Supporting Information

In situ Structure of Mo-doped Pt-Ni Catalyst during Electrochemical Oxygen Reduction Resolved from Machine Learning Based Grand Canonical Global Optimization

Ji-Li Li, Ye-Fei Li*, and Zhi-Pan Liu*

Collaborative Innovation Center of Chemistry for Energy Material, Shanghai Key Laboratory of Molecular Catalysis and Innovative Materials, Key Laboratory of Computational Physical Science, Department of Chemistry, Fudan University, Shanghai 200433, China

Table of Contents

1.Methodology and Calculation Details

1.1 Stochastic surface walking global optimization using neural network potential energy surface (SSW-NN)

Architecture of the high dimensional neural network (HDNN)

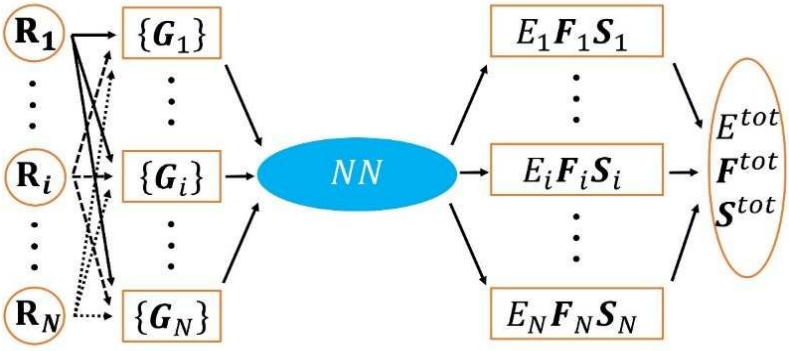

Scheme S1. Scheme for HDNN architecture. The subscript i is atom index; N is the number of atoms. The inputs of HDNN are a set of atom-centered symmetry functions $\{G_i\}$, which is constructed from a set of Cartesian coordinates $\{R_i\}$. The outputs are the atomic properties $\{E_i, \boldsymbol{F_i}, \boldsymbol{S_i}\}$, i.e., energy, force and stress. The overall properties of a structure, namely, E^{tot}, $\boldsymbol{F^{tot}}$, or $\boldsymbol{S}^{tot}$, are calculated by summing the atomic properties, E_i, $\boldsymbol{F_i}$, $\boldsymbol{S_i}$.

To build the high dimensional neural network (HDNN) potential energy surface[1-2], we utilized the SSW global optimization to generate the global dataset for Pt-Ni-Mo-O-H system. The HDNN architecture is schematically shown in Scheme S1. The total energy $\boldsymbol{E^{tot}}$ is obtained by summing the atomic energy $\boldsymbol{E_i}$, which is the output of the standard neural network (see Eq. 1,). The inputs, $\{\boldsymbol{G_i}\}$, are a set of atom-centered symmetry functions (also called geometry-based structural descriptors).

$$E^{tot} = \sum_i E_i \#(1.)$$

Structure Descriptors

The atom-centered symmetry functions are calculated a series of power-type structure descriptors (PTSDs)[1-2], which is developed by our group. There are six types of PTSDs, namely $\boldsymbol{S^1}$ to $\boldsymbol{S^6}$, which have the following mathematic forms:

$$f_c(R_{ij}) = \begin{cases} 0.5 \times tanh^3\left[1 - \frac{r_{ij}}{r_c}\right], for\ r_{ij} \le r_c \#(2.) \\ 0, for\ r_{ij} > r_c \end{cases}$$

$$R^n(r_{ij}) = r_{ij}^n \cdot \mathrm{f}_c(r_{ij}) \#()$$

$$S_i^1 = \sum_{j \neq i} R^n(r_{ij}) \#()$$

$$S_i^2 = \left[\sum_{m=-L}^{L} |\sum GU_2|^2\right]^{\frac{1}{2}} = \left[\sum_{m=-L}^{L} |\sum_{j \neq i} R^n(r_{ij}) Y_{Lm}(r_{ij})|^2\right]^{\frac{1}{2}} \#()$$

$$S_i^3 = 2^{1-\zeta} \sum GU_3 = 2^{1-\zeta} \sum_{j,k \neq i} (1 + \lambda cos\theta_{ijk})^{\zeta} \cdot R^n(r_{ij}) \cdot R^m(r_{ik}) \#()$$

$$S_i^4 = 2^{1-\zeta}\sum GU_4 = 2^{1-\zeta}\sum_{j,k\neq i}(1+\lambda cos\theta_{ijk})^{\zeta}\cdot R^n(r_{ij})\cdot R^m(r_{ik})\cdot R^p(r_{ik})\#()$$

$$S_i^5 = \left[\sum_{m=-L}^{L}|\sum GU_5|^2\right]^{\frac{1}{2}}$$

$$= \left[\sum_{m=-L}^{L}|\sum_{j,k\neq i} R^n(r_{ij})\cdot R^m(r_{ik})\cdot R^p(r_{ik})\cdot (Y_{Lm}(r_{ij})+Y_{Lm}(r_{ik})|^2\right]^{\frac{1}{2}}\#(8.)$$

$$S_i^6 = 2^{1-\zeta}\sum GU_6 = 2^{1-\zeta}\sum_{j,k,l\neq i}(1+\lambda cos\theta_{ijk})^{\zeta}\cdot R^n(r_{ij})\cdot R^m(r_{ik})\cdot R^p(r_{il})\#()$$

Each PTSD can be considered as a sum of the n-body functions, named as the group unit (GU). The power function $R^n(r_{ij})$ represents the radial function in the GU. In the equations, r_{ij} is the distance of atomic pairs, r_c is the cutoff, beyond which the value of Eq. 2 is equal to zero, $Y_{Lm}(r_{ik})$ is the spherical harmonic function, and n, m, p, λ, and ζ are power parameters. Depending on the functional form of GU, the PTSDs S_i^1, S_i^2, S_i^3, S_i^4, S_i^5 and S_i^6 can be considered as 2-body, 3-body and 4-body functions, respectively, where the S_i^2 and S_i^5 involve also spherical function.

Construction of global dataset for HDNN training (G-NN)

The building of dataset is the key factor that determines the accuracy of the potential energy surface (PES) of G-NN. Our previous works have shown that, the SSW[3-5] global optimization can fast generate a global dataset, which incorporates structures with notably different structural patterns on the global PES. The SSW global optimization is fully automated and does not need a priori knowledge on the system, such as the structure motif (e.g., bonding patterns, symmetry) of the materials.

The overall approach to generate G-NN and its implementations are briefly divided into six steps (see in Scheme S2):

(i) Generating the global dataset by computing the selected structures from the SSW trajectories using DFT.

(ii) Training the G-NN potential with the global dataset.

(iii) Benchmarking the accuracy between the current G-NN potential and DFT values for a few randomly selected structures from a trial SSW-NN calculations. The structures with large error are added in the dataset to retrain the G-NN potential.

(iv) Iteratively performing (i)-(iii) steps until the PES deviation is low enough. The RMSE for G-NN potential is typically 5~10 meV/atom for energy and 0.1~0.2 eV/Å for force.

(v) Performing the SSW global optimization on the NN PES for target problem.

(vi) Recomputing the energy of key structures with DFT calculations, in which Bayesian optimization is utilized to drive the iterative acquisition-surrogate procedure.

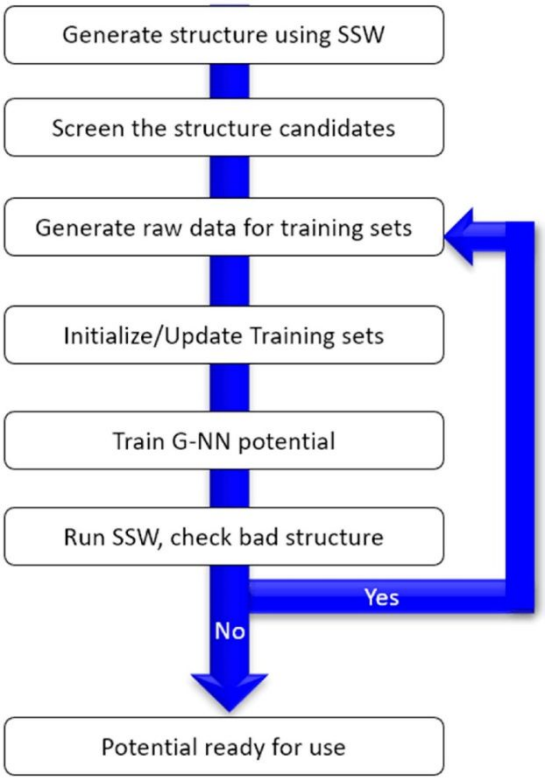

Scheme S2. Overall procedure for generating the training dataset using SSW global optimization.

Table S1. Number of structures for the global data set to train the Pt-Ni-Mo-O-H potential.

Species	N_{atom}	$N_{cluster}$	N_{layer}	N_{bulk}	total
Pt16	16	3107	7	10606	13720
Mo1-Pt15	16	0	0	113	113
Mo2-Pt14	16	0	0	165	165
Mo3-Pt13	16	0	0	150	150
Mo4-Pt12	16	0	0	140	140
Mo5-Pt10	15	0	0	3	3
Mo5-Pt11	16	0	0	137	137
Mo6-Pt9	15	0	0	5	5
Mo6-Pt10	16	0	0	132	132
Mo6-Pt42	48	0	0	4	4
Mo7-Pt8	15	0	0	7	7
Mo7-Pt9	16	0	0	151	151
Mo8-Pt7	15	0	0	6	6
Mo8-Pt8	16	0	1	157	158
Mo8-Pt24	32	0	36	40	76
Mo9-Pt6	15	0	0	13	13
Mo9-Pt7	16	0	0	177	177
Mo10-Pt5	15	0	0	21	21
Mo10-Pt6	16	0	0	115	115

Mo11-Pt4	15	0	0	14	14
Mo11-Pt5	16	0	0	162	162
Mo12-Pt3	15	0	0	20	20
Mo12-Pt4	16	0	1	147	148
Mo12-Pt36	48	0	0	7	7
Mo13-Pt2	15	0	0	25	25
Mo13-Pt3	16	0	0	154	154
Mo14-Pt1	15	0	0	24	24
Mo14-Pt2	16	0	0	149	149
Mo14-Pt15	29	0	37	23	60
Mo15	15	0	0	154	154
Mo15-Pt1	16	0	0	122	122
Mo16	16	0	0	363	363
Mo18-Pt46	64	0	7	3	10
Mo23-Pt6	29	0	68	123	191
Mo24-Pt24	48	0	0	8	8
Mo28	28	0	1	0	1
Mo29-Pt19	48	0	0	15	15
Mo30-Pt2	32	0	146	227	373
Mo31-Pt1	32	0	177	142	319
Mo32	32	0	0	1	1
Mo36-Pt12	48	0	0	9	9
Mo42-Pt6	48	0	0	58	58
Mo46-Pt18	64	0	17	9	26
Mo48	48	0	0	11	11
Ni1-Pt15	16	0	2	2	4
Ni1-Mo1-Pt13	15	0	0	2	2
Ni1-Mo2-Pt12	15	0	0	7	7
Ni1-Mo3-Pt11	15	0	0	8	8
Ni1-Mo4-Pt10	15	0	0	11	11
Ni1-Mo5-Pt9	15	0	0	13	13
Ni1-Mo6-Pt8	15	0	0	15	15
Ni1-Mo7-Pt7	15	0	0	21	21
Ni1-Mo8-Pt6	15	0	0	12	12
Ni1-Mo9-Pt5	15	0	0	18	18
Ni1-Mo9-Pt6	16	0	0	1	1
Ni1-Mo10-Pt4	15	0	0	13	13
Ni1-Mo10-Pt5	16	0	0	1	1
Ni1-Mo11-Pt3	15	0	0	10	10
Ni1-Mo11-Pt4	16	0	1	2	3
Ni1-Mo11-Pt36	48	0	0	26	26

Ni1-Mo12-Pt2	15	0	0	4	4
Ni1-Mo12-Pt3	16	0	0	7	7
Ni1-Mo13-Pt1	15	0	0	4	4
Ni1-Mo13-Pt2	16	0	0	5	5
Ni1-Mo14	15	0	0	25	25
Ni1-Mo14-Pt1	16	0	0	9	9
Ni1-Mo15	16	0	1	10	11
Ni1-Mo22-Pt6	29	0	75	78	153
Ni1-Mo22-Pt9	32	0	0	1	1
Ni1-Mo23-Pt24	48	0	0	7	7
Ni1-Mo28-Pt3	32	0	0	1	1
Ni1-Mo28-Pt19	48	0	0	27	27
Ni2-Pt13	15	0	0	2176	2176
Ni2-Mo1-Pt12	15	0	0	16	16
Ni2-Mo2-Pt11	15	0	0	32	32
Ni2-Mo3-Pt10	15	0	0	24	24
Ni2-Mo3-Pt11	16	0	1	0	1
Ni2-Mo4-Pt9	15	0	0	16	16
Ni2-Mo5-Pt8	15	0	0	13	13
Ni2-Mo6-Pt7	15	0	0	7	7
Ni2-Mo6-Pt8	16	0	0	1	1
Ni2-Mo7-Pt6	15	0	0	3	3
Ni2-Mo8-Pt5	15	0	0	6	6
Ni2-Mo8-Pt6	16	0	0	2	2
Ni2-Mo9-Pt4	15	0	0	2	2
Ni2-Mo9-Pt5	16	0	0	3	3
Ni2-Mo10-Pt3	15	0	0	2	2
Ni2-Mo10-Pt4	16	0	0	3	3
Ni2-Mo10-Pt20	32	0	55	45	100
Ni2-Mo10-Pt36	48	0	0	19	19
Ni2-Mo11-Pt3	16	0	0	4	4
Ni2-Mo12-Pt2	16	0	1	7	8
Ni2-Mo13	15	0	0	33	33
Ni2-Mo13-Pt1	16	0	0	7	7
Ni2-Mo14	16	0	1	7	8
Ni2-Mo21-Pt9	32	0	0	1	1
Ni2-Mo22-Pt24	48	0	0	10	10
Ni2-Mo24-Pt6	32	0	34	66	100
Ni3-Pt13	16	0	6	0	6
Ni3-Mo3-Pt18	24	0	0	26	26
Ni3-Mo7-Pt22	32	0	18	22	40

Ni3-Mo8-Pt5	16	0	0	7	7
Ni3-Mo9-Pt4	16	0	0	10	10
Ni3-Mo9-Pt36	48	0	0	13	13
Ni3-Mo10-Pt3	16	0	0	6	6
Ni3-Mo11-Pt2	16	0	0	15	15
Ni3-Mo12	15	0	0	41	41
Ni3-Mo12-Pt1	16	0	0	6	6
Ni3-Mo12-Pt17	32	0	0	1	1
Ni3-Mo13	16	0	0	12	12
Ni3-Mo13-Pt16	32	0	0	1	1
Ni3-Mo16-Pt13	32	0	44	46	90
Ni3-Mo21-Pt8	32	0	203	309	512
Ni3-Mo21-Pt24	48	0	0	15	15
Ni3-Mo26-Pt3	32	0	0	1	1
Ni3-Mo26-Pt19	48	0	0	11	11
Ni4-Mo2-Pt42	48	0	0	6	6
Ni4-Mo4-Pt8	16	0	0	2	2
Ni4-Mo5-Pt7	16	0	0	2	2
Ni4-Mo6-Pt6	16	0	0	7	7
Ni4-Mo7-Pt5	16	0	0	6	6
Ni4-Mo8-Pt4	16	0	0	10	10
Ni4-Mo8-Pt20	32	0	0	1	1
Ni4-Mo8-Pt36	48	0	0	8	8
Ni4-Mo9-Pt3	16	0	0	5	5
Ni4-Mo10-Pt2	16	0	0	3	3
Ni4-Mo11	15	0	0	57	57
Ni4-Mo11-Pt1	16	0	0	2	2
Ni4-Mo12	16	0	0	11	11
Ni4-Mo20-Pt24	48	0	0	12	12
Ni4-Mo21-Pt7	32	0	31	69	100
Ni4-Mo26-Pt34	64	0	6	5	11
Ni4-Mo30-Pt24	58	0	22	8	30
Ni4-Mo32-Pt12	48	0	0	10	10
Ni5-Pt11	16	10	1	0	11
Ni5-Mo3-Pt8	16	0	0	1	1
Ni5-Mo4-Pt7	16	0	0	6	6
Ni5-Mo5-Pt6	16	0	0	13	13
Ni5-Mo6-Pt5	16	0	0	10	10
Ni5-Mo7-Pt4	16	0	0	7	7
Ni5-Mo7-Pt36	48	0	0	2	2
Ni5-Mo8-Pt3	16	0	0	4	4

Ni5-Mo9-Pt2	16	0	0	5	5
Ni5-Mo9-Pt18	32	0	30	23	53
Ni5-Mo10	15	0	0	49	49
Ni5-Mo11	16	0	0	8	8
Ni5-Mo16-Pt11	32	0	41	50	91
Ni5-Mo19-Pt8	32	0	47	62	109
Ni5-Mo19-Pt24	48	0	0	16	16
Ni5-Mo23-Pt4	32	0	39	83	122
Ni5-Mo24-Pt3	32	0	1	0	1
Ni5-Mo24-Pt19	48	0	0	14	14
Ni6-Pt26	32	0	0	8	8
Ni6-Pt42	48	0	0	9	9
Ni6-Mo2-Pt8	16	0	0	5	5
Ni6-Mo3-Pt7	16	0	0	7	7
Ni6-Mo4-Pt6	16	0	0	3	3
Ni6-Mo5-Pt5	16	0	0	10	10
Ni6-Mo6-Pt4	16	0	0	1	1
Ni6-Mo6-Pt36	48	0	0	8	8
Ni6-Mo7-Pt3	16	0	0	1	1
Ni6-Mo8-Pt2	16	0	0	2	2
Ni6-Mo9	15	0	0	52	52
Ni6-Mo10	16	0	0	12	12
Ni6-Mo16-Pt10	32	0	0	1	1
Ni6-Mo18-Pt24	48	0	0	21	21
Ni6-Mo36-Pt6	48	0	0	1	1
Ni7-Mo1-Pt8	16	0	0	11	11
Ni7-Mo2-Pt7	16	0	0	12	12
Ni7-Mo2-Pt23	32	75	0	0	75
Ni7-Mo2-Pt27	36	0	0	35	35
Ni7-Mo3-Pt6	16	0	0	14	14
Ni7-Mo4-Pt5	16	0	0	3	3
Ni7-Mo5-Pt4	16	0	0	4	4
Ni7-Mo5-Pt20	32	0	16	44	60
Ni7-Mo5-Pt36	48	0	0	3	3
Ni7-Mo6-Pt3	16	0	0	3	3
Ni7-Mo8	15	0	0	46	46
Ni7-Mo9	16	0	0	6	6
Ni7-Mo15-Pt10	32	0	31	50	81
Ni7-Mo17-Pt24	48	0	0	8	8
Ni7-Mo19-Pt6	32	0	0	1	1
Ni7-Mo22-Pt19	48	0	0	20	20

Ni8-Pt8	16	0	5	1403	1408
Ni8-Mo1-Pt7	16	0	0	11	11
Ni8-Mo1-Pt23	32	0	21	11	32
Ni8-Mo2-Pt6	16	0	0	4	4
Ni8-Mo2-Pt22	32	0	20	12	32
Ni8-Mo3-Pt21	32	28	14	7	49
Ni8-Mo4-Pt4	16	0	0	2	2
Ni8-Mo7	15	0	0	42	42
Ni8-Mo7-Pt1	16	0	0	1	1
Ni8-Mo8	16	0	0	11	11
Ni8-Mo10-Pt14	32	0	47	56	103
Ni8-Mo13-Pt11	32	0	72	63	135
Ni8-Mo14-Pt7	29	0	103	138	241
Ni8-Mo14-Pt10	32	0	0	1	1
Ni8-Mo16-Pt8	32	0	58	70	128
Ni8-Mo16-Pt24	48	0	0	4	4
Ni8-Mo18-Pt6	32	0	37	63	100
Ni8-Mo28-Pt12	48	0	0	9	9
Ni9-Mo2-Pt53	64	0	2	0	2
Ni9-Mo2-Pt54	65	0	1	0	1
Ni9-Mo3-Pt36	48	0	0	2	2
Ni9-Mo4-Pt19	32	0	1	0	1
Ni9-Mo6	15	0	0	48	48
Ni9-Mo7	16	0	0	4	4
Ni9-Mo15-Pt4	28	0	1	0	1
Ni9-Mo15-Pt24	48	0	0	8	8
Ni9-Mo20-Pt19	48	0	0	15	15
Ni9-Mo23	32	0	71	128	199
Ni10-Mo2-Pt36	48	0	0	8	8
Ni10-Mo2-Pt60	72	0	8	0	8
Ni10-Mo2-Pt61	73	0	3	0	3
Ni10-Mo5	15	0	0	50	50
Ni10-Mo5-Pt17	32	190	0	0	190
Ni10-Mo6	16	0	0	10	10
Ni10-Mo6-Pt15	31	24	0	0	24
Ni10-Mo6-Pt16	32	204	0	0	204
Ni10-Mo12-Pt7	29	0	1	0	1
Ni10-Mo14-Pt24	48	0	0	8	8
Ni10-Mo38-Pt16	64	0	4	10	14
Ni11-Pt21	32	0	5	6	11
Ni11-Mo1-Pt36	48	0	0	2	2

Ni11-Mo4	15	0	0	41	41
Ni11-Mo4-Pt17	32	0	1	0	1
Ni11-Mo5	16	0	0	10	10
Ni11-Mo13-Pt24	48	0	0	7	7
Ni11-Mo18-Pt19	48	0	0	22	22
Ni12-Pt4	16	0	2	0	2
Ni12-Mo3	15	0	0	48	48
Ni12-Mo4	16	0	0	6	6
Ni12-Mo7-Pt13	32	0	1	0	1
Ni12-Mo8-Pt12	32	0	0	1	1
Ni12-Mo12-Pt24	48	0	0	5	5
Ni12-Mo24-Pt12	48	0	0	8	8
Ni12-Mo30-Pt6	48	0	0	15	15
Ni13-Pt3	16	0	0	5	5
Ni13-Mo1-Pt18	32	0	189	104	293
Ni13-Mo2	15	0	0	41	41
Ni13-Mo3	16	0	0	9	9
Ni13-Mo11-Pt24	48	0	0	9	9
Ni14-Pt14	28	0	10	0	10
Ni14-Pt15	29	0	12	0	12
Ni14-Pt18	32	0	6	1	7
Ni14-Mo1	15	0	0	29	29
Ni14-Mo2	16	0	0	5	5
Ni14-Mo2-Pt48	64	0	1	0	1
Ni14-Mo6-Pt44	64	0	6	6	12
Ni14-Mo10-Pt8	32	0	185	134	319
Ni14-Mo10-Pt24	48	0	0	2	2
Ni15	15	0	0	2695	2695
Ni15-Pt1	16	0	7	17	24
Ni15-Mo1	16	0	0	5	5
Ni15-Mo2-Pt15	32	0	0	2	2
Ni15-Mo9-Pt24	48	0	0	11	11
Ni15-Mo14-Pt19	48	0	0	8	8
Ni15-Mo16-Pt1	32	0	35	59	94
Ni16	16	0	0	507	507
Ni16-Pt16	32	0	3	63	66
Ni16-Mo2-Pt54	72	0	1	0	1
Ni16-Mo8-Pt8	32	0	103	121	224
Ni16-Mo8-Pt24	48	0	0	2	2
Ni16-Mo14-Pt2	32	0	50	77	127
Ni16-Mo20-Pt12	48	0	0	4	4

Ni17-Pt15	32	0	3	0	3
Ni17-Mo7-Pt24	48	0	0	13	13
Ni17-Mo12-Pt19	48	0	0	7	7
Ni18-Pt54	72	0	1	0	1
Ni18-Mo1-Pt13	32	0	47	45	92
Ni18-Mo6-Pt24	48	0	0	5	5
Ni18-Mo14	32	0	101	119	220
Ni19-Mo5-Pt24	48	0	0	2	2
Ni19-Mo9-Pt20	48	0	0	8	8
Ni19-Mo10-Pt19	48	0	0	6	6
Ni19-Mo13	32	0	88	45	133
Ni20-Mo4-Pt24	48	0	0	5	5
Ni20-Mo8-Pt20	48	0	0	4	4
Ni20-Mo9-Pt19	48	0	0	4	4
Ni20-Mo10-Pt18	48	0	0	7	7
Ni20-Mo16-Pt12	48	0	0	7	7
Ni21-Mo3-Pt24	48	0	0	4	4
Ni22-Mo7-Pt19	48	0	0	24	24
Ni22-Mo8-Pt18	48	0	0	10	10
Ni23-Mo1-Pt24	48	0	0	20	20
Ni23-Mo4-Pt4	31	16	0	0	16
Ni23-Mo6-Pt19	48	0	0	3	3
Ni24-Mo3-Pt5	32	85	0	0	85
Ni24-Mo4-Pt4	32	104	0	0	104
Ni24-Mo12-Pt12	48	0	0	1	1
Ni24-Mo18-Pt6	48	0	0	5	5
Ni25-Mo4-Pt19	48	0	0	4	4
Ni27-Mo2-Pt19	48	0	0	4	4
Ni28-Mo8-Pt12	48	0	0	3	3
Ni30-Mo12-Pt6	48	0	0	1	1
Ni30-Mo32-Pt2	64	0	1	7	8
Ni32-Mo28-Pt4	64	0	2	2	4
Ni36-Pt12	48	0	0	2	2
Ni36-Mo6-Pt6	48	0	0	4	4
Ni36-Mo28	64	0	5	11	16
Ni42-Pt6	48	0	0	1	1
O1-Pt12	13	0	175	0	175
O1-Mo1-Pt11	13	0	3	0	3
O1-Mo2-Pt10	13	0	7	0	7
O1-Mo3-Pt9	13	0	3	0	3
O1-Mo4-Pt8	13	0	3	0	3

O1-Mo5-Pt7	13	0	5	0	5
O1-Mo6-Pt6	13	0	6	0	6
O1-Mo6-Pt18	25	0	0	20	20
O1-Mo7-Pt5	13	0	3	0	3
O1-Mo8-Pt4	13	0	7	0	7
O1-Mo8-Pt23	32	0	20	15	35
O1-Mo9-Pt3	13	0	1	0	1
O1-Mo10-Pt2	13	0	3	0	3
O1-Mo11-Pt1	13	0	7	0	7
O1-Ni1-Pt11	13	0	1	0	1
O1-Ni1-Mo13-Pt17	32	0	26	16	42
O1-Ni1-Mo15	17	0	2	0	2
O1-Ni2-Pt10	13	0	4	0	4
O1-Ni3	4	0	5	11	16
O1-Ni3-Pt9	13	0	3	0	3
O1-Ni3-Pt13	17	0	1	0	1
O1-Ni3-Mo3-Pt18	25	0	0	23	23
O1-Ni3-Mo11-Pt17	32	0	8	7	15
O1-Ni3-Mo13	17	0	1	0	1
O1-Ni4-Pt8	13	0	1	0	1
O1-Ni4-Pt12	17	0	1	0	1
O1-Ni5-Pt11	17	0	3	0	3
O1-Ni5-Mo11	17	0	3	0	3
O1-Ni6-Pt10	17	0	1	0	1
O1-Ni6-Mo2-Pt23	32	0	10	8	18
O1-Ni6-Mo3-Pt22	32	0	21	14	35
O1-Ni6-Mo9-Pt15	31	43	0	0	43
O1-Ni6-Mo10	17	0	1	0	1
O1-Ni6-Mo19-Pt6	32	0	9	12	21
O1-Ni7-Pt5	13	0	1	0	1
O1-Ni7-Pt9	17	0	2	0	2
O1-Ni7-Mo9	17	0	3	0	3
O1-Ni8-Mo8	17	0	2	0	2
O1-Ni9-Mo2-Pt53	65	0	5	0	5
O1-Ni9-Mo7	17	0	3	0	3
O1-Ni10-Pt6	17	0	1	0	1
O1-Ni10-Mo2-Pt60	73	0	15	0	15
O1-Ni10-Mo2-Pt61	74	0	1	0	1
O1-Ni10-Mo5-Pt15	31	75	0	0	75
O1-Ni10-Mo6	17	0	3	0	3
O1-Ni11-Pt5	17	0	1	0	1

O1-Ni11-Pt20	32	0	7	8	15
O1-Ni11-Mo2-Pt17	31	24	0	0	24
O1-Ni11-Mo5	17	0	5	0	5
O1-Ni11-Mo8-Pt12	32	0	18	15	33
O1-Ni12-Mo4	17	0	2	0	2
O1-Ni13-Mo1-Pt17	32	0	16	14	30
O1-Ni13-Mo2-Pt49	65	0	1	0	1
O1-Ni13-Mo3	17	0	5	0	5
O1-Ni14-Mo2	17	0	3	0	3
O1-Ni15	16	0	1	4	5
O1-Ni15-Mo1	17	0	3	0	3
O1-Ni16-Mo2-Pt54	73	0	3	0	3
O1-Ni18-Pt54	73	0	1	0	1
O1-Ni23-Mo3-Pt4	31	43	0	0	43
O2-Pt10	12	0	161	0	161
O2-Mo1-Pt9	12	0	8	0	8
O2-Mo2-Pt8	12	0	11	0	11
O2-Mo3-Pt7	12	0	4	0	4
O2-Mo4-Pt6	12	0	4	0	4
O2-Mo5-Pt5	12	0	4	0	4
O2-Mo6-Pt4	12	0	5	0	5
O2-Mo7-Pt3	12	0	3	0	3
O2-Mo8-Pt2	12	0	5	0	5
O2-Mo9-Pt1	12	0	7	0	7
O2-Mo21-Pt9	32	0	52	32	84
O2-Ni1-Pt9	12	0	2	0	2
O2-Ni2-Pt8	12	0	3	0	3
O2-Ni2-Mo11-Pt17	32	0	3	4	7
O2-Ni2-Mo13-Pt12	29	0	43	43	86
O2-Ni2-Mo14	18	0	0	1	1
O2-Ni2-Mo21-Pt7	32	0	6	6	12
O2-Ni3-Pt7	12	0	3	0	3
O2-Ni3-Mo13	18	0	0	1	1
O2-Ni5-Pt11	18	0	0	1	1
O2-Ni5-Mo2-Pt23	32	0	5	4	9
O2-Ni5-Mo11	18	0	0	2	2
O2-Ni6-Mo9-Pt12	29	0	26	20	46
O2-Ni7-Pt9	18	0	0	1	1
O2-Ni7-Mo25	34	0	2	0	2
O2-Ni8-Pt8	18	0	0	1	1
O2-Ni8-Mo8	18	0	0	4	4

O2-Ni8-Mo13-Pt9	32	0	30	19	49
O2-Ni9-Pt7	18	0	0	1	1
O2-Ni9-Mo2-Pt53	66	0	3	0	3
O2-Ni9-Mo2-Pt54	67	0	2	0	2
O2-Ni10-Pt20	32	0	2	0	2
O2-Ni10-Pt22	34	0	1	0	1
O2-Ni10-Mo2-Pt60	74	0	3	0	3
O2-Ni10-Mo2-Pt61	75	0	1	0	1
O2-Ni10-Mo6	18	0	0	2	2
O2-Ni11-Mo5	18	0	0	1	1
O2-Ni12-Mo4	18	0	0	1	1
O2-Ni13-Pt19	34	0	2	0	2
O2-Ni13-Mo2-Pt49	66	0	1	0	1
O2-Ni13-Mo3	18	0	0	1	1
O2-Ni14	16	0	4	7	11
O2-Ni14-Mo2	18	0	0	2	2
O2-Ni14-Mo9-Pt7	32	0	12	15	27
O2-Ni15-Pt17	34	0	1	0	1
O2-Ni15-Mo1	18	0	0	5	5
O2-Ni15-Mo13-Pt2	32	0	17	27	44
O2-Ni15-Mo14-Pt1	32	0	32	53	85
O2-Ni16-Mo2-Pt54	74	0	8	0	8
O2-Ni16-Mo2-Pt55	75	0	2	0	2
O2-Ni16-Mo9-Pt2	29	0	18	25	43
O2-Ni18-Pt54	74	0	1	0	1
O2-Ni20-Mo12	34	0	1	0	1
O2-Ni22-Mo10	34	0	1	0	1
O2-Ni25-Mo7	34	0	1	0	1
O2-Ni28-Mo4	34	0	1	0	1
O2-Ni29-Mo3	34	0	1	0	1
O3-Pt16	19	24	0	0	24
O3-Mo1-Pt15	19	1	0	0	1
O3-Mo2-Pt14	19	3	0	0	3
O3-Mo3-Pt13	19	1	0	0	1
O3-Mo5-Pt11	19	1	0	0	1
O3-Mo7-Pt9	19	1	0	0	1
O3-Mo9-Pt7	19	2	0	0	2
O3-Mo13-Pt3	19	3	0	0	3
O3-Ni2-Mo19-Pt8	32	0	16	22	38
O3-Ni2-Mo21-Pt6	32	0	2	7	9
O3-Ni3-Mo19-Pt7	32	0	4	13	17

O3-Ni4-Mo2-Pt23	32	0	11	18	29
O3-Ni5-Pt11	19	1	0	0	1
O3-Ni9-Mo2-Pt53	67	0	1	0	1
O3-Ni9-Mo2-Pt54	68	0	1	0	1
O3-Ni9-Mo2-Pt55	69	0	1	0	1
O3-Ni10-Mo2-Pt60	75	0	2	0	2
O3-Ni10-Mo2-Pt61	76	0	1	0	1
O3-Ni10-Mo2-Pt62	77	0	8	0	8
O3-Ni13-Mo2-Pt49	67	0	1	0	1
O3-Ni13-Mo2-Pt50	68	0	1	0	1
O3-Ni13-Mo14-Pt2	32	0	24	15	39
O3-Ni14-Mo13-Pt2	32	0	9	8	17
O3-Ni15-Mo9-Pt2	29	0	6	9	15
O3-Ni16-Mo2-Pt54	75	0	1	0	1
O3-Ni16-Mo2-Pt55	76	0	1	0	1
O3-Ni18-Mo4-Pt7	32	0	20	15	35
O3-Ni18-Mo11	32	0	58	46	104
O4-Pt8	12	0	0	4604	4604
O4-Pt27	31	0	0	116	116
O4-Mo1-Pt7	12	0	0	215	215
O4-Mo1-Pt26	31	0	0	2	2
O4-Mo2-Pt6	12	0	0	173	173
O4-Mo2-Pt25	31	0	0	6	6
O4-Mo3-Pt5	12	0	0	170	170
O4-Mo3-Pt24	31	0	0	3	3
O4-Mo4-Pt4	12	0	0	187	187
O4-Mo5-Pt3	12	0	0	179	179
O4-Mo5-Pt22	31	0	0	1	1
O4-Mo6-Pt2	12	0	0	198	198
O4-Mo6-Pt21	31	0	0	1	1
O4-Mo7-Pt1	12	0	0	211	211
O4-Mo7-Pt20	31	0	0	1	1
O4-Mo8-Pt19	31	0	0	2	2
O4-Mo9-Pt18	31	0	0	1	1
O4-Mo10-Pt17	31	0	0	2	2
O4-Mo11-Pt16	31	0	0	3	3
O4-Mo13-Pt14	31	0	0	3	3
O4-Mo14-Pt13	31	0	0	1	1
O4-Mo16-Pt11	31	0	0	3	3
O4-Mo18-Pt9	31	0	0	1	1
O4-Mo19-Pt8	31	0	0	3	3

O4-Mo20-Pt7	31	0	0	1	1
O4-Mo21-Pt6	31	0	0	1	1
O4-Mo22-Pt5	31	0	0	1	1
O4-Mo23-Pt4	31	0	0	2	2
O4-Mo24-Pt3	31	0	0	3	3
O4-Mo25-Pt2	31	0	0	4	4
O4-Mo26-Pt1	31	0	0	2	2
O4-Ni1-Pt7	12	0	0	144	144
O4-Ni2-Pt6	12	0	0	111	111
O4-Ni2-Pt25	31	0	0	2	2
O4-Ni2-Mo30	36	0	1	0	1
O4-Ni3-Pt5	12	0	0	58	58
O4-Ni3-Pt24	31	0	0	1	1
O4-Ni3-Mo19-Pt6	32	0	26	12	38
O4-Ni4-Pt4	12	0	0	28	28
O4-Ni4-Pt23	31	0	0	3	3
O4-Ni4-Mo22-Pt34	64	0	17	13	30
O4-Ni5-Pt3	12	0	0	1	1
O4-Ni5-Pt22	31	0	0	2	2
O4-Ni5-Mo27	36	0	1	0	1
O4-Ni6-Pt21	31	0	0	5	5
O4-Ni9-Mo2-Pt53	68	0	2	0	2
O4-Ni9-Mo2-Pt54	69	0	2	0	2
O4-Ni9-Mo2-Pt55	70	0	2	0	2
O4-Ni9-Mo2-Pt56	71	0	1	0	1
O4-Ni9-Mo23	36	0	1	0	1
O4-Ni10-Pt17	31	0	0	1	1
O4-Ni10-Mo2-Pt60	76	0	3	0	3
O4-Ni10-Mo2-Pt61	77	0	10	0	10
O4-Ni10-Mo2-Pt62	78	0	2	0	2
O4-Ni10-Mo2-Pt63	79	0	1	0	1
O4-Ni10-Mo4-Pt46	64	0	20	2	22
O4-Ni12-Mo10-Pt6	32	0	3	6	9
O4-Ni13-Mo2-Pt49	68	0	1	0	1
O4-Ni13-Mo2-Pt50	69	0	1	0	1
O4-Ni16-Mo2-Pt54	76	0	2	0	2
O4-Ni16-Mo2-Pt55	77	0	7	0	7
O4-Ni16-Mo2-Pt56	78	0	1	0	1
O4-Ni17-Mo1-Pt52	74	0	89	0	89
O4-Ni17-Mo15	36	0	1	0	1
O4-Ni18-Pt54	76	0	1	0	1

O4-Ni18-Mo22-Pt20	64	0	5	6	11
O4-Ni20-Pt40	64	0	10	15	25
O4-Ni22-Mo10	36	0	1	0	1
O4-Ni28-Mo4	36	0	1	0	1
O4-Ni36-Mo6-Pt18	64	0	10	7	17
O4-Ni43-Mo2-Pt133	182	0	85	0	85
O4-Ni44-Pt16	64	0	4	2	6
O5-Ni2-Mo29	36	0	1	0	1
O5-Ni3-Mo28	36	0	1	0	1
O5-Ni8-Pt23	36	0	1	0	1
O5-Ni9-Mo2-Pt53	69	0	1	0	1
O5-Ni9-Mo2-Pt54	70	0	3	0	3
O5-Ni9-Mo2-Pt55	71	0	2	0	2
O5-Ni9-Mo2-Pt56	72	0	1	0	1
O5-Ni10-Mo2-Pt60	77	0	13	0	13
O5-Ni10-Mo2-Pt61	78	0	8	0	8
O5-Ni10-Mo2-Pt62	79	0	9	0	9
O5-Ni10-Mo2-Pt63	80	0	1	0	1
O5-Ni13-Pt18	36	0	1	0	1
O5-Ni13-Mo2-Pt50	70	0	1	0	1
O5-Ni16-Pt15	36	0	1	0	1
O5-Ni16-Mo2-Pt54	77	0	1	0	1
O5-Ni16-Mo2-Pt55	78	0	2	0	2
O5-Ni16-Mo2-Pt56	79	0	1	0	1
O5-Ni16-Mo2-Pt57	80	0	1	0	1
O5-Ni18-Pt54	77	0	1	0	1
O5-Ni22-Mo9	36	0	1	0	1
O5-Ni29-Mo2	36	0	1	0	1
O5-Ni30-Mo1	36	0	1	0	1
O6-Pt4	10	0	65	214	279
O6-Pt26	32	0	0	97	97
O6-Mo1-Pt25	32	0	0	2	2
O6-Mo2-Pt24	32	0	0	3	3
O6-Mo3-Pt23	32	0	0	7	7
O6-Mo5-Pt21	32	0	0	2	2
O6-Mo7-Pt19	32	0	0	3	3
O6-Mo9-Pt17	32	0	0	3	3
O6-Mo10-Pt16	32	0	0	2	2
O6-Mo11-Pt15	32	0	0	3	3
O6-Mo12-Pt14	32	0	0	3	3
O6-Mo13-Pt13	32	0	0	2	2

O6-Mo14-Pt12	32	0	0	5	5
O6-Mo15-Pt11	32	0	0	3	3
O6-Mo16-Pt10	32	0	0	1	1
O6-Mo17-Pt9	32	0	0	3	3
O6-Mo18-Pt8	32	0	0	3	3
O6-Mo19-Pt7	32	0	0	4	4
O6-Mo20-Pt6	32	0	0	2	2
O6-Mo22-Pt4	32	0	0	2	2
O6-Mo23-Pt3	32	0	0	3	3
O6-Mo24-Pt2	32	0	0	3	3
O6-Mo25-Pt1	32	0	0	1	1
O6-Ni2-Pt24	32	0	0	1	1
O6-Ni3-Mo6-Pt16	31	13	0	0	13
O6-Ni4-Pt22	32	0	0	1	1
O6-Ni4-Mo42-Pt12	64	0	14	15	29
O6-Ni5-Pt21	32	0	0	2	2
O6-Ni6-Pt20	32	0	0	4	4
O6-Ni7-Pt19	32	0	0	2	2
O6-Ni8-Pt18	32	0	0	1	1
O6-Ni9-Mo2-Pt53	70	0	1	0	1
O6-Ni9-Mo2-Pt54	71	0	2	0	2
O6-Ni9-Mo2-Pt55	72	0	2	0	2
O6-Ni9-Mo2-Pt56	73	0	1	0	1
O6-Ni9-Mo2-Pt57	74	0	1	0	1
O6-Ni10-Mo2-Pt60	78	0	6	0	6
O6-Ni10-Mo2-Pt61	79	0	2	0	2
O6-Ni10-Mo2-Pt62	80	0	2	0	2
O6-Ni10-Mo6-Pt36	58	0	9	13	22
O6-Ni10-Mo14-Pt34	64	0	11	1	12
O6-Ni11-Mo2-Pt12	31	19	0	0	19
O6-Ni13-Mo1-Pt11	31	35	0	0	35
O6-Ni13-Mo2-Pt49	70	0	1	0	1
O6-Ni13-Mo2-Pt51	72	0	1	0	1
O6-Ni13-Mo2-Pt52	73	0	1	0	1
O6-Ni16-Mo2-Pt54	78	0	1	0	1
O6-Ni16-Mo2-Pt55	79	0	2	0	2
O6-Ni16-Mo2-Pt56	80	0	1	0	1
O6-Ni16-Mo2-Pt57	81	0	1	0	1
O6-Ni18-Pt54	78	0	2	0	2
O6-Ni26-Mo4-Pt16	52	0	11	0	11
O6-Ni28-Mo16-Pt14	64	0	14	10	24

O6-Ni28-Mo26-Pt4	64	0	30	16	46
O6-Ni30-Mo18-Pt4	58	0	60	37	97
O7-Pt8	15	0	0	4554	4554
O7-Ni9-Mo2-Pt53	71	0	1	0	1
O7-Ni9-Mo2-Pt54	72	0	3	0	3
O7-Ni9-Mo2-Pt55	73	0	4	0	4
O7-Ni9-Mo2-Pt56	74	0	2	0	2
O7-Ni9-Mo2-Pt57	75	0	2	0	2
O7-Ni9-Mo2-Pt58	76	0	2	0	2
O7-Ni9-Mo2-Pt59	77	0	1	0	1
O7-Ni10-Mo2-Pt60	79	0	1	0	1
O7-Ni10-Mo2-Pt61	80	0	2	0	2
O7-Ni10-Mo2-Pt62	81	0	2	0	2
O7-Ni10-Mo2-Pt63	82	0	3	0	3
O7-Ni13-Mo2-Pt49	71	0	1	0	1
O7-Ni13-Mo2-Pt50	72	0	1	0	1
O7-Ni13-Mo2-Pt51	73	0	1	0	1
O7-Ni13-Mo2-Pt52	74	0	1	0	1
O7-Ni13-Mo2-Pt53	75	0	1	0	1
O7-Ni13-Mo2-Pt54	76	0	1	0	1
O7-Ni16-Mo2-Pt54	79	0	1	0	1
O7-Ni16-Mo2-Pt55	80	0	12	0	12
O7-Ni16-Mo2-Pt56	81	0	1	0	1
O7-Ni16-Mo2-Pt57	82	0	1	0	1
O7-Ni18-Pt54	79	0	1	0	1
O8-Pt6	14	0	19	172	191
O8-Pt8	16	42	5	5704	5751
O8-Pt16	24	26	0	0	26
O8-Mo1-Pt15	24	1	0	0	1
O8-Mo4-Pt12	24	1	0	0	1
O8-Mo7-Pt9	24	1	0	0	1
O8-Mo9-Pt7	24	2	0	0	2
O8-Mo10-Pt6	24	1	0	0	1
O8-Mo13-Pt3	24	2	0	0	2
O8-Mo15-Pt1	24	1	0	0	1
O8-Mo15-Pt8	31	81	0	0	81
O8-Ni1-Mo3-Pt19	31	27	0	0	27
O8-Ni4-Pt12	24	1	0	0	1
O8-Ni4-Mo2-Pt18	32	0	23	9	32
O8-Ni6-Pt26	40	0	1	0	1
O8-Ni6-Mo9-Pt8	31	36	0	0	36

O8-Ni6-Mo10-Pt8	32	0	10	9	19
O8-Ni9-Mo2-Pt55	74	0	1	0	1
O8-Ni9-Mo2-Pt56	75	0	1	0	1
O8-Ni9-Mo2-Pt57	76	0	2	0	2
O8-Ni9-Mo2-Pt58	77	0	2	0	2
O8-Ni9-Mo2-Pt59	78	0	1	0	1
O8-Ni9-Mo2-Pt60	79	0	1	0	1
O8-Ni10-Mo2-Pt60	80	0	7	0	7
O8-Ni10-Mo2-Pt61	81	0	1	0	1
O8-Ni10-Mo2-Pt62	82	0	1	0	1
O8-Ni10-Mo2-Pt63	83	0	1	0	1
O8-Ni12-Pt12	32	0	3	5	8
O8-Ni13-Mo2-Pt49	72	0	1	0	1
O8-Ni13-Mo2-Pt50	73	0	1	0	1
O8-Ni13-Mo2-Pt51	74	0	1	0	1
O8-Ni13-Mo2-Pt53	76	0	11	0	11
O8-Ni13-Mo2-Pt55	78	0	2	0	2
O8-Ni16-Pt16	40	0	1	0	1
O8-Ni16-Mo2-Pt54	80	0	1	0	1
O8-Ni16-Mo2-Pt55	81	0	2	0	2
O8-Ni16-Mo2-Pt56	82	0	1	0	1
O8-Ni16-Mo2-Pt57	83	0	1	0	1
O8-Ni18-Pt54	80	0	1	0	1
O8-Ni18-Mo2-Pt54	82	0	4	59	63
O8-Ni22-Mo10	40	0	1	0	1
O9-Mo15-Pt8	32	0	34	8	42
O9-Ni5-Mo10-Pt8	32	0	21	7	28
O9-Ni9-Mo2-Pt55	75	0	1	0	1
O9-Ni9-Mo2-Pt56	76	0	1	0	1
O9-Ni9-Mo2-Pt57	77	0	8	0	8
O9-Ni9-Mo2-Pt58	78	0	1	0	1
O9-Ni9-Mo2-Pt59	79	0	1	0	1
O9-Ni10-Mo2-Pt62	83	0	5	0	5
O9-Ni13-Mo2-Pt51	75	0	8	0	8
O9-Ni13-Mo2-Pt54	78	0	0	1	1
O9-Ni13-Mo2-Pt55	79	0	1	0	1
O9-Ni16-Mo2-Pt54	81	0	1	0	1
O9-Ni16-Mo2-Pt55	82	0	1	0	1
O9-Ni18-Pt54	81	0	1	0	1
O10-Pt6	16	0	90	139	229
O10-Mo6-Pt15	31	39	0	0	39

O10-Ni3-Mo3-Pt15	31	35	0	0	35
O10-Ni6-Mo2-Pt14	32	0	14	8	22
O10-Ni9-Mo11-Pt2	32	0	17	3	20
O10-Ni13-Mo2-Pt53	78	0	1	0	1
O10-Ni13-Mo2-Pt54	79	0	7	0	7
O11-Mo5-Pt15	31	77	0	0	77
O11-Ni5-Pt15	31	81	0	0	81
O11-Ni6-Mo1-Pt14	32	0	8	3	11
O11-Ni10-Mo4-Pt26	51	28	0	0	28
O11-Ni12-Mo4-Pt24	51	9	0	0	9
O11-Ni15-Mo6-Pt19	51	12	0	0	12
O11-Ni21-Mo9-Pt16	57	0	8	0	8
O12-Mo10-Pt40	62	22	0	0	22
O12-Ni7-Mo6-Pt37	62	34	0	0	34
O12-Ni7-Mo10-Pt33	62	20	0	0	20
O12-Ni20-Mo10-Pt16	58	0	13	0	13
O13-Ni21-Mo9-Pt16	59	0	6	0	6
O14-Pt7	21	0	54	138	192
O14-Ni2-Mo6-Pt36	58	0	15	21	36
O14-Ni14-Mo16-Pt20	64	0	11	5	16
O14-Ni26-Mo4-Pt16	60	0	3	0	3
O15-Ni11-Mo5-Pt31	62	19	0	0	19
O16-Pt16	32	28	0	24	52
O16-Mo6-Pt36	58	0	62	53	115
O16-Mo28-Pt20	64	0	33	7	40
O16-Mo30-Pt18	64	0	24	11	35
O16-Ni10-Mo4-Pt34	64	0	2	2	4
O16-Ni10-Mo14-Pt24	64	0	15	4	19
O16-Ni14-Mo14-Pt20	64	0	41	2	43
O16-Ni18-Mo16-Pt14	64	0	27	8	35
O16-Ni24-Pt24	64	0	22	5	27
O16-Ni24-Mo6-Pt18	64	0	21	10	31
O16-Ni26-Mo4-Pt16	62	0	7	0	7
O16-Ni32-Pt16	64	0	10	5	15
O18-Pt7	25	0	65	116	181
O18-Pt8	26	0	50	86	136
O18-Pt9	27	0	61	100	161
O18-Pt12	30	0	2	133	135
O18-Mo24-Pt22	64	0	31	2	33
O18-Mo28-Pt18	64	0	39	6	45
O18-Mo30-Pt16	64	0	27	3	30

O18-Mo32-Pt14	64	0	77	18	95
O18-Ni6-Pt40	64	0	21	0	21
O18-Ni10-Mo14-Pt22	64	0	17	7	24
O18-Ni14-Mo8-Pt24	64	0	9	0	9
O18-Ni16-Mo16-Pt14	64	0	58	12	70
O18-Ni22-Mo6-Pt18	64	0	16	5	21
O18-Ni26-Mo4-Pt16	64	0	5	0	5
O18-Ni30-Pt16	64	0	18	2	20
O22-Mo14-Pt28	64	0	22	8	30
O22-Mo16-Pt26	64	0	53	7	60
O22-Ni4-Mo4-Pt34	64	0	12	2	14
O22-Ni10-Mo4-Pt28	64	0	23	10	33
O22-Ni12-Mo2-Pt28	64	0	27	3	30
O22-Ni14-Mo2-Pt26	64	0	26	7	33
O32-Pt16	48	33	70	17	120
H1-Pt15	16	0	0	364	364
H1-Pt23	24	0	7	32	39
H1-Pt26	27	0	17	0	17
H1-Pt27	28	0	18	0	18
H1-Ni15	16	0	1	15	16
H1-Ni21	22	0	21	2	23
H1-Ni23	24	0	1	0	1
H1-Ni26	27	0	7	0	7
H1-Ni27	28	0	1	0	1
H1-Ni31	32	0	0	3	3
H2-Pt14	16	0	69	626	695
H2-Pt27	29	0	24	22	46
H2-Pt28	30	0	29	0	29
H2-Ni14	16	0	20	17	37
H2-Ni16	18	0	72	31	103
H2-Ni21	23	0	0	1	1
H2-Ni22	24	0	1	0	1
H2-Ni27	29	0	1	3	4
H2-Ni28	30	0	1	0	1
H2-Ni30	32	1	0	0	1
H2-O1-Ni15	18	0	3	4	7
H3-Pt26	29	0	33	0	33
H3-Ni26	29	0	13	0	13
H4-Pt12	16	2122	0	256	2378
H4-Pt17	21	0	0	170	170
H4-Pt20	24	0	28	0	28

H4-Pt24	28	0	28	0	28
H4-Ni12	16	104	104	12	220
H4-Ni17	21	0	5	4	9
H4-Ni20	24	0	3	0	3
H4-Ni32	36	0	5	0	5
H4-O1-Ni11	16	0	7	14	21
H4-O2-Ni10	16	0	3	8	11
H4-O2-Ni30	36	0	3	2	5
H5-Pt16	21	0	182	38	220
H5-Ni16	21	0	8	0	8
H5-Ni27	32	0	1	0	1
H6-Pt10	16	0	0	360	360
H6-Pt15	21	0	286	5	291
H6-Pt25	31	0	133	0	133
H6-Pt26	32	95	72	106	273
H6-Ni10	16	0	23	14	37
H6-Ni15	21	0	20	0	20
H6-Ni16	22	0	79	24	103
H6-Ni25	31	0	65	37	102
H6-Ni26	32	7	10	11	28
H6-O1-Ni15	22	0	4	0	4
H6-O2-Ni14	22	0	7	0	7
H7-Pt25	32	0	0	117	117
H7-Ni25	32	0	0	5	5
H8-Pt8	16	2986	0	1459	4445
H8-Pt16	24	0	27	21	48
H8-Pt20	28	0	16	0	16
H8-Ni8	16	87	145	63	295
H8-Ni16	24	0	1	0	1
H8-Ni20	28	0	5	1	6
H8-O1-Ni7	16	0	33	10	43
H8-O2-Ni6	16	0	2	0	2
H9-Pt23	32	145	0	0	145
H9-Ni23	32	9	11	0	20
H10-Pt21	31	0	135	0	135
H10-Pt22	32	0	54	206	260
H10-Ni21	31	0	15	9	24
H10-Ni22	32	0	20	9	29
H10-O5-Pt12	27	0	623	13	636
H10-O5-Mo1-Pt11	27	0	6	8	14
H10-O5-Mo2-Pt10	27	0	4	7	11

H10-O5-Ni1-Pt11	27	0	13	9	22
H10-O5-Ni1-Mo1-Pt10	27	0	8	5	13
H10-O5-Ni1-Mo2-Pt9	27	0	7	5	12
H10-O5-Ni1-Mo3-Pt8	27	0	9	11	20
H10-O5-Ni1-Mo4-Pt7	27	0	5	8	13
H10-O5-Ni2-Pt10	27	0	73	47	120
H10-O5-Ni2-Mo1-Pt9	27	0	12	13	25
H10-O5-Ni2-Mo2-Pt8	27	0	96	70	166
H10-O5-Ni2-Mo4-Pt6	27	0	7	7	14
H10-O5-Ni3-Pt9	27	0	7	7	14
H10-O5-Ni3-Mo1-Pt8	27	0	48	18	66
H10-O5-Ni3-Mo2-Pt7	27	0	16	17	33
H10-O5-Ni3-Mo3-Pt6	27	0	21	25	46
H10-O5-Ni4-Pt8	27	0	12	4	16
H10-O5-Ni4-Mo2-Pt6	27	0	8	8	16
H10-O5-Ni5-Mo1-Pt6	27	0	2	3	5
H10-O5-Ni5-Mo3-Pt4	27	0	11	4	15
H10-O5-Ni6-Pt6	27	0	9	3	12
H11-Pt5	16	0	41	1334	1375
H11-Pt21	32	0	0	218	218
H11-Ni5	16	0	36	68	104
H11-Ni17	28	0	22	0	22
H11-Ni21	32	0	0	5	5
H11-O1-Ni4	16	0	12	0	12
H11-O5-Pt12	28	0	258	22	280
H11-O5-Ni1-Pt11	28	0	6	5	11
H11-O5-Ni1-Mo1-Pt10	28	0	3	7	10
H11-O5-Ni1-Mo2-Pt9	28	0	2	1	3
H11-O5-Ni2-Pt10	28	0	15	10	25
H11-O5-Ni2-Mo1-Pt9	28	0	2	3	5
H11-O5-Ni2-Mo2-Pt8	28	0	4	1	5
H11-O5-Ni2-Mo3-Pt7	28	0	4	8	12
H11-O5-Ni3-Pt9	28	0	7	8	15
H11-O5-Ni3-Mo1-Pt8	28	0	19	23	42
H11-O5-Ni4-Mo1-Pt7	28	0	1	0	1
H11-O5-Ni4-Mo2-Pt6	28	0	5	1	6
H12-Pt16	28	0	2	126	128
H12-Ni19	31	0	15	20	35
H12-Ni32	44	0	8	0	8
H12-O5-Pt12	29	0	267	32	299
H12-O5-Ni1-Mo1-Pt10	29	0	23	18	41

H12-O5-Ni1-Mo2-Pt9	29	0	7	6	13
H12-O5-Ni2-Pt10	29	0	7	3	10
H12-O5-Ni2-Mo1-Pt9	29	0	42	34	76
H12-O5-Ni2-Mo2-Pt8	29	0	9	6	15
H12-O5-Ni3-Mo2-Pt7	29	0	45	64	109
H13-Pt19	32	0	0	53	53
H13-Ni16	29	0	109	79	188
H13-Ni19	32	0	0	1	1
H13-O1-Ni15	29	0	6	8	14
H13-O2-Ni14	29	0	1	7	8
H13-O5-Pt12	30	0	244	8	252
H13-O5-Mo2-Pt10	30	0	9	10	19
H13-O5-Ni1-Pt11	30	0	8	2	10
H13-O5-Ni1-Mo1-Pt10	30	0	6	1	7
H13-O5-Ni1-Mo2-Pt9	30	0	3	10	13
H13-O5-Ni2-Mo1-Pt9	30	0	18	9	27
H13-O5-Ni3-Mo1-Pt8	30	0	5	6	11
H13-O5-Ni4-Mo1-Pt7	30	0	18	17	35
H13-O5-Ni4-Mo2-Pt6	30	0	5	6	11
H14-Pt16	30	0	1	53	54
H14-Pt17	31	0	0	165	165
H14-Pt18	32	0	0	138	138
H14-Ni16	30	0	0	3	3
H14-Ni17	31	0	0	4	4
H14-Ni18	32	0	0	1	1
H14-O7	21	0	1	756	757
H15-Pt6	21	0	650	0	650
H15-Pt16	31	0	1	254	255
H15-Pt17	32	0	0	257	257
H15-Ni6	21	0	18	8	26
H15-Ni16	31	0	7	5	12
H15-Ni17	32	0	1	14	15
H15-O1-Ni5	21	0	10	0	10
H16-Pt5	21	0	950	58	1008
H16-Pt16	32	0	1	507	508
H16-Ni5	21	0	38	29	67
H16-Ni16	32	0	9	18	27
H16-O8	24	0	14	3911	3925
H17-Pt15	32	0	0	140	140
H17-Ni15	32	0	0	4	4
H18-Pt13	31	0	0	80	80

H18-Ni13	31	0	0	1	1
H19-Pt13	32	0	0	64	64
H19-Ni12	31	0	44	9	53
H19-Ni13	32	0	7	1	8
H19-Ni21	40	0	8	11	19
H19-O1-Ni11	31	0	2	10	12
H23-Pt8	31	0	255	85	340
H23-Pt9	32	0	233	132	365
H23-Ni8	31	0	13	4	17
H23-Ni9	32	0	11	18	29
H23-O1-Ni8	32	0	5	0	5
H23-O11-Pt16	50	0	145	1855	2000
H23-O11-Mo1-Pt15	50	0	18	55	73
H23-O11-Mo3-Pt13	50	0	5	22	27
H23-O11-Ni1-Pt15	50	0	2	19	21
H23-O11-Ni1-Mo1-Pt14	50	0	2	6	8
H23-O11-Ni1-Mo2-Pt13	50	0	11	29	40
H23-O11-Ni1-Mo3-Pt12	50	0	5	16	21
H23-O11-Ni1-Mo4-Pt11	50	0	2	15	17
H23-O11-Ni1-Mo5-Pt10	50	0	7	19	26
H23-O11-Ni2-Pt14	50	0	11	47	58
H23-O11-Ni2-Mo1-Pt13	50	0	11	35	46
H23-O11-Ni2-Mo2-Pt12	50	0	13	63	76
H23-O11-Ni2-Mo3-Pt11	50	0	3	24	27
H23-O11-Ni2-Mo4-Pt10	50	0	7	20	27
H23-O11-Ni3-Pt13	50	0	9	41	50
H23-O11-Ni3-Mo1-Pt12	50	0	10	49	59
H23-O11-Ni3-Mo2-Pt11	50	0	6	25	31
H23-O11-Ni3-Mo3-Pt10	50	0	37	111	148
H23-O11-Ni3-Mo4-Pt9	50	0	3	10	13
H23-O11-Ni3-Mo5-Pt8	50	0	6	20	26
H23-O11-Ni4-Pt12	50	0	7	29	36
H23-O11-Ni4-Mo1-Pt11	50	0	14	77	91
H23-O11-Ni4-Mo2-Pt10	50	0	10	33	43
H23-O11-Ni4-Mo3-Pt9	50	0	10	51	61
H23-O11-Ni4-Mo4-Pt8	50	0	3	21	24
H23-O11-Ni5-Pt11	50	0	3	12	15
H23-O11-Ni5-Mo1-Pt10	50	0	9	26	35
H23-O11-Ni5-Mo2-Pt9	50	0	30	63	93
H23-O11-Ni5-Mo3-Pt8	50	0	3	11	14
H23-O11-Ni5-Mo4-Pt7	50	0	1	2	3

H23-O11-Ni6-Mo1-Pt9	50	0	2	4	6
H23-O11-Ni6-Mo2-Pt8	50	0	21	104	125
H23-O11-Ni6-Mo3-Pt7	50	0	2	19	21
H23-O11-Ni7-Mo2-Pt7	50	0	1	7	8
H24-Pt8	32	0	62	113	175
H24-Ni8	32	0	0	1	1
H24-O11-Pt16	51	0	83	923	1006
H24-O11-Mo1-Pt15	51	0	2	18	20
H24-O11-Mo2-Pt14	51	0	1	3	4
H24-O11-Ni1-Mo1-Pt14	51	0	2	9	11
H24-O11-Ni1-Mo3-Pt12	51	0	3	17	20
H24-O11-Ni2-Pt14	51	0	1	4	5
H24-O11-Ni2-Mo1-Pt13	51	0	9	40	49
H24-O11-Ni2-Mo2-Pt12	51	0	25	113	138
H24-O11-Ni2-Mo3-Pt11	51	0	0	14	14
H24-O11-Ni2-Mo4-Pt10	51	0	2	17	19
H24-O11-Ni2-Mo5-Pt9	51	0	0	25	25
H24-O11-Ni3-Pt13	51	0	2	16	18
H24-O11-Ni3-Mo1-Pt12	51	0	5	35	40
H24-O11-Ni3-Mo2-Pt11	51	0	8	40	48
H24-O11-Ni3-Mo3-Pt10	51	0	1	11	12
H24-O11-Ni3-Mo4-Pt9	51	0	0	11	11
H24-O11-Ni4-Pt12	51	0	1	8	9
H24-O11-Ni4-Mo1-Pt11	51	0	3	5	8
H24-O11-Ni4-Mo2-Pt10	51	0	5	18	23
H24-O11-Ni4-Mo3-Pt9	51	0	2	3	5
H24-O11-Ni5-Pt11	51	0	1	6	7
H24-O11-Ni5-Mo2-Pt9	51	0	6	12	18
H24-O11-Ni6-Mo1-Pt9	51	0	10	59	69
H25-O11-Pt16	52	0	52	746	798
H25-O11-Mo1-Pt15	52	0	0	4	4
H25-O11-Mo2-Pt14	52	0	3	13	16
H25-O11-Ni1-Pt15	52	0	3	9	12
H25-O11-Ni1-Mo2-Pt13	52	0	2	9	11
H25-O11-Ni1-Mo3-Pt12	52	0	2	20	22
H25-O11-Ni1-Mo4-Pt11	52	0	0	5	5
H25-O11-Ni2-Pt14	52	0	0	4	4
H25-O11-Ni2-Mo1-Pt13	52	0	6	27	33
H25-O11-Ni2-Mo2-Pt12	52	0	1	20	21
H25-O11-Ni2-Mo3-Pt11	52	0	4	23	27
H25-O11-Ni3-Pt13	52	0	1	11	12

H25-O11-Ni3-Mo1-Pt12	52	0	6	15	21
H25-O11-Ni3-Mo2-Pt11	52	0	2	26	28
H25-O11-Ni3-Mo3-Pt10	52	0	3	13	16
H25-O11-Ni3-Mo4-Pt9	52	0	2	5	7
H25-O11-Ni3-Mo5-Pt8	52	0	0	5	5
H25-O11-Ni4-Pt12	52	0	2	7	9
H25-O11-Ni4-Mo1-Pt11	52	0	9	87	96
H25-O11-Ni4-Mo2-Pt10	52	0	4	20	24
H25-O11-Ni4-Mo3-Pt9	52	0	17	69	86
H25-O11-Ni6-Pt10	52	0	0	10	10
H25-O11-Ni6-Mo1-Pt9	52	0	2	6	8
H27-O23-Ni18-Mo2-Pt54	124	0	6	74	80
H28-O22-Ni18-Mo2-Pt54	124	0	11	76	87
H30-O15	45	124	4	94	222
H32-O19-Ni18-Pt54	123	0	11	42	53
H42-O25-Pt72	139	0	0	26	26
H43-O25-Pt72	140	0	0	73	73
H43-O31-Ni18-Mo2-Pt54	148	0	0	1	1
H45-O22-Pt32	99	0	350	0	350
H45-O22-Ni3-Mo5-Pt24	99	0	1	8	9
H45-O22-Ni4-Mo2-Pt26	99	0	2	4	6
H45-O22-Ni4-Mo3-Pt25	99	0	1	1	2
H45-O22-Ni4-Mo4-Pt24	99	0	1	0	1
H45-O22-Ni4-Mo6-Pt22	99	0	7	5	12
H45-O22-Ni6-Mo4-Pt22	99	0	2	2	4
H45-O22-Ni7-Mo3-Pt22	99	0	1	0	1
H45-O22-Ni7-Mo6-Pt19	99	0	0	3	3
H45-O22-Ni8-Mo4-Pt20	99	0	1	3	4
H45-O22-Ni9-Pt23	99	0	1	2	3
H45-O22-Ni9-Mo4-Pt19	99	0	1	3	4
H45-O22-Ni11-Mo4-Pt17	99	0	1	0	1
H48-O24-Pt24	96	0	14	104	118
H48-O24-Ni2-Mo2-Pt20	96	0	0	1	1
H48-O24-Ni3-Mo6-Pt15	96	0	1	3	4
H48-O24-Ni4-Mo4-Pt16	96	0	0	2	2
H48-O24-Ni5-Mo1-Pt18	96	0	0	2	2
H48-O24-Ni5-Mo2-Pt17	96	0	0	1	1
H48-O24-Ni6-Mo1-Pt17	96	0	0	1	1
H48-O24-Ni6-Mo2-Pt16	96	0	2	1	3
H52-O22-Pt32	106	0	765	0	765
H52-O22-Ni1-Mo6-Pt25	106	0	0	6	6

H52-O22-Ni2-Mo2-Pt28	106	0	1	3	4
H52-O22-Ni2-Mo3-Pt27	106	0	3	1	4
H52-O22-Ni2-Mo5-Pt25	106	0	1	0	1
H52-O22-Ni2-Mo6-Pt24	106	0	4	5	9
H52-O22-Ni3-Pt29	106	0	0	1	1
H52-O22-Ni3-Mo3-Pt26	106	0	1	5	6
H52-O22-Ni3-Mo4-Pt25	106	0	16	21	37
H52-O22-Ni3-Mo5-Pt24	106	0	3	2	5
H52-O22-Ni3-Mo6-Pt23	106	0	1	3	4
H52-O22-Ni3-Mo10-Pt19	106	0	1	1	2
H52-O22-Ni4-Mo1-Pt27	106	0	1	0	1
H52-O22-Ni4-Mo3-Pt25	106	0	1	0	1
H52-O22-Ni4-Mo4-Pt24	106	0	2	6	8
H52-O22-Ni4-Mo5-Pt23	106	0	2	15	17
H52-O22-Ni4-Mo6-Pt22	106	0	2	9	11
H52-O22-Ni4-Mo10-Pt18	106	0	2	12	14
H52-O22-Ni5-Mo1-Pt26	106	0	4	14	18
H52-O22-Ni5-Mo2-Pt25	106	0	2	5	7
H52-O22-Ni5-Mo3-Pt24	106	0	2	22	24
H52-O22-Ni5-Mo4-Pt23	106	0	1	2	3
H52-O22-Ni5-Mo5-Pt22	106	0	2	6	8
H52-O22-Ni5-Mo6-Pt21	106	0	1	5	6
H52-O22-Ni5-Mo7-Pt20	106	0	2	2	4
H52-O22-Ni6-Mo1-Pt25	106	0	1	4	5
H52-O22-Ni6-Mo3-Pt23	106	0	10	26	36
H52-O22-Ni6-Mo4-Pt22	106	0	3	7	10
H52-O22-Ni6-Mo5-Pt21	106	0	1	2	3
H52-O22-Ni6-Mo6-Pt20	106	0	5	26	31
H52-O22-Ni7-Mo2-Pt23	106	0	3	9	12
H52-O22-Ni7-Mo3-Pt22	106	0	1	2	3
H52-O22-Ni7-Mo5-Pt20	106	0	1	2	3
H52-O22-Ni8-Mo1-Pt23	106	0	1	5	6
H52-O22-Ni8-Mo2-Pt22	106	0	1	2	3
H52-O22-Ni8-Mo3-Pt21	106	0	1	2	3
H52-O22-Ni8-Mo4-Pt20	106	0	1	4	5
H52-O22-Ni8-Mo5-Pt19	106	0	3	4	7
H52-O22-Ni9-Mo2-Pt21	106	0	2	0	2
H52-O22-Ni9-Mo3-Pt20	106	0	4	5	9
H52-O22-Ni9-Mo5-Pt18	106	0	3	11	14
H52-O22-Ni10-Mo1-Pt21	106	0	3	3	6
H52-O22-Ni10-Mo6-Pt16	106	0	2	3	5

H52-O22-Ni11-Mo4-Pt17	106	0	1	0	1
H58-O32-Ni18-Pt54	162	0	0	8	8
H58-O37-Ni18-Mo2-Pt54	169	0	1	3	4
H58-O39-Ni18-Mo2-Pt54	171	0	0	4	4
H59-O32-Ni18-Pt54	163	0	1	1	2
H59-O39-Ni18-Mo2-Pt54	172	0	0	25	25
H64-O35-Ni18-Pt54	171	0	0	2	2
H67-O32-Pt48	147	0	0	2	2
H70-O32-Pt48	150	0	0	11	11
H78-O32-Pt48	158	0	1	70	71
H78-O32-Ni5-Mo3-Pt40	158	0	0	2	2
H78-O32-Ni6-Mo1-Pt41	158	0	3	16	19
H78-O32-Ni8-Mo3-Pt37	158	0	0	2	2
H78-O32-Ni11-Mo5-Pt32	158	0	0	1	1
H78-O32-Ni14-Mo4-Pt30	158	0	0	1	1
H80-O32-Pt48	160	0	0	72	72
H80-O32-Ni5-Mo7-Pt36	160	0	0	4	4
H80-O32-Ni6-Mo7-Pt35	160	0	0	1	1
H84-O50-Pt62	196	0	0	51	51
H84-O50-Pt64	198	0	0	56	56
H84-O50-Ni10-Mo8-Pt44	196	0	0	1	1
H84-O50-Ni10-Mo8-Pt46	198	0	1	16	17
H84-O50-Ni11-Mo8-Pt45	198	0	0	4	4
H84-O50-Ni16-Mo11-Pt35	196	0	0	3	3
H98-O44-Pt64	206	0	127	0	127
H98-O44-Ni6-Mo6-Pt52	206	0	1	1	2
H98-O44-Ni8-Mo11-Pt45	206	0	1	1	2
H98-O44-Ni9-Mo6-Pt49	206	0	1	0	1
H98-O44-Ni10-Mo6-Pt48	206	0	4	0	4
H98-O44-Ni10-Mo8-Pt46	206	0	1	0	1
H98-O44-Ni11-Mo4-Pt49	206	0	1	0	1
H98-O44-Ni12-Mo12-Pt40	206	0	1	0	1
H98-O44-Ni13-Mo1-Pt50	206	0	1	0	1
H98-O44-Ni14-Mo7-Pt43	206	0	1	0	1
total	--	10471	14400	64379	89250

1.2 Benchmark of G-NN potential against DFT calculations

To benchmark the accuracy of G-NN potential, we compare NN energies with DFT results for 83 selected PtNiMo bulk structures. The RMSE of the energy difference is 2.227 meV/atom, accurate enough for searching stable structures. The details for energies between NN and DFT

results are given in Table S2.

Table S2. Benchmark of G-NN potential.

Composition	E_{DFT} (eV)	E_{NN} (eV)	E_{diff} (meV/atom)
$Pt_{19}Ni_{13}Mo_{16}$	-375.26	-375.38	2.43
$Pt_{19}Ni_{11}Mo_{18}$	-383.46	-383.21	-5.03
$Pt_{19}Ni_{5}Mo_{24}$	-417.93	-417.97	0.80
$Pt_{19}Ni_{15}Mo_{14}$	-363.32	-363.29	-0.75
$Pt_{19}Ni_{9}Mo_{20}$	-391.71	-391.62	-1.81
$Pt_{19}Ni_{3}Mo_{26}$	-428.38	-428.32	-1.31
$Pt_{19}Ni_{0}Mo_{29}$	-444.10	-443.99	-2.31
$Pt_{19}Ni_{1}Mo_{28}$	-438.83	-438.72	-2.39
$Pt_{19}Ni_{7}Mo_{22}$	-406.72	-406.57	-3.05
$Pt_{19}Ni_{17}Mo_{12}$	-352.90	-352.81	-1.81
$Pt_{19}Ni_{19}Mo_{10}$	-341.20	-341.17	-0.66
$Pt_{19}Ni_{21}Mo_{8}$	-341.20	-341.17	-0.66
$Pt_{19}Ni_{22}Mo_{7}$	-323.20	-323.04	-3.23
$Pt_{19}Ni_{20}Mo_{9}$	-335.08	-334.96	-2.64
$Pt_{18}Ni_{22}Mo_{8}$	-328.33	-328.26	-1.46
$Pt_{18}Ni_{20}Mo_{10}$	-340.35	-340.29	-1.31
$Pt_{20}Ni_{20}Mo_{8}$	-329.62	-329.56	-1.12
$Pt_{20}Ni_{19}Mo_{9}$	-334.86	-335.06	4.12
$Pt_{19}Ni_{23}Mo_{6}$	-317.03	-317.02	-0.12
$Pt_{19}Ni_{25}Mo_{4}$	-304.86	-304.92	1.22
$Pt_{19}Ni_{27}Mo_{2}$	-292.84	-292.88	0.88
$Pt_{19}Ni_{29}Mo_{0}$	-280.61	-280.56	-1.12
$Pt_{24}Ni_{1}Mo_{23}$	-417.63	-417.67	0.73
$Pt_{24}Ni_{8}Mo_{16}$	-379.24	-379.22	-0.47
$Pt_{24}Ni_{2}Mo_{22}$	-411.84	-411.75	-1.96
$Pt_{24}Ni_{0}Mo_{24}$	-422.49	-422.40	-1.87
$Pt_{24}Ni_{9}Mo_{15}$	-373.23	-373.15	-1.50
$Pt_{24}Ni_{10}Mo_{14}$	-367.44	-367.41	-0.56
$Pt_{24}Ni_{5}Mo_{19}$	-395.36	-395.38	0.49
$Pt_{24}Ni_{7}Mo_{17}$	-383.44	-383.47	0.64
$Pt_{24}Ni_{3}Mo_{21}$	-406.43	-406.29	-2.91
$Pt_{24}Ni_{4}Mo_{20}$	-400.42	-400.40	-0.39
$Pt_{24}Ni_{6}Mo_{18}$	-389.48	-389.35	-2.84
$Pt_{24}Ni_{11}Mo_{13}$	-361.14	-361.03	-2.29
$Pt_{24}Ni_{12}Mo_{12}$	-355.46	-355.43	-0.75
$Pt_{24}Ni_{13}Mo_{11}$	-349.31	-349.26	-1.17
$Pt_{24}Ni_{14}Mo_{10}$	-343.84	-343.72	-2.38

$Pt_{24}Ni_{15}Mo_9$	-338.31	-338.19	-2.60
$Pt_{24}Ni_{16}Mo_8$	-332.00	-332.15	3.02
$Pt_{24}Ni_{17}Mo_7$	-325.97	-326.12	3.23
$Pt_{24}Ni_{18}Mo_6$	-320.17	-320.05	-2.46
$Pt_{24}Ni_{19}Mo_5$	-313.89	-313.84	-0.97
$Pt_{24}Ni_{20}Mo_4$	-308.02	-307.98	-0.99
$Pt_{24}Ni_{21}Mo_3$	-301.80	-301.79	-0.16
$Pt_{24}Ni_{22}Mo_2$	-295.76	-295.78	0.43
$Pt_{24}Ni_{23}Mo_1$	-289.39	-289.37	-0.54
$Pt_{24}Ni_{24}Mo_0$	-283.46	-283.35	-2.24
$Pt_{36}Ni_{12}Mo_0$	-287.83	-287.84	0.26
$Pt_{36}Ni_{11}Mo_1$	-294.86	-294.85	-0.40
$Pt_{36}Ni_{10}Mo_2$	-300.86	-300.89	0.55
$Pt_{36}Ni_9Mo_3$	-307.30	-307.35	1.11
$Pt_{36}Ni_8Mo_4$	-313.88	-313.78	-2.12
$Pt_{36}Ni_7Mo_5$	-320.46	-320.51	1.20
$Pt_{36}Ni_6Mo_6$	-326.72	-326.67	-1.10
$Pt_{36}Ni_5Mo_7$	-332.79	-332.93	2.91
$Pt_{36}Ni_4Mo_8$	-339.15	-339.17	0.40
$Pt_{36}Ni_3Mo_9$	-345.04	-344.96	-1.67
$Pt_{36}Ni_2Mo_{10}$	-351.15	-351.14	-0.26
$Pt_{36}Ni_1Mo_{11}$	-357.54	-357.41	-2.70
$Pt_{36}Ni_0Mo_{12}$	-363.85	-363.80	-1.08
$Pt_{12}Ni_{36}Mo_0$	-276.68	-276.67	-0.20
$Pt_{12}Ni_{32}Mo_4$	-300.07	-299.79	-5.80
$Pt_{12}Ni_{28}Mo_8$	-323.62	-323.55	-1.47
$Pt_{12}Ni_{24}Mo_{12}$	-345.61	-345.62	0.36
$Pt_{12}Ni_{20}Mo_{16}$	-368.73	-368.81	1.59
$Pt_{12}Ni_{16}Mo_{20}$	-388.25	-388.18	-1.42
$Pt_{12}Ni_{12}Mo_{24}$	-410.18	-410.16	-0.39
$Pt_{12}Ni_8Mo_{28}$	-429.99	-429.92	-1.39
$Pt_{12}Ni_4Mo_{32}$	-450.27	-450.36	1.74
$Pt_{12}Ni_0Mo_{36}$	-472.72	-472.87	3.16
$Pt_{42}Ni_6Mo_0$	-289.26	-289.40	3.08
$Pt_{42}Ni_5Mo_1$	-296.08	-296.31	4.74
$Pt_{42}Ni_4Mo_2$	-302.84	-302.81	-0.70
$Pt_{42}Ni_0Mo_6$	-328.89	-328.88	-0.16
$Pt_{48}Ni_0Mo_0$	-290.97	-290.90	-1.44
$Pt_6Ni_{42}Mo_0$	-271.99	-271.92	-1.33
$Pt_6Ni_{36}Mo_6$	-306.84	-306.87	0.61
$Pt_6Ni_{30}Mo_{12}$	-341.45	-341.06	-8.27

$Pt_6Ni_{24}Mo_{18}$	-371.76	-371.61	-3.16
$Pt_6Ni_{12}Mo_{30}$	-433.28	-433.14	-3.04
$Pt_6Ni_6Mo_{36}$	-466.06	-465.88	-3.69
$Pt_6Ni_0Mo_{42}$	-499.03	-498.95	-1.64
$Pt_0Ni_{48}Mo_0$	-267.56	-267.57	0.26
$Pt_0Ni_0Mo_{48}$	-525.60	-525.72	2.41

Table S3. Benchmark for the DFT setups of Monkhorst-Pack k mesh and plane-wave-basis set cutoff energy

composition	**25times-450eV**	**30times-500eV**	**E_{diff} (eV)**
$Pt_{19}Ni_{11}Mo_{18}$	-383.46	-383.46	0.00
$Pt_{19}Ni_5Mo_{24}$	-417.93	-417.91	0.02
$Pt_{19}Ni_{15}Mo_{14}$	-363.32	-363.29	0.03
$Pt_{19}Ni_9Mo_{20}$	-391.71	-391.72	0.00
$Pt_{19}Ni_3Mo_{26}$	-428.38	-428.38	0.00
$Pt_{19}Ni_1Mo_{28}$	-438.83	-438.84	-0.01
$Pt_{19}Ni_{17}Mo_{12}$	-352.90	-352.92	-0.02
$Pt_{19}Ni_{20}Mo_9$	-335.08	-335.07	0.01
$Pt_{19}Ni_{25}Mo_4$	-304.86	-304.87	-0.01
$Pt_{24}Ni_1Mo_{23}$	-417.63	-417.63	0.00
$Pt_{24}Ni_8Mo_{16}$	-379.24	-379.24	0.01
$Pt_{24}Ni_2Mo_{22}$	-411.84	-411.84	0.00
$Pt_{24}Ni_9Mo_{15}$	-373.23	-373.24	-0.01
$Pt_{24}Ni_{10}Mo_{14}$	-367.44	-367.45	-0.01
$Pt_{24}Ni_5Mo_{19}$	-395.36	-395.39	-0.03
$Pt_{24}Ni_7Mo_{17}$	-383.44	-383.45	-0.01
$Pt_{24}Ni_3Mo_{21}$	-406.43	-406.44	-0.01
$Pt_{24}Ni_6Mo_{18}$	-389.48	-389.52	-0.03
$Pt_{24}Ni_{11}Mo_{13}$	-361.14	-361.15	0.00
$Pt_{24}Ni_{12}Mo_{12}$	-355.46	-355.46	0.01
$Pt_{24}Ni_{15}Mo_9$	-338.31	-338.35	-0.03
$Pt_{24}Ni_{16}Mo_8$	-332.00	-332.02	-0.02
$Pt_{24}Ni_{18}Mo_6$	-320.17	-320.20	-0.03
$Pt_{24}Ni_{19}Mo_5$	-313.89	-313.88	0.01
$Pt_{24}Ni_{22}Mo_2$	-295.76	-295.79	-0.03

$Pt_{36}Ni_{11}Mo_1$	-294.86	-294.88	-0.02
$Pt_{36}Ni_{10}Mo_2$	-300.86	-300.88	-0.02
$Pt_{36}Ni_4Mo_8$	-339.15	-339.12	0.03
$Pt_{36}Ni_3Mo_9$	-345.04	-345.02	0.02
$Pt_{36}Ni_2Mo_{10}$	-351.15	-351.14	0.01
$Pt_{12}Ni_{32}Mo_4$	-300.07	-300.06	0.01
$Pt_{12}Ni_{28}Mo_8$	-323.62	-323.63	-0.01
$Pt_{12}Ni_{24}Mo_{12}$	-345.61	-345.60	0.01
$Pt_{12}Ni_{20}Mo_{16}$	-368.73	-368.76	-0.02
$Pt_{12}Ni_8Mo_{28}$	-429.99	-430.01	-0.02
$Pt_6Ni_{36}Mo_6$	-306.84	-306.80	0.03
$Pt_6Ni_{30}Mo_{12}$	-341.45	-341.47	-0.02
$Pt_6Ni_{24}Mo_{18}$	-371.76	-371.80	-0.03
$Pt_6Ni_{12}Mo_{30}$	-433.28	-433.29	-0.01
$Pt_{19}Ni_{11}Mo_{18}$	-383.46	-383.46	0.00
$Pt_{19}Ni_5Mo_{24}$	-417.93	-417.91	0.02
$Pt_{19}Ni_{15}Mo_{14}$	-363.32	-363.29	0.03
$Pt_{19}Ni_9Mo_{20}$	-391.71	-391.72	0.00
$Pt_{19}Ni_3Mo_{26}$	-428.38	-428.38	0.00
$Pt_{19}Ni_1Mo_{28}$	-438.83	-438.84	-0.01
$Pt_{19}Ni_{17}Mo_{12}$	-352.90	-352.92	-0.02
$Pt_{19}Ni_{20}Mo_9$	-335.08	-335.07	0.01
$Pt_{19}Ni_{25}Mo_4$	-304.86	-304.87	-0.01
$Pt_{24}Ni_1Mo_{23}$	-417.63	-417.63	0.00
$Pt_{24}Ni_8Mo_{16}$	-379.24	-379.24	0.01
$Pt_{24}Ni_2Mo_{22}$	-411.84	-411.84	0.00
$Pt_{24}Ni_9Mo_{15}$	-373.23	-373.24	-0.01
$Pt_{24}Ni_{10}Mo_{14}$	-367.44	-367.45	-0.01
$Pt_{24}Ni_5Mo_{19}$	-395.36	-395.39	-0.03
$Pt_{24}Ni_7Mo_{17}$	-383.44	-383.45	-0.01
$Pt_{24}Ni_3Mo_{21}$	-406.43	-406.44	-0.01
$Pt_{24}Ni_6Mo_{18}$	-389.48	-389.52	-0.03
$Pt_{24}Ni_{11}Mo_{13}$	-361.14	-361.15	0.00
$Pt_{24}Ni_{12}Mo_{12}$	-355.46	-355.46	0.01
$Pt_{24}Ni_{15}Mo_9$	-338.31	-338.35	-0.03

$Pt_{24}Ni_{16}Mo_8$	-332.00	-332.02	-0.02
$Pt_{24}Ni_{18}Mo_6$	-320.17	-320.20	-0.03
$Pt_{24}Ni_{19}Mo_5$	-313.89	-313.88	0.01
$Pt_{24}Ni_{22}Mo_2$	-295.76	-295.79	-0.03
$Pt_{36}Ni_{11}Mo_1$	-294.86	-294.88	-0.02
$Pt_{36}Ni_{10}Mo_2$	-300.86	-300.88	-0.02
$Pt_{36}Ni_4Mo_8$	-339.15	-339.12	0.03
$Pt_{36}Ni_3Mo_9$	-345.04	-345.02	0.02
$Pt_{36}Ni_2Mo_{10}$	-351.15	-351.14	0.01

1.3 Calculation Details of GCMC/SSW-NN method

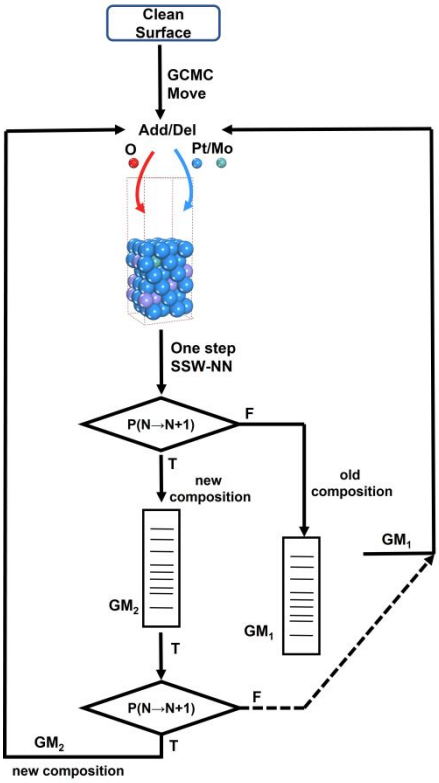

Scheme S3. Overall procedure of the GCMC/SSW-NN method.

Upper limit of surface Mo coverage in GCMC/SSW-NN simulations

The upper limit of surface Mo coverage during GCMC/SSW-NN simulations is restricted to below 0.2 monolayer (ML). This is because, in practice, the amount of surface Mo is limited, which is determined by the size of nanoparticle. In experiment, the size of PtNiMo nanoparticle is typical around 4.1 nm[6]. In this case, Wulff construction shows that the upper limit of surface Mo coverage is 0.2 ML. The details are described as follows.

Wulff construction states that a particle reaches the lowest surface free energy when its shape satisfies the criterion that the surface energy (γ_i) of a given face is proportional to the distance h_i

from the center of the polyhedron to that surface, as shown in Eq. 10-11.

$$\gamma_i/h_i = constant\#(10.)$$

$$\gamma_i = [E_{slab} - N * E_{bulk}]/2A\#(11.)$$

Here we set $\gamma_{(111)}$ = 1.41 J/m^2 and $\gamma_{(100)}$ = 1.61 J/m^2, respectively. According to Wulff construction, the equilibrium shape of PtNiMo is cuboctahedral, which exposes eight {111} and six {100} (see Figure 1)[6-7]. The particle size is defined by the distance between (111) and $(\bar{1}\bar{1}\bar{1})$, which is denoted as $d_{(111)}$. We set the $d_{(111)}$ to 4.1 nm, and obtain the side length of (100) surface is 3 nm and its area is 9 nm^2 for each face. The side length of (111) is 3.1 nm and its area is 25.73 nm^2 (see Figure S1b). Altogether, the total area of six (100) surfaces and eight (111) surfaces is 259.83 nm^2, and the volume of PtNiMo particle is 322.67 nm^3. The total number of atoms is 22019. According to the ratio of the surface area to volume, it indicates that the number of surface atoms is 1774, and the total number of Mo (at 1.6% Mo content) in the particle is 353. Thus, the upper limit of surface Mo is 353/1774 = 0.20 ML.

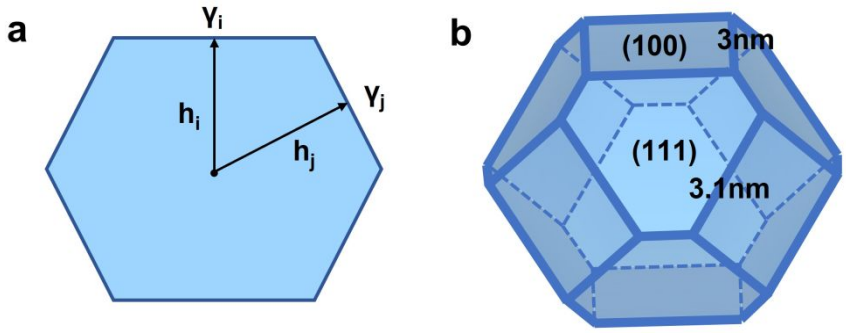

Figure S1. (a) Illustration of the Wulff construction. (b) Wulff shape of PtNiMo nanoparticles with $d_{(111)}$ = 4.1 nm.

Chemical potentials for Mo

To calculate the chemical potential of Mo, we calculated all forms that can appear in nature, either neutral metal atoms in bulk phase or free ions in the electrolyte from experiments.

(i) Neutral Mo metal atoms in bulk PtNiMo alloy

$$PtNi - nMo \rightarrow PtNi - (n-1)Mo + [Mo]\#(12)$$

where $[Mo]$ represents an atom in the reservoir. In this case, the chemical potential of Mo is then defined as

$$\mu_{Mo'} = G(PtNi - nMo) - G[PtNi - (n-1)Mo] = -13.23eV\#(13)$$

(ii) Mo^{3+} cation in electrolyte

$$Mo^{3+} + 3e^- \rightarrow [Mo]\#(14)$$

where $[Mo]$ represents an atom in the reservoir. The chemical potential of Mo is defined as

$$\mu_{Mo''} = \mu_{Mo^{3+}} + 3\mu_{e^-}\#(15)$$

$\mu_{Mo^{3+}}$ is the electrochemical potential of Mo^{3+}, μ_{e^-} is the electrochemical potential of electron. $\mu_{Mo^{3+}}$ can be derived by the redox reaction on the Mo^{3+}/Mo electrode:

$$Mo^{3+} + 3e^- \rightarrow Mo\#(16)$$

At the standard electrode potential ($E^0_{Mo^{3+}/Mo}$) and standard conditions, the redox reaction is in equilibrium, and thereby

$$\Delta G = G^0_{Mo} - \mu^0_{Mo^{3+}} - 3\mu_{e^-_{Mo^{3+}/Mo}} = 0\#(17)$$

$$\mu^0_{Mo^{3+}} = G^0_{Mo} - 3\mu_{e^-_{Mo^{3+}/Mo}}\#(18)$$

where $\mu^0_{Mo^{3+}}$ is the electrochemical potential of Mo^{3+} at standard conditions (c^0 = 1 M), $\mu_{e^-_{Mo^{3+}/Mo}}$ is the electrochemical potential of electron in the Mo^{3+}/Mo electrode. For Mo^{3+} with other concentrations (c), we get

$$\mu_{Mo^{3+}} = \mu^0_{Mo^{3+}} - 3\mu_{e^-_{Mo^{3+}/Mo}} + k_B T ln(c/c^0)\#(19)$$

The concentration of Mo is set as $c = 10^{-4}$ mol/L. Substituting Eq. 19 into Eq. 15, we get

$$\mu_{Mo''} = \mu_{Mo^{3+}} + 3\mu_{e^-} = G^0_{Mo} - 3\mu_{e^-_{Mo^{3+}/Mo}} + k_B T ln(c/c^0) + 3\mu_{e^-} \quad (20)$$

Reformulate Eq. (22), we get

$$\begin{aligned}\mu_{Mo''} &= G^0_{Mo} - 3\mu_{e^-_{Mo^{3+}/Mo}} + k_B T ln(c/c^0) + 3\mu_{e^-} \\ &= G^0_{Mo} + 3\left(\mu^{SHE}_{e^-} - \mu_{e^-_{Mo^{3+}/Mo}}\right) + k_B T ln(c/c^0) - 3(\mu^{SHE}_{e^-} - \mu_{e^-})\end{aligned} \quad (21)$$

where $\mu^{SHE}_{e^-}$ is the electrochemical potential of electron in SHE. Since the electrode potential U is defined as

$$U = \frac{\left(\mu^{SHE}_{e^-} - \mu_{e^-}\right)}{e} \quad (22)$$

Where U is the electrode potential vs. SHE, while e is the element charge. Substituting Eq. 22 into Eq. 23, we get

$$\begin{aligned}\mu_{Mo''} &= G^0_{Mo} + 3\left(\mu^{SHE}_{e^-} - \mu_{e^-_{Mo^{3+}/Mo}}\right) + k_B T ln(c/c^0) - 3\left(\mu^{SHE}_{e^-} - \mu_{e^-}\right) \\ &= G^0_{Mo} + 3E^0_{Mo^{3+}/Mo} + k_B T ln(c/c^0) - 3eU\#\end{aligned} \quad (23)$$

At U = 0.9 V, the $\mu_{Mo''}$ is calculated to be

$$\mu_{Mo''} = -14.49\ \text{eV} \quad (24)$$

(iii) H_2MoO_4(aq) in the electrolyte

$$H_2MoO_4(aq) + 6H^+ + 6e^- \rightarrow [Mo] + 4H_2O\#(25)$$

where $[Mo]$ represents an atom in the reservoir. The chemical potential of Mo is defined as

$$\mu_{Mo'''} = G_{H_2MoO_4} + 6\mu_{H^+} + 6\mu_{e^-} - 4G_{H_2O}\#(26)$$

μ_{H^+} is the electrochemical potential of H^+(aq). $G_{H_2MoO_4}$ can be derived by the redox reaction on the H_2MoO_4/Mo electrode:

$$H_2MoO_4(aq) + 6H^+ + 6e^- \rightarrow \text{Mo} + 4H_2O\#(27)$$

At the standard electrode potential ($E^0_{H_2MoO_4/Mo}$) and standard conditions, the above redox reaction is in equilibrium, and thereby

$$\mu^0_{H_2MoO_4} = G^0_{Mo} + 4G^0_{H_2O} - 6\mu^0_{H^+} - 6\mu_{e^-_{H_2MoO_4/Mo}}\# \quad (28)$$

Substituting Eq. 28 into Eq. 26, we get

$$\begin{aligned}\mu_{Mo'''} &= G_{H_2MoO_4} + 6\mu_{H^+} + 6\mu_{e^-} - 4G_{H_20} \\ &= G^0_{Mo} + 4G^0_{H_2O} - 6\mu^0_{H^+} - 6\mu_{e^-_{H_2MoO_4/Mo}} + k_B T ln(c/c^0) + 6\mu^0_{H^+} + 6\mu_{e^-} - 4G^0_{H_2O}\# \\ &= G^0_{Mo} - 6\mu_{e^-_{H_2MoO_4/Mo}} + k_B T ln(c/c^0) + 6\mu_{e^-} \\ &= G^0_{Mo} + 6\left(\mu^{SHE}_{e^-} - \mu_{e^-_{H_2MoO_4/Mo}}\right) + k_B T ln(c/c^0) - 6\left(\mu^{SHE}_{e^-} - \mu_{e^-}\right) \\ &= G^0_{Mo} + 6E^0_{H_2MoO_4/Mo} + k_B T ln(c/c^0) - 6eU\end{aligned} \quad (29)$$

The concentration of H_2MoO_4 is set as c = 10^{-4} mol/L. The $\mu_{Mo'''}$ is calculated to be

$$\mu_{Mo'''} = -15.93eV \quad (30)$$

The final μ_{Mo} is then the maximum of $\mu_{Mo'}$,$\mu_{Mo''}$, and $\mu_{Mo'''}$

$$\mu_{Mo} = max\{\mu_{Mo'},\mu_{Mo''},\mu_{Mo'''}\} = -13.23eV\#(31)$$

Table S4. Chemical potentials of Mo derived from Eq. 13 with different Mo contents

Mo%	Reactions	μ_{Mo} (eV)
2.08%	$Pt_{36}Ni_{11}Mo_1 \rightarrow Pt_{36}Ni_{11}+[Mo]$	-13.23
1.39%	$Pt_{54}Ni_{17}Mo_1 \rightarrow Pt_{54}Ni_{17}+[Mo]$	-13.30
0.55%	$Pt_{135}Ni_{44}Mo_1 \rightarrow Pt_{135}Ni_{44}+[Mo]$	-13.38

Chemical potential for Pt

$$nPt - Ni \rightarrow (n-1)Pt - Ni + [Pt] \#(32)$$

$$\mu_{Pt} = G(nPt - Ni) - G[(n-1)Pt - Ni] = -6.21eV \#(33)$$

Chemical potential for O

$$H_2O \rightarrow 2H^+ + 2e^- + [O] \#(34)$$

$$\mu_O = G^0_{H_2O} - 2\mu^0_{H^+} - 2\mu_{e^-} \#(35)$$

For the Standard Hydrogen Electrode (SHE: $H^+ + e^- \rightarrow 1/2\ H_2$, pH = 0, p = 1bar, T = 298.15 K) as reference, where we get

$$\Delta G = \frac{1}{2}G^0_{H_2} - 2\mu^0_{H^+} - \mu^{SHE}_{e^-} = 0 \#(36)$$

μ_{H^+} can be estimated as

$$\mu^0_{H^+} = \frac{1}{2}G^0(H_2) - \mu^{SHE}_{e^-} \#(37)$$

Substituting Eq. 37 into Eq. 35, we get

$$\begin{aligned} \mu_O &= G^0_{H_2O} - 2\mu^0_{H^+} - 2\mu_{e^-} \# \\ &= G^0_{H_2O} - 2\left(\frac{1}{2}G^0(H_2) - \mu^{SHE}_{e^-}\right) - 2\mu_{e^-} \\ &= G^0_{H_2O} - G^0(H_2) + 2(\mu^{SHE}_{e^-} - \mu_{e^-}) \\ &= G^0_{H_2O} - G^0(H_2) + 2eU = -5.62\ eV \end{aligned} \quad (38)$$

The [Pt], [Mo], and [O] represent an atom in the reservoir, G(nPt-Ni), G[(n-1)Pt-Ni], G(PtNi-nMo), and G[PtNi-(n-1)Mo] are energies of GM for the corresponding bulk phase determined by SSW-NN. In Eq. 13, we use two PtNiMo bulks with of $Pt_{54}Ni_{18}$ for nPt-Ni and $Pt_{53}Ni_{18}$ for (n-1)Pt-Ni. G(Pt) and G(Mo) are the Gibbs free energy of pure Pt and Mo metals. $E^0_{Mo3+/Mo}$, and $E^0_{H2MoO4/Mo}$ are standard electrode potentials from experiments[8-9]. The concentration of ions (Eq. 19, 20, 21, 23, and 29) are set as c = 10^{-4} mol/L.

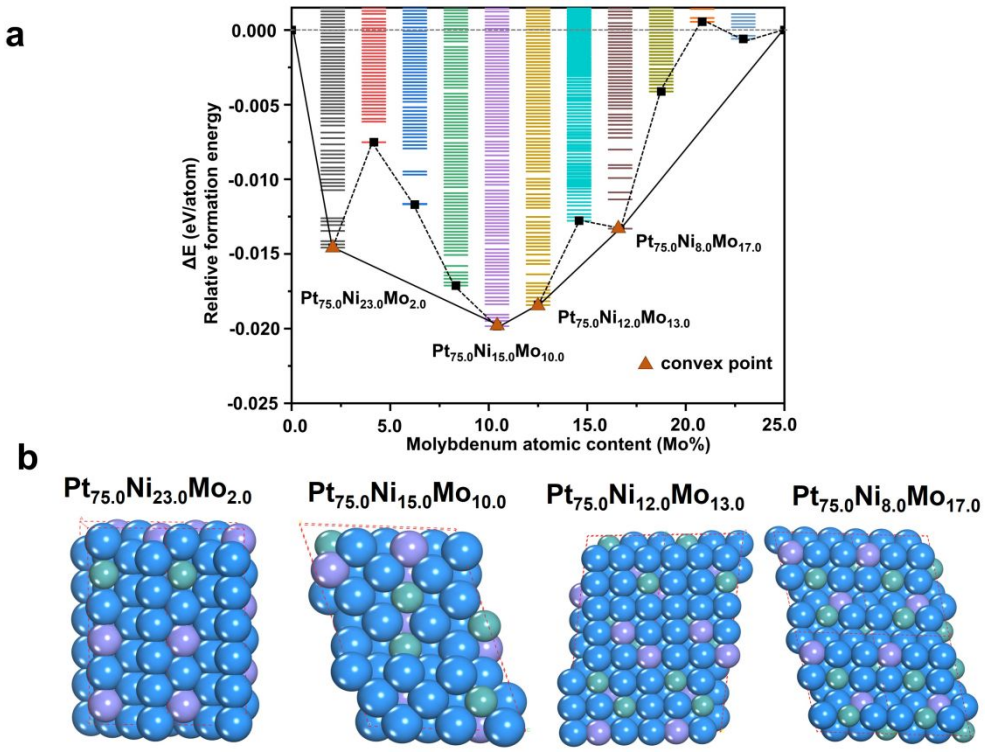

Figure S2. (a) Thermodynamic convex hull diagram of $Pt_{75.0}Ni_{25.0-x}Mo_x$; (b) GM structures of the convex points. Blue balls are Pt; violet balls are Ni; cyan balls are Mo.

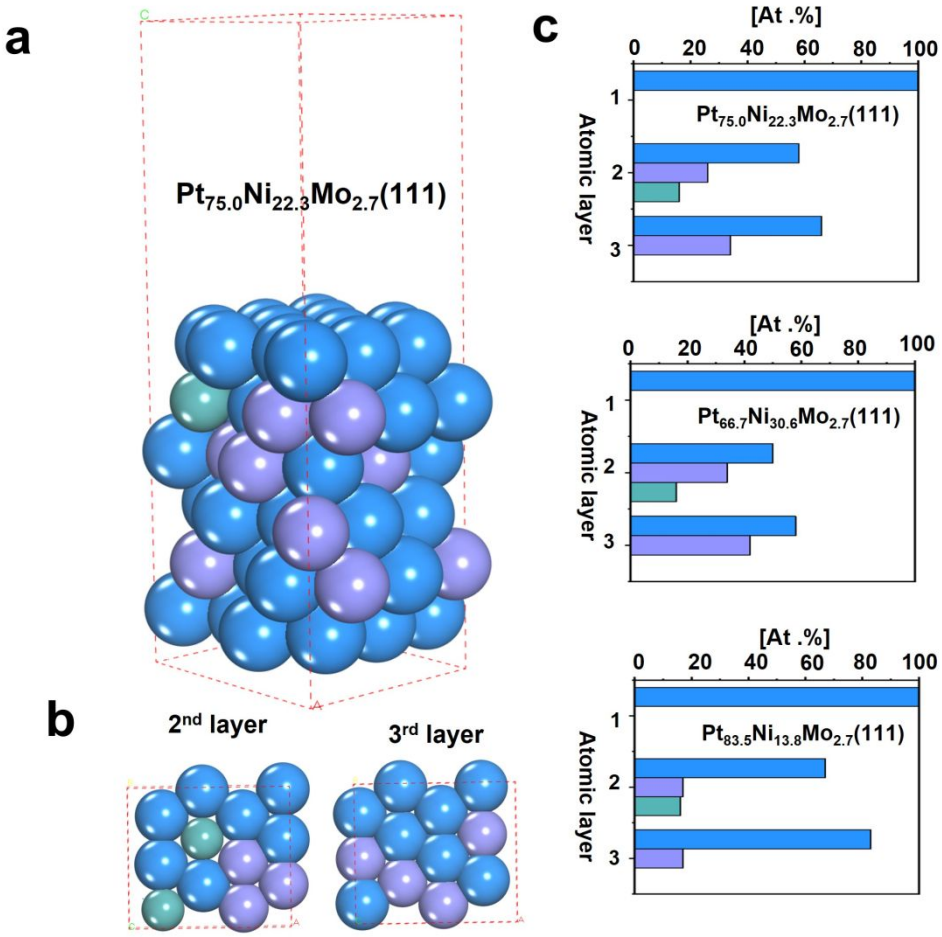

Figure S3. (a) Sideview of GM structure for the $Pt_{75.0}Ni_{22.3}Mo_{2.7}(111)$; (b) Cross section for the 1st and 2nd atomic layer of $Pt_{75.0}Ni_{22.3}Mo_{2.7}(111)$. (c) Atomic contents for the first three surface layers of $Pt_{75.0}Ni_{22.3}Mo_{2.7}(111)$, $Pt_{66.7}Ni_{30.6}Mo_{2.7}(111)$, and $Pt_{83.5}Ni_{13.8}Mo_{2.7}(111)$.

2. GCMC/SSW-NN trajectory of $Pt_{75.0}Ni_{25.0}$ surface

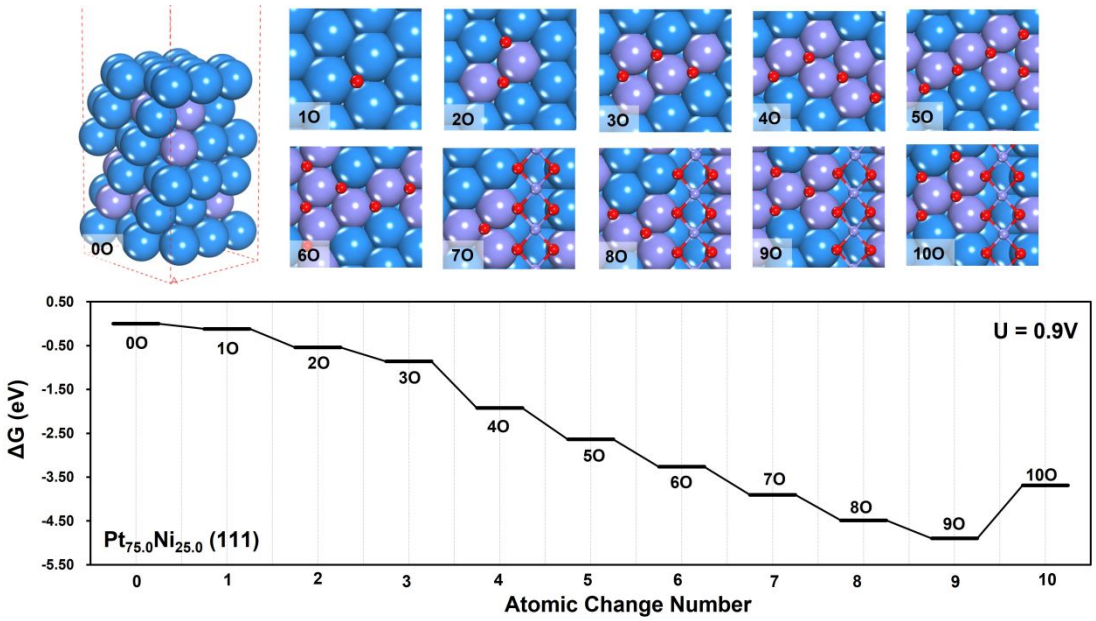

Figure S4. Structures and energetic profiles for the intermediate states and the evolution of $Pt_{75.0}Ni_{25.0}$ (111) at 0.9V vs. RHE. Each state is named as nO + mPt, where n and m represent the number of O and Pt atoms that are added in the unit cell at the current GCMC step. The atoms above the surface plane are depicted in the ball-and-stick style, while other atoms are depicted in the CPK style. Colors in figure: Blue balls are Pt; Violet balls are Ni; Cyan balls are Mo; Red balls are O.

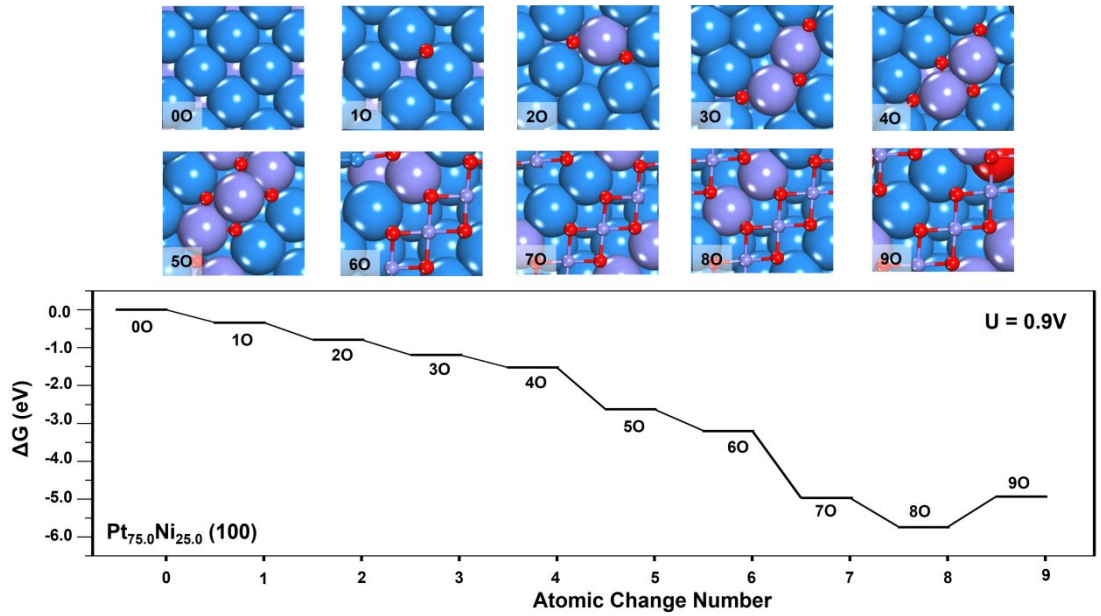

Figure S5. Structures and energetic profiles for the intermediate states and the evolution of $Pt_{75.0}Ni_{25.0}$ (100) at 0.9V vs. RHE. Each state is named as nO + mPt, where n and m represent the number of O and Pt atoms that are added in the unit cell at the current GCMC step. The atoms above the surface plane are depicted in the ball-and-stick style, while other atoms are depicted in the CPK style. Colors in figure: Blue balls are Pt; Violet balls are Ni; Cyan balls are Mo; Red balls are O.

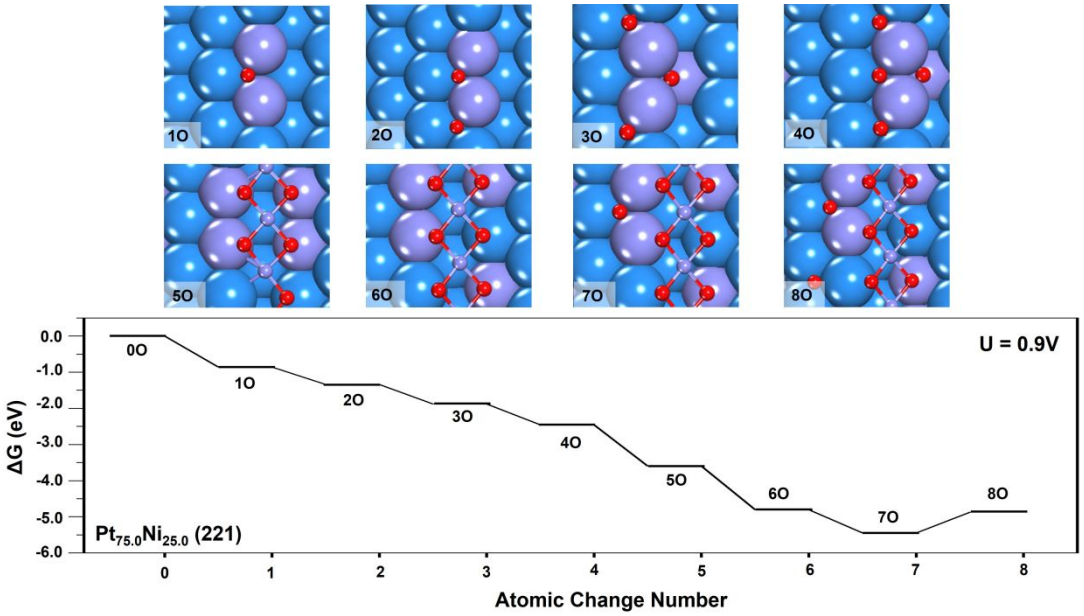

Figure S6. Structures and energetic profiles for the intermediate states and the evolution of $Pt_{75.0}Ni_{25.0}$ (221) at 0.9V vs. RHE. Each state is named as nO + mPt, where n and m represent the number of O and Pt atoms that are added in the unit cell at the current GCMC step. The atoms above the surface plane are depicted in the ball-and-stick style, while other atoms are depicted in the CPK style. Colors in figure: Blue balls are Pt; Violet balls are Ni; Cyan balls are Mo; Red balls are O.

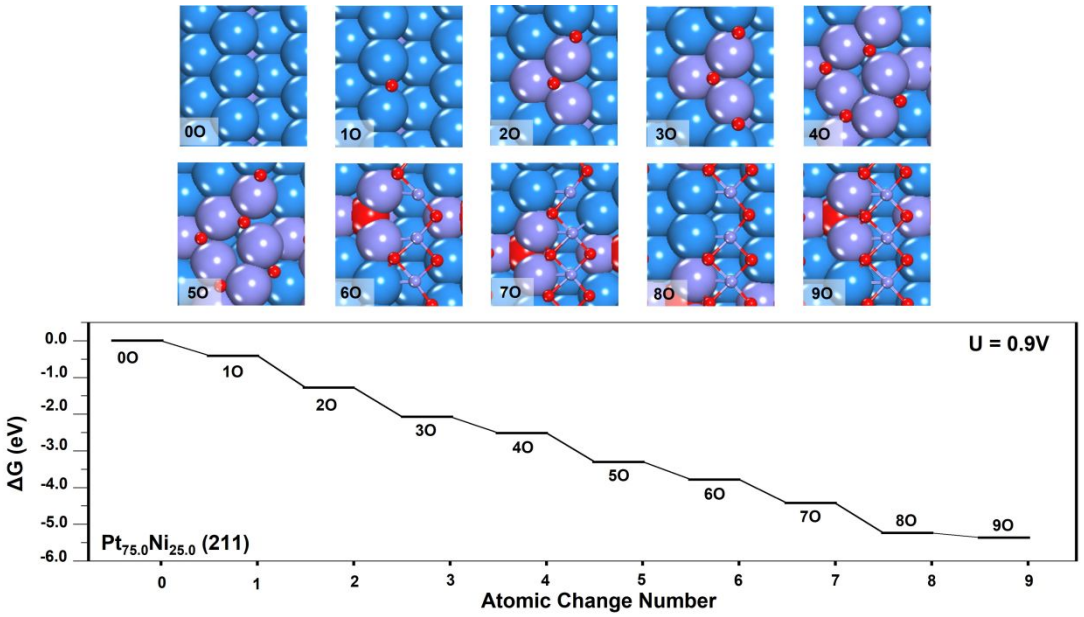

Figure S7. Structures and energetic profiles for the intermediate states and the evolution of $Pt_{75.0}Ni_{25.0}$ (211) at 0.9V vs. RHE. Each state is named as nO + mPt, where n and m represent the number of O and Pt atoms that are added in the unit cell at the current GCMC step. The atoms above the surface plane are depicted in the ball-and-stick style, while other atoms are depicted in the CPK style. Colors in figure: Blue balls are Pt; Violet balls are Ni; Cyan balls are Mo; Red balls are O.

3. GCMC/SSW-NN trajectories of PtNiMo Surfaces

Due to the importance of the surface $^{*}MoO_4$, it is intriguing to investigate the formation mechanism of $^{*}MoO_4$. To this end, we take a close look at the GCMC/SSW-NN trajectory of the $Pt_{75.0}Ni_{22.3}Mo_{2.7}$ (111) surface at $0.9V_{RHE}$, as shown in Figure S8. The bare surface (*0O state) contains two Mo atoms at the subsurface in each unit cell. Then, one O atom attaches on the surface, whilst one Mo atom migrates on the surface, forming a metal-oxo complex, *Mo=O (*1O state). Next, the second terminal *Mo=O group forms by adding another O on the surface (*2O state). Then, the third O atom is added on the surface, which links two Mo=O groups to a $^{*}Mo^{\#}O_2$-O-Mo moiety (*3O state). The superscript "#" indicates that this Mo atom leaches out from the lattice site, leaving a lattice vacancy beneath the $Mo^{\#}$ atom. The fourth O attaches on the leached $Mo^{\#}$ atom to form a $Mo^{\#}O_3$-O-Mo moiety (*4O state). Meanwhile, the lattice vacancy moves from the surface to the third layer of the slab. Subsequently, a Pt atom is added to this system to heal this lattice vacancy (4O+1Pt state). The fifth O atom is added to the $^{*}Mo^{\#}O_3$-O-Mo moiety to form a $^{*}Mo^{\#}O_2$-O-$^{*}Mo^{\#}O_2$ group (5O+1Pt state). In this state, the remaining lattice Mo leaches out of the surface, while the lattice vacancy site locates at the second atomic layer of the slab. The sixth O atom attaches to the surface to form a $^{*}Mo^{\#}O_3$-O-$^{*}Mo^{\#}O_2$ group. The seventh O attaches on the surface to further form a $^{*}Mo^{\#}O_3$-O-$^{*}Mo^{\#}O_3$ group. Then, the second Pt atom is added to the system to fill the lattice vacancy at the second atomic layer. Finally, the eighth O is added on the $^{*}Mo^{\#}O_3$-O-$^{*}Mo^{\#}O_3$ moiety to form two tetrahedral-coordinated $^{*}Mo^{\#}O_4$ groups, and further addition of O atoms to the 9O+2Pt state is endothermal.

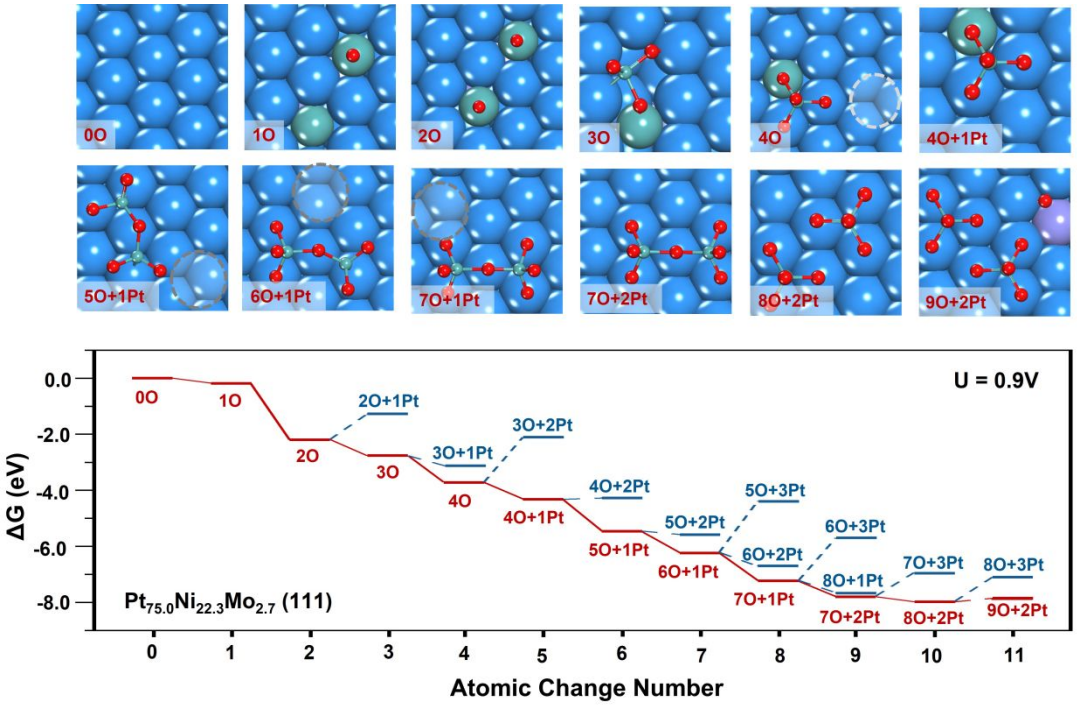

Figure S8. Structures and energetic profiles for the intermediate states and the evolution of $Pt_{75.0}Ni_{22.3}Mo_{2.7}$ (111) at 0.9V vs. RHE. Each state is named as nO + mPt, where n and m represent the number of O and Pt atoms that are added in the unit cell at the current GCMC step. The atoms above the surface plane are depicted in the ball-and-stick style, while other atoms are depicted in the CPK style. Colors in figure: Blue balls are Pt; Violet balls are Ni; Cyan balls are Mo; Red balls are O.

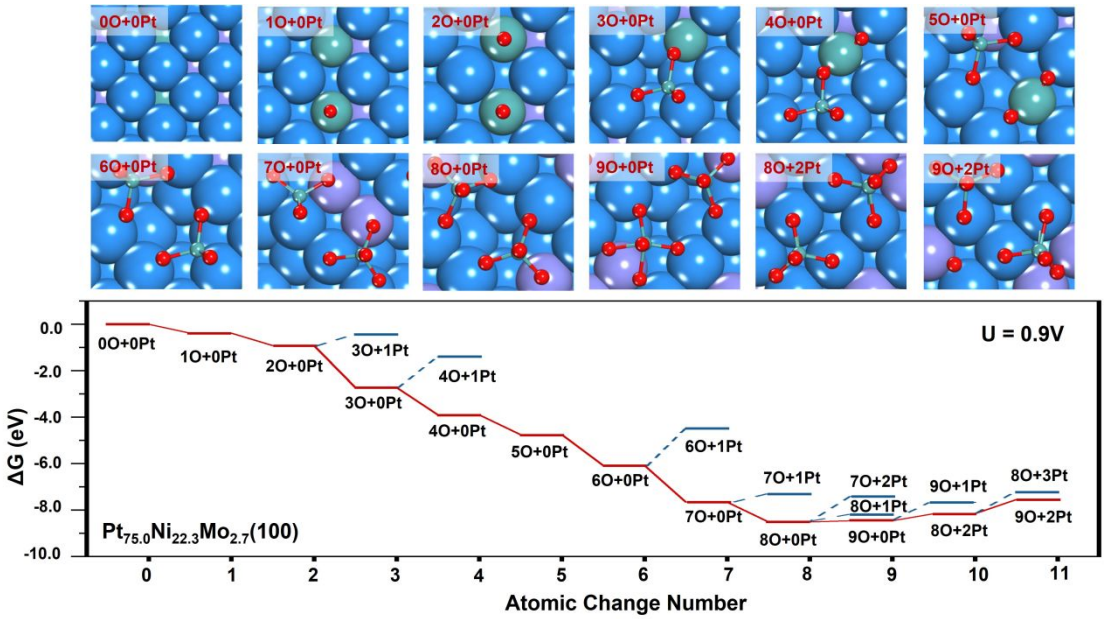

Figure S9. Structures and energetic profiles for the intermediate states and the evolution of $Pt_{75.0}Ni_{22.3}Mo_{2.7}$ (100) at 0.9V vs. RHE. Each state is named as nO + mPt, where n and m represent the number of O and Pt atoms that are added in the unit cell at the current GCMC step. The atoms above the surface plane are depicted in the ball-and-stick style, while other atoms are depicted in the CPK style. Colors in figure: Blue balls are Pt; Violet balls are Ni; Cyan balls are Mo; Red balls are O.

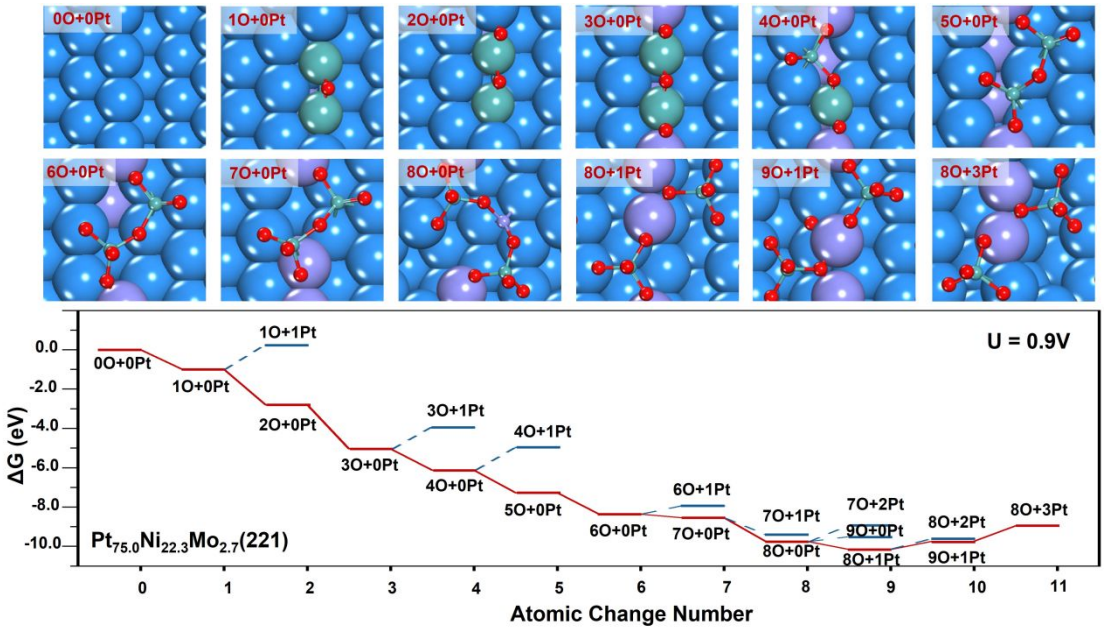

Figure S10. Structures and energetic profiles for the intermediate states and the evolution of $Pt_{75.0}Ni_{22.3}Mo_{2.7}$ (221) at 0.9V vs. RHE. Each state is named as nO + mPt, where n and m represent the number of O and Pt atoms that are added in the unit cell at the current GCMC step. The atoms above the surface plane are depicted in the ball-and-stick style, while other atoms are depicted in the CPK style. Colors in figure: Blue balls are Pt; Violet balls are Ni; Cyan balls are Mo; Red balls are O.

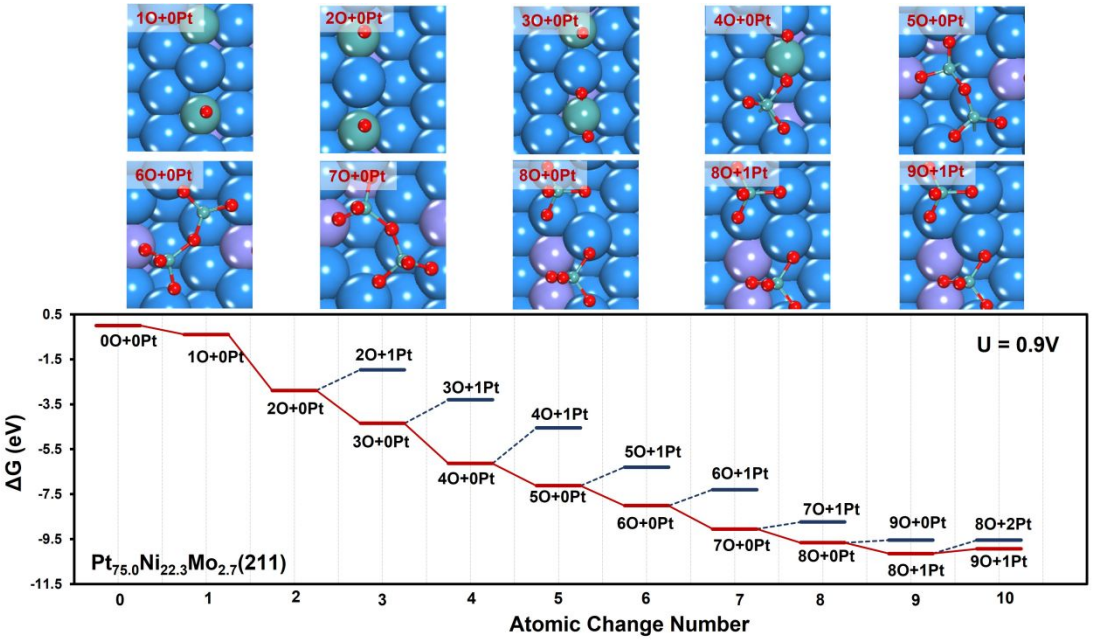

Figure S11. Structures and energetic profiles for the intermediate states and the evolution of $Pt_{75.0}Ni_{22.3}Mo_{2.7}$ (211) at 0.9V vs. RHE. Each state is named as nO + mPt, where n and m represent the number of O and Pt atoms that are added in the unit cell at the current GCMC step. The atoms above the surface plane are depicted in the ball-and-stick style, while other atoms are depicted in the CPK style. Colors in figure: Blue balls are Pt; Violet balls are Ni; Cyan balls are Mo; Red balls are O.

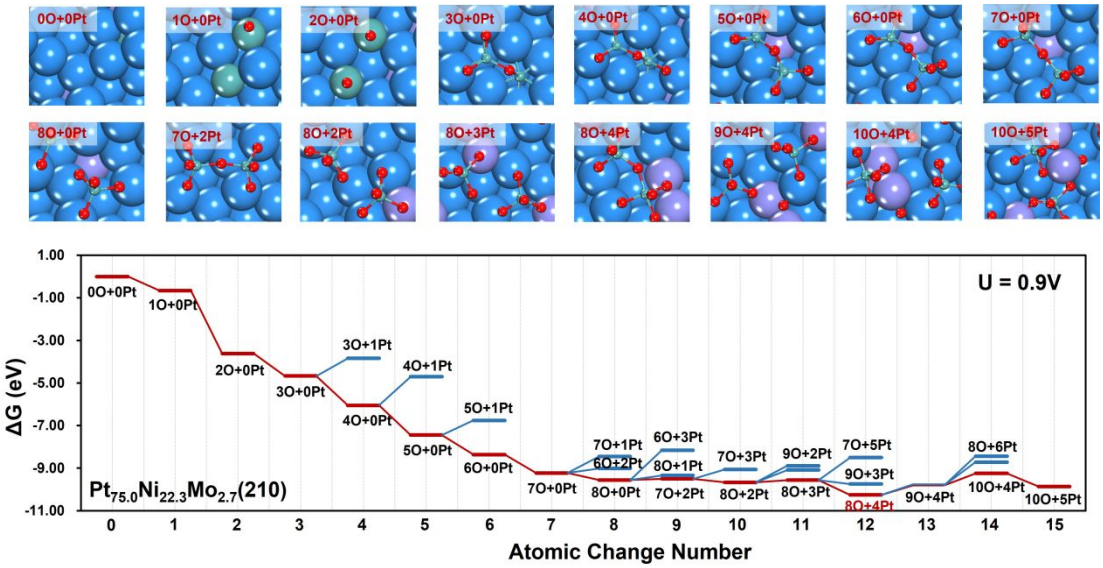

Figure S12. Structures and energetic profiles for the intermediate states and the evolution of $Pt_{75.0}Ni_{22.3}Mo_{2.7}$ (210) at 0.9V vs. RHE. Each state is named as nO + mPt, where n and m represent the number of O and Pt atoms that are added in the unit cell at the current GCMC step. The atoms above the surface plane are depicted in the ball-and-stick style, while other atoms are depicted in the CPK style. Colors in figure: Blue balls are Pt; Violet balls are Ni; Cyan balls are Mo; Red balls are O.

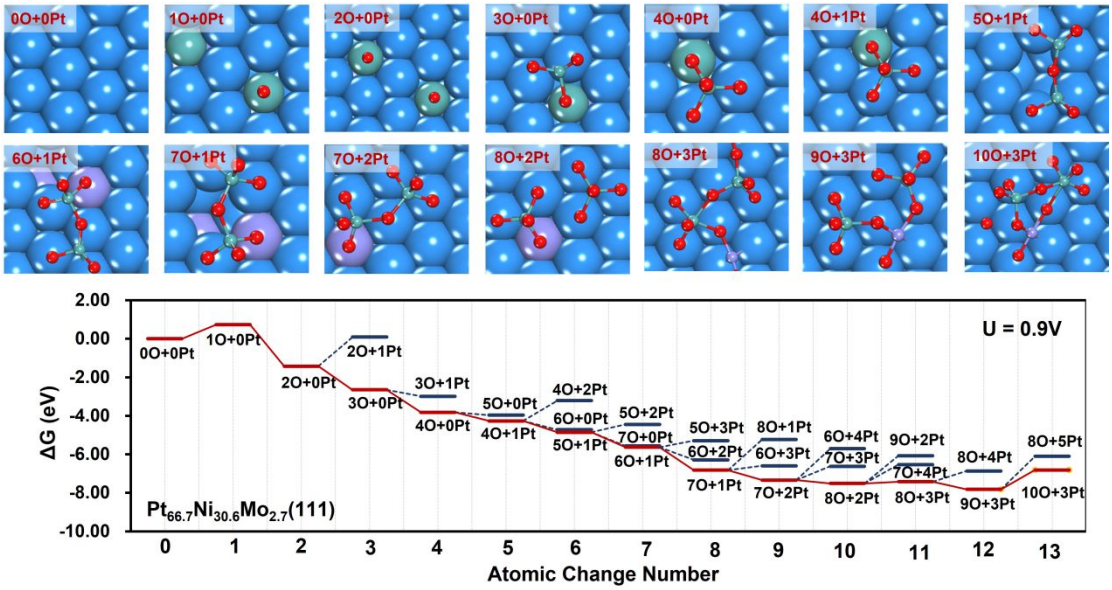

Figure S13. Structures and energetic profiles for the intermediate states and the evolution of $Pt_{66.7}Ni_{30.6}Mo_{2.7}$ (111) at 0.9V vs. RHE. Each state is named as nO + mPt, where n and m represent the number of O and Pt atoms that are added in the unit cell at the current GCMC step. The atoms above the surface plane are depicted in the ball-and-stick style, while other atoms are depicted in the CPK style. Colors in figure: Blue balls are Pt; Violet balls are Ni; Cyan balls are Mo; Red balls are O.

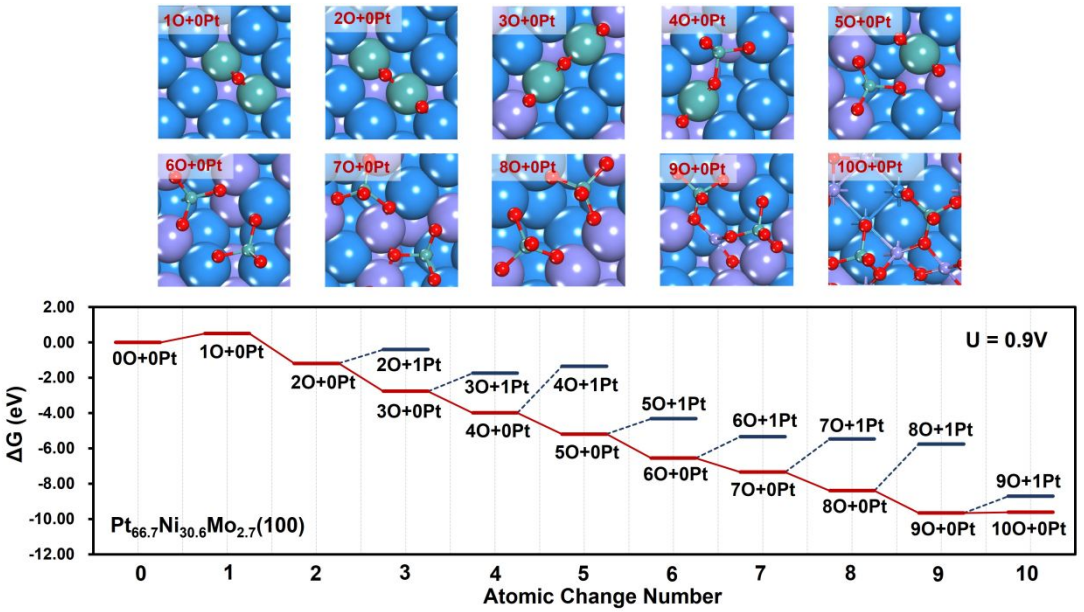

Figure S14. Structures and energetic profiles for the intermediate states and the evolution of $Pt_{66.7}Ni_{30.6}Mo_{2.7}$ (100) at 0.9V vs. RHE. Each state is named as nO + mPt, where n and m represent the number of O and Pt atoms that are added in the unit cell at the current GCMC step. The atoms above the surface plane are depicted in the ball-and-stick style, while other atoms are depicted in the CPK style. Colors in figure: Blue balls are Pt; Violet balls are Ni; Cyan balls are Mo; Red balls are O.

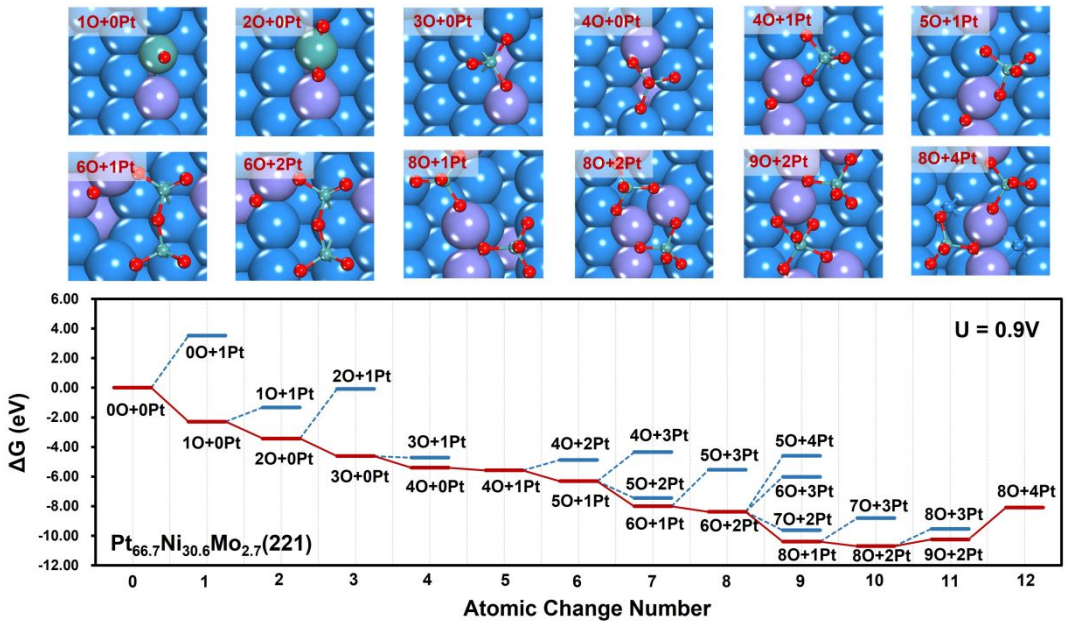

Figure S15. Structures and energetic profiles for the intermediate states and the evolution of $Pt_{66.7}Ni_{30.6}Mo_{2.7}$ (221) at 0.9V vs. RHE. Each state is named as nO + mPt, where n and m represent the number of O and Pt atoms that are added in the unit cell at the current GCMC step. The atoms above the surface plane are depicted in the ball-and-stick style, while other atoms are depicted in the CPK style. Colors in figure: Blue balls are Pt; Violet balls are Ni; Cyan balls are Mo; Red balls are O.

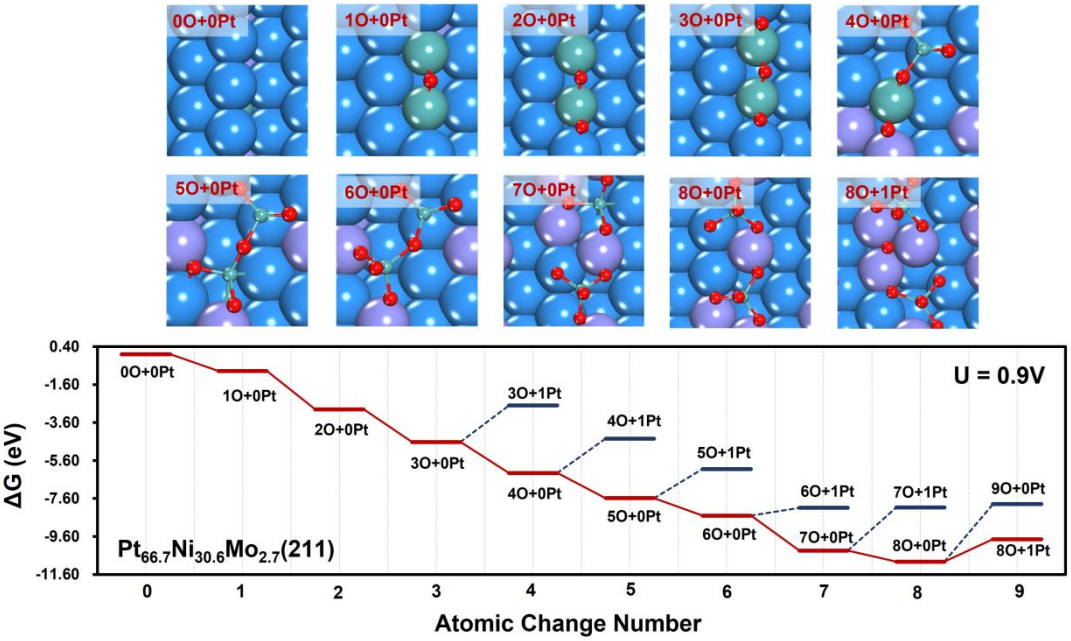

Figure S16. Structures and energetic profiles for the intermediate states and the evolution of $Pt_{66.7}Ni_{30.6}Mo_{2.7}$ (211) at 0.9V vs. RHE. Each state is named as nO + mPt, where n and m represent the number of O and Pt atoms that are added in the unit cell at the current GCMC step. The atoms above the surface plane are depicted in the ball-and-stick style, while other atoms are depicted in the CPK style. Colors in figure: Blue balls are Pt; Violet balls are Ni; Cyan balls are Mo; Red balls are O.

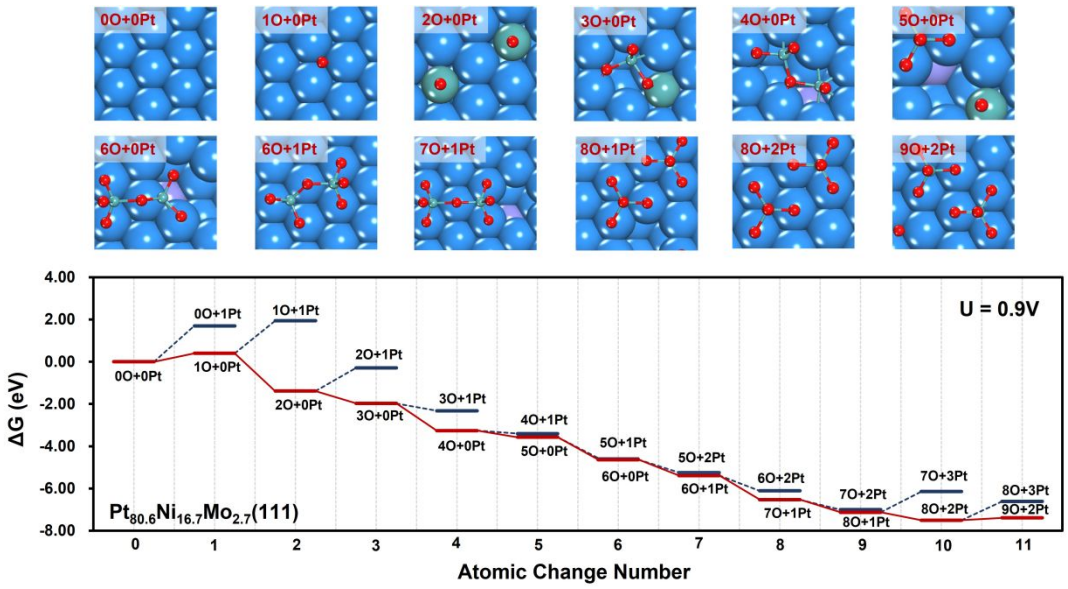

Figure S17. Structures and energetic profiles for the intermediate states and the evolution of $Pt_{80.6}Ni_{16.7}Mo_{2.7}$ (111) at 0.9V vs. RHE. Each state is named as nO + mPt, where n and m represent the number of O and Pt atoms that are added in the unit cell at the current GCMC step. The atoms above the surface plane are depicted in the ball-and-stick style, while other atoms are depicted in the CPK style. Colors in figure: Blue balls are Pt; Violet balls are Ni; Cyan balls are Mo; Red balls are O.

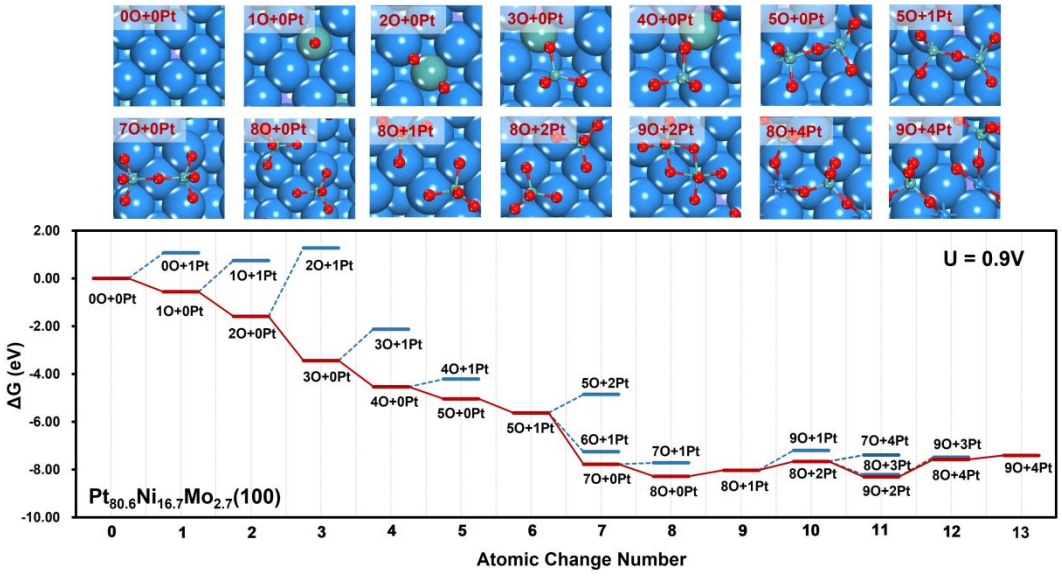

Figure S18. Structures and energetic profiles for the intermediate states and the evolution of $Pt_{80.6}Ni_{16.7}Mo_{2.7}$ (100) at 0.9V vs. RHE. Each state is named as nO + mPt, where n and m represent the number of O and Pt atoms that are added in the unit cell at the current GCMC step. The atoms above the surface plane are depicted in the ball-and-stick style, while other atoms are depicted in the CPK style. Colors in figure: Blue balls are Pt; Violet balls are Ni; Cyan balls are Mo; Red balls are O.

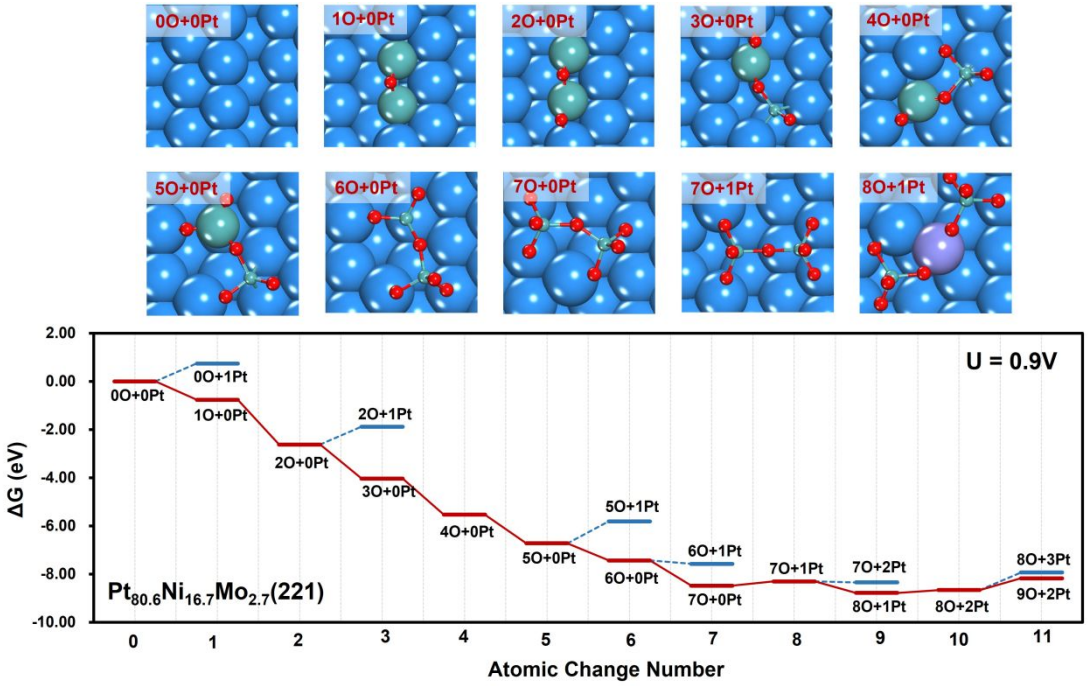

Figure S19. Structures and energetic profiles for the intermediate states and the evolution of $Pt_{80.6}Ni_{16.7}Mo_{2.7}$ (221) at 0.9V vs. RHE. Each state is named as nO + mPt, where n and m represent the number of O and Pt atoms that are added in the unit cell at the current GCMC step. The atoms above the surface plane are depicted in the ball-and-stick style, while other atoms are depicted in the CPK style. Colors in figure: Blue balls are Pt; Violet balls are Ni; Cyan balls are Mo; Red balls are O.

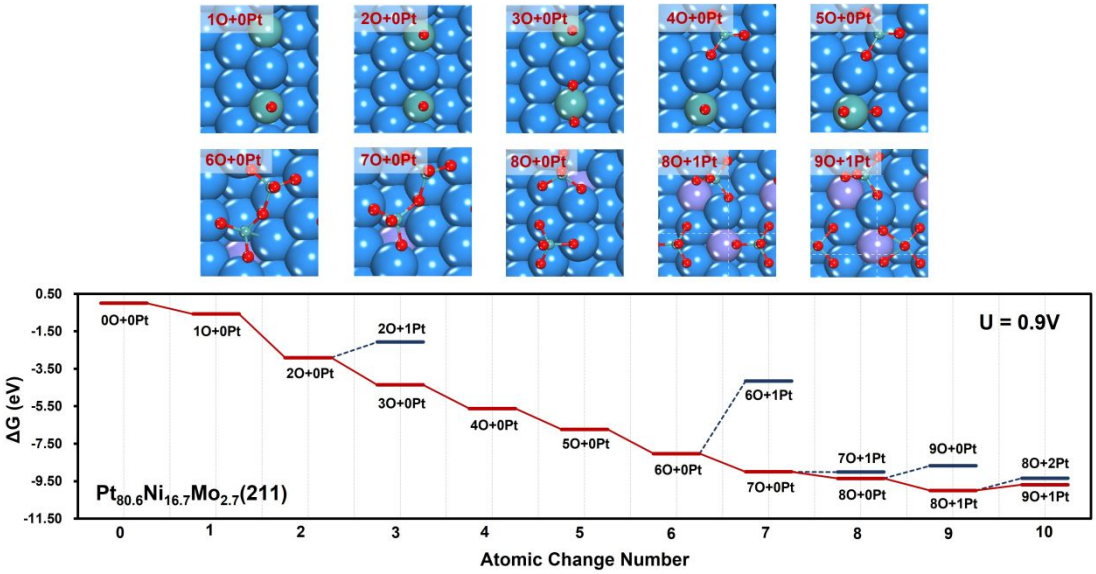

Figure S20. Structures and energetic profiles for the intermediate states and the evolution of $Pt_{80.6}Ni_{16.7}Mo_{2.7}$ (211) at 0.9V vs. RHE. Each state is named as nO + mPt, where n and m represent the number of O and Pt atoms that are added in the unit cell at the current GCMC step. The atoms above the surface plane are depicted in the ball-and-stick style, while other atoms are depicted in the CPK style. Colors in figure: Blue balls are Pt; Violet balls are Ni; Cyan balls are Mo; Red balls are O.

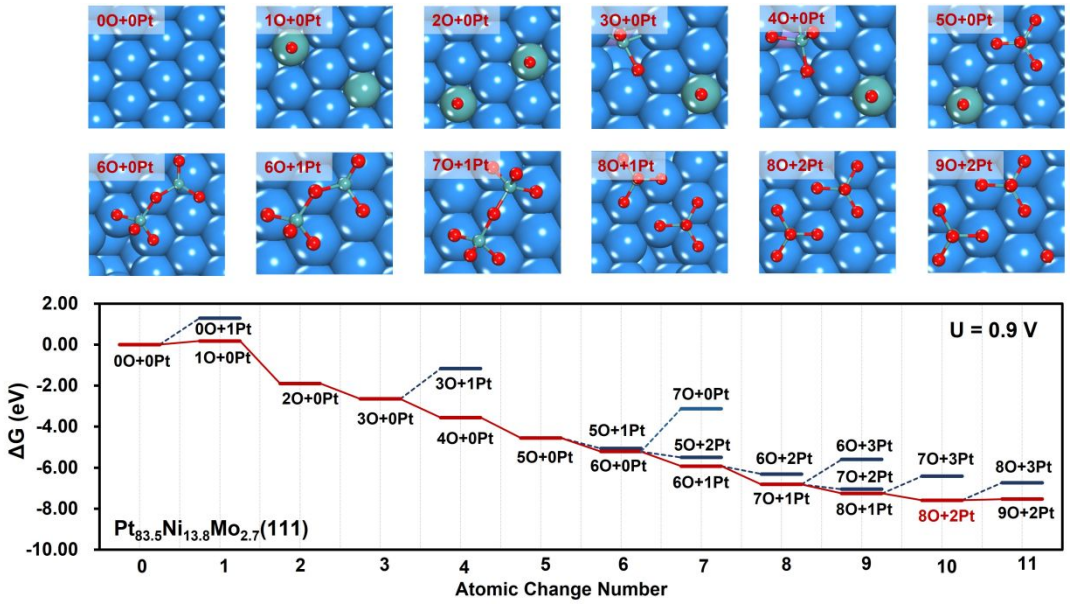

Figure S21. Structures and energetic profiles for the intermediate states and the evolution of $Pt_{83.5}Ni_{13.8}Mo_{2.7}$ (111) at 0.9V vs. RHE. Each state is named as nO + mPt, where n and m represent the number of O and Pt atoms that are added in the unit cell at the current GCMC step. The atoms above the surface plane are depicted in the ball-and-stick style, while other atoms are depicted in the CPK style. Colors in figure: Blue balls are Pt; Violet balls are Ni; Cyan balls are Mo; Red balls are O.

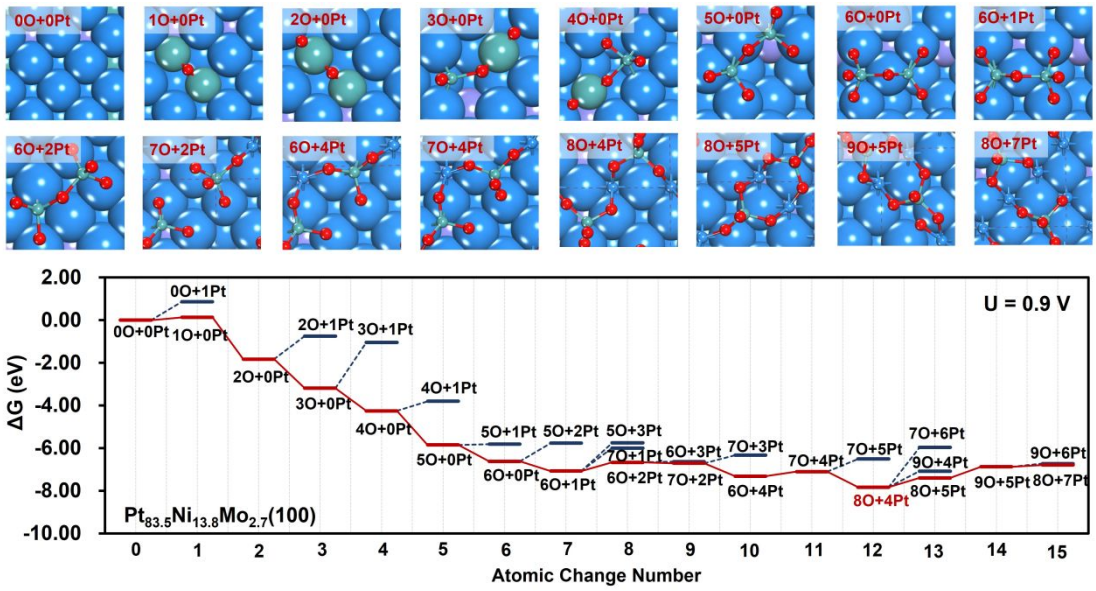

Figure S22. Structures and energetic profiles for the intermediate states and the evolution of $Pt_{83.5}Ni_{13.8}Mo_{2.7}$ (100) at 0.9V vs. RHE. Each state is named as nO + mPt, where n and m represent the number of O and Pt atoms that are added in the unit cell at the current GCMC step. The atoms above the surface plane are depicted in the ball-and-stick style, while other atoms are depicted in the CPK style. Colors in figure: Blue balls are Pt; Violet balls are Ni; Cyan balls are Mo; Red balls are O.

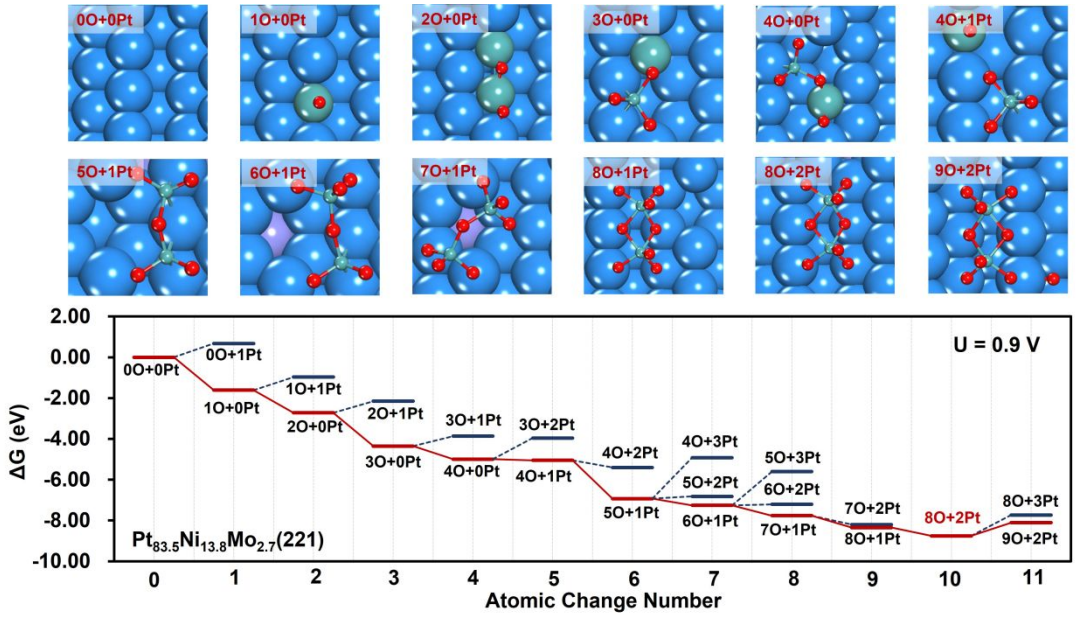

Figure S23. Structures and energetic profiles for the intermediate states and the evolution of $Pt_{83.5}Ni_{13.8}Mo_{2.7}$ (221) at 0.9V vs. RHE. Each state is named as nO + mPt, where n and m represent the number of O and Pt atoms that are added in the unit cell at the current GCMC step. The atoms above the surface plane are depicted in the ball-and-stick style, while other atoms are depicted in the CPK style. Colors in figure: Blue balls are Pt; Violet balls are Ni; Cyan balls are Mo; Red balls are O.

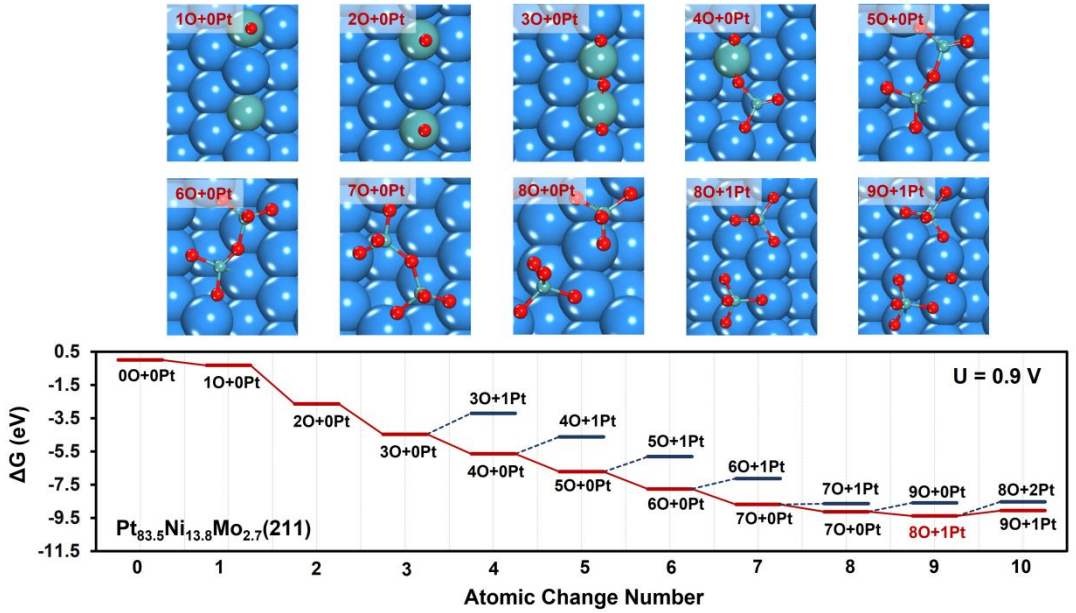

Figure S24. Structures and energetic profiles for the intermediate states and the evolution of $Pt_{83.5}Ni_{13.8}Mo_{2.7}$ (211) at 0.9V vs. RHE. Each state is named as nO + mPt, where n and m represent the number of O and Pt atoms that are added in the unit cell at the current GCMC step. The atoms above the surface plane are depicted in the ball-and-stick style, while other atoms are depicted in the CPK style. Colors in figure: Blue balls are Pt; Violet balls are Ni; Cyan balls are Mo; Red balls are O.

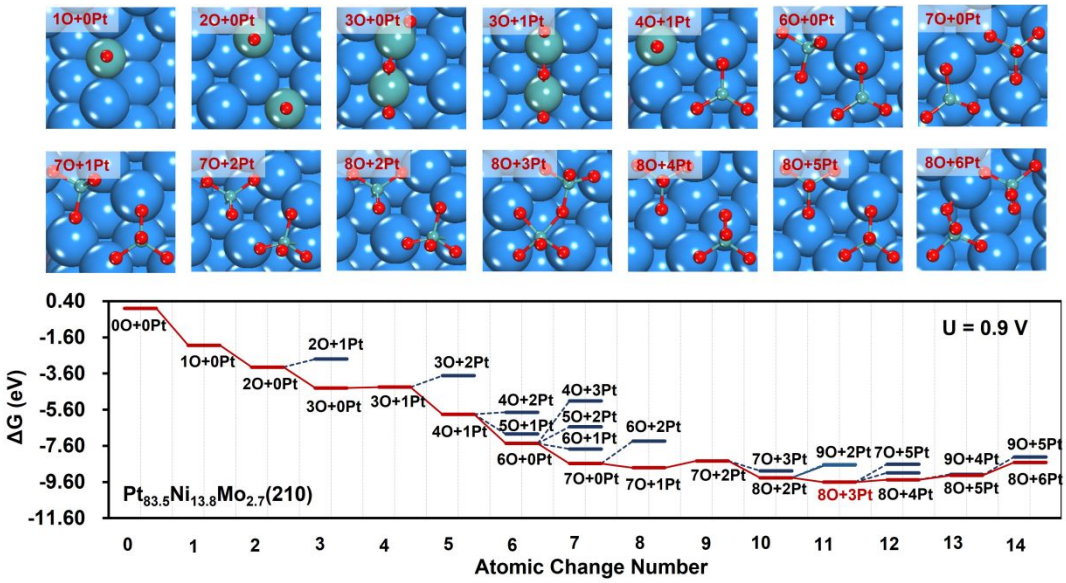

Figure S25. Structures and energetic profiles for the intermediate states and the evolution of $Pt_{83.5}Ni_{13.8}Mo_{2.7}$ (210) at 0.9V vs. RHE. Each state is named as nO + mPt, where n and m represent the number of O and Pt atoms that are added in the unit cell at the current GCMC step. The atoms above the surface plane are depicted in the ball-and-stick style, while other atoms are depicted in the CPK style. Colors in figure: Blue balls are Pt; Violet balls are Ni; Cyan balls are Mo; Red balls are O.

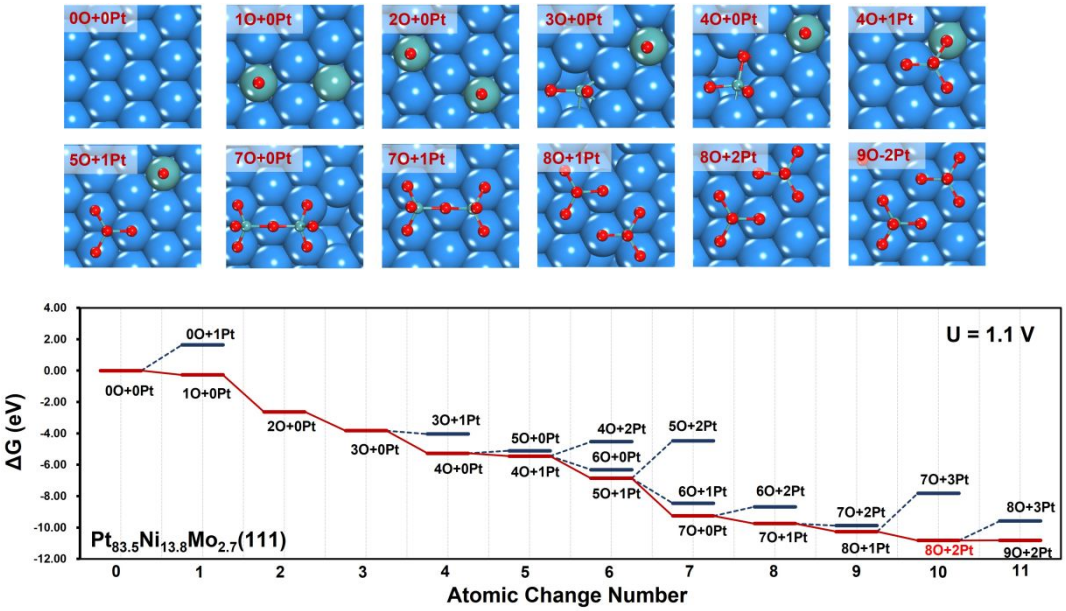

Figure S26. Structures and energetic profiles for the intermediate states and the evolution of $Pt_{83.5}Ni_{13.8}Mo_{2.7}$ (111) at 1.1V vs. RHE. Each state is named as nO + mPt, where n and m represent the number of O and Pt atoms that are added in the unit cell at the current GCMC step. The atoms above the surface plane are depicted in the ball-and-stick style, while other atoms are depicted in the CPK style. Colors in figure: Blue balls are Pt; Violet balls are Ni; Cyan balls are Mo; Red balls are O.

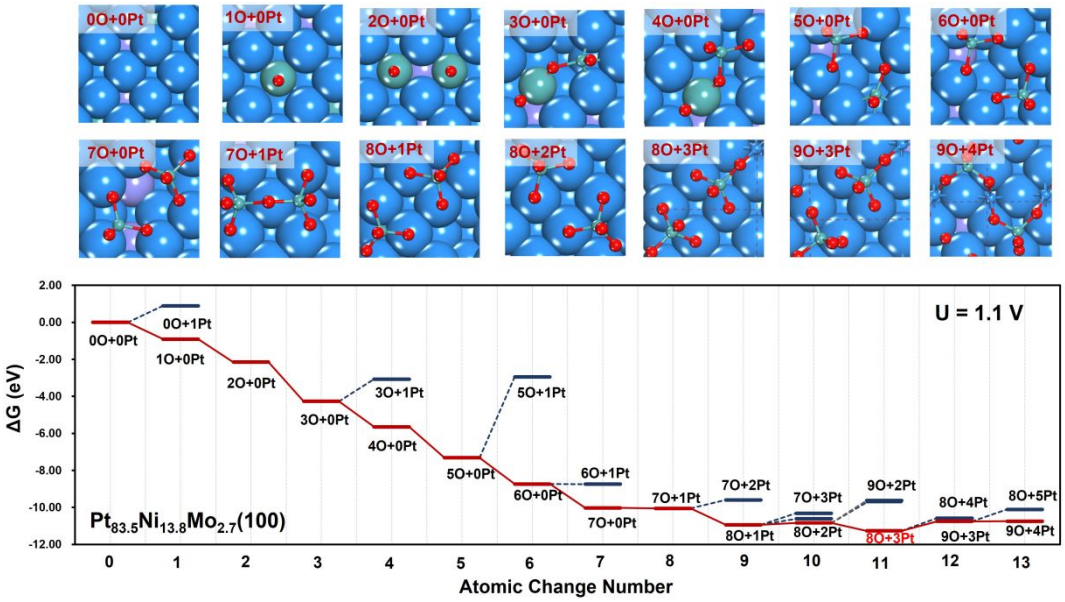

Figure S27. Structures and energetic profiles for the intermediate states and the evolution of $Pt_{83.5}Ni_{13.8}Mo_{2.7}$ (100) at 1.1V vs. RHE. Each state is named as nO + mPt, where n and m represent the number of O and Pt atoms that are added in the unit cell at the current GCMC step. The atoms above the surface plane are depicted in the ball-and-stick style, while other atoms are depicted in the CPK style. Colors in figure: Blue balls are Pt; Violet balls are Ni; Cyan balls are Mo; Red balls are O.

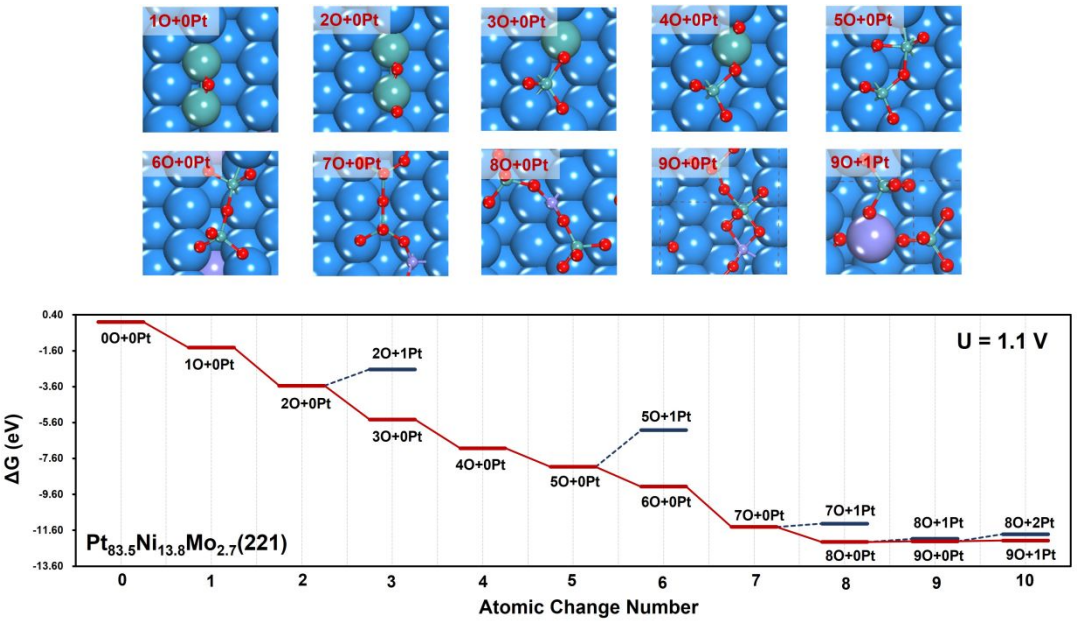

Figure S28. Structures and energetic profiles for the intermediate states and the evolution of $Pt_{83.5}Ni_{13.8}Mo_{2.7}$ (221) at 1.1V vs. RHE. Each state is named as nO + mPt, where n and m represent the number of O and Pt atoms that are added in the unit cell at the current GCMC step. The atoms above the surface plane are depicted in the ball-and-stick style, while other atoms are depicted in the CPK style. Colors in figure: Blue balls are Pt; Violet balls are Ni; Cyan balls are Mo; Red balls are O.

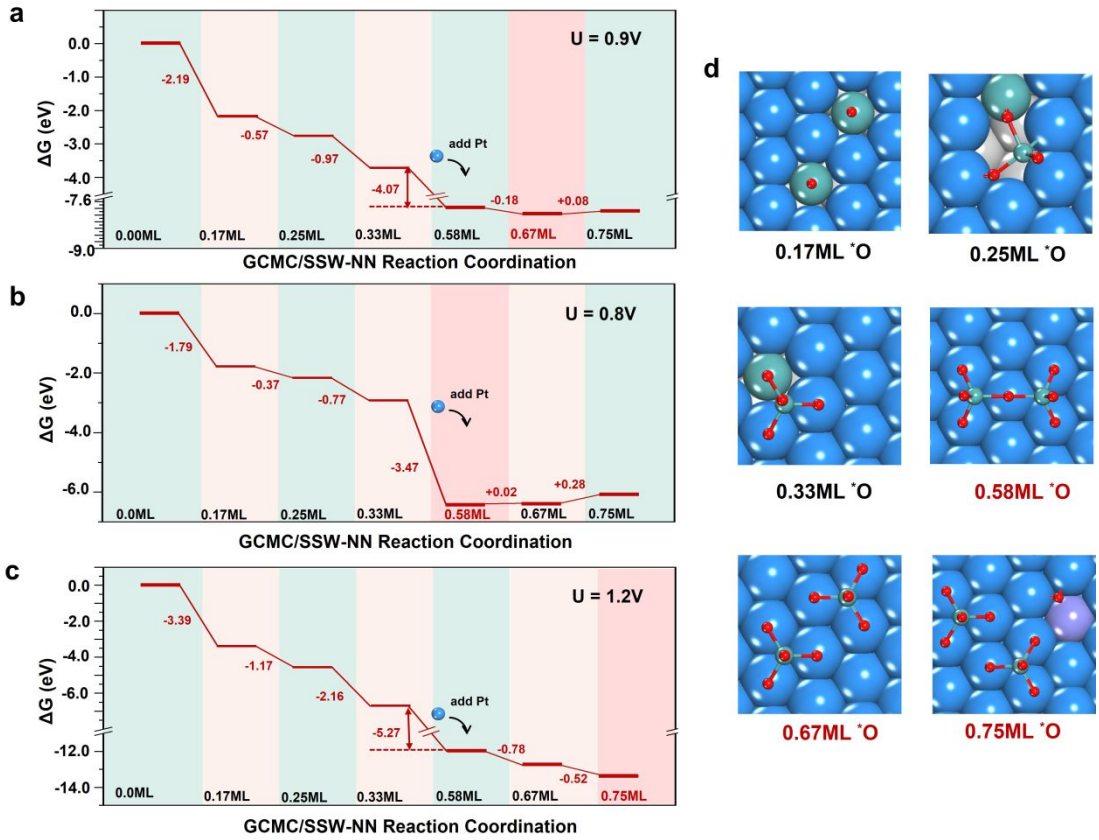

Figure S29. Energy profiles for the GCMC/SSW-NN trajectories of $Pt_{75.0}Ni_{22.3}Mo_{2.7}(111)$ at 0.8, 0.9, and 1.2V vs RHE. Colors in the right column: blue balls are Pt; violet balls are Ni; cyan balls are Mo; red balls are O.

4. ORR Activity on $Pt_{75.0}Ni_{22.3}Mo_{2.7}(111)$, $Pt_{83.5}Ni_{13.8}Mo_{2.7}(111)$, and $Pt_{75.0}Ni_{25.0}(111)$-0.16 ML O

As the electrode potential increases, the *O adatom would gradually appear on the clean electrode surface. We calculate the *O coverage for $Pt_{75.0}Ni_{22.3}Mo_{2.7}(111)$ and $Pt_{75.0}Ni_{25.0}(111)$, as shown in Figure S31. Note that we did not perform SSW global optimization in this calculation, so the surface would not reconstruct during simulation. At 0 ~ 0.8 V, both surfaces are clean. At 0.8 ~ 0.9 V, $Pt_{75.0}Ni_{25.0}(111)$ surface starts to be covered by 0.08 ML *O, while at 0.9 V, the *O coverage increases to 0.16 ML. For $Pt_{75.0}Ni_{22.3}Mo_{2.7}(111)$, it starts to be covered by 0.08 ML *O at 0.83 V, while at 0.94 V, the *O coverage increases to 0.16 ML. So, at 0.9 V, the *O coverage on the clean $Pt_{75.0}Ni_{25.0}(111)$ surface can reach up to 0.16 ML before surface reconstruction.

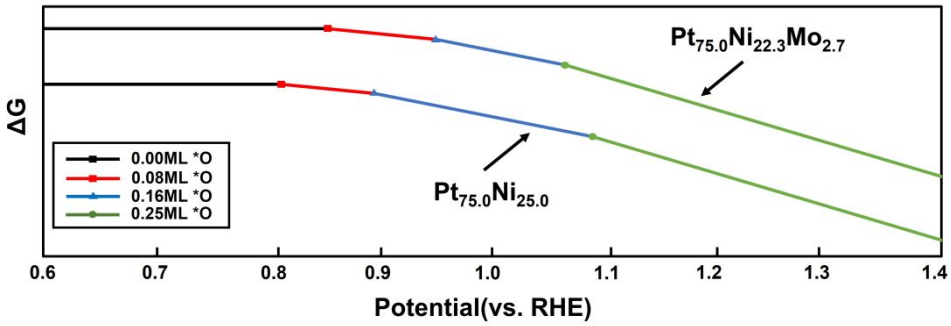

Figure S30. A surface phase diagram of $Pt_{75.0}Ni_{25.0}$ (111) and $Pt_{75.0}Ni_{22.3}Mo_{2.7}$(111). To illustrate curve clearly, a constant spacing in the y-axis is applied for the ΔG of the clean surfaces for $Pt_{75.0}Ni_{25.0}$ (111).

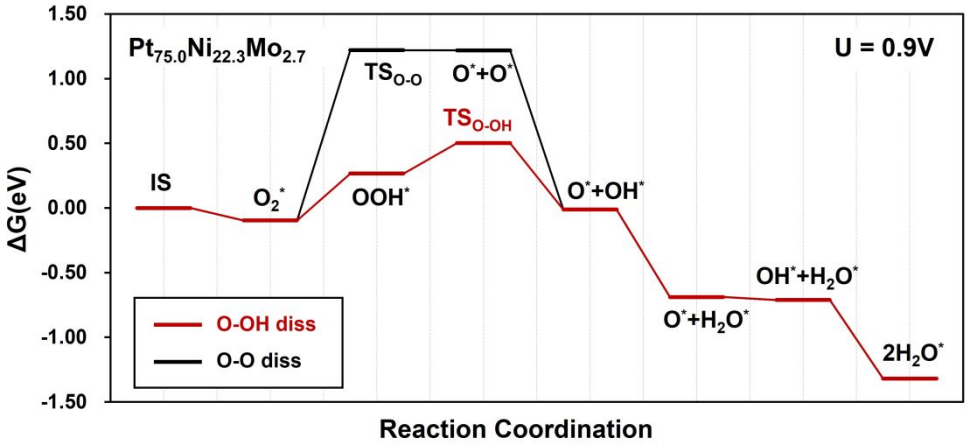

Figure S31. Free energy profile for ORR on in-situ $Pt_{75.0}Ni_{22.3}Mo_{2.7}$(111) at 0.9V.

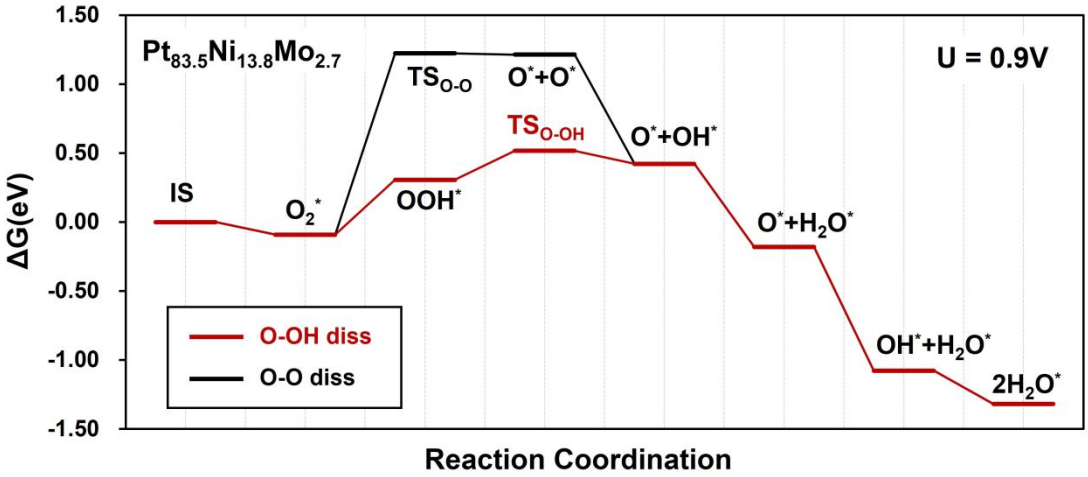

Figure S32. Free energy profile for ORR on the in-situ $Pt_{83.5}Ni_{13.8}Mo_{2.7}$(111) at 0.9V.

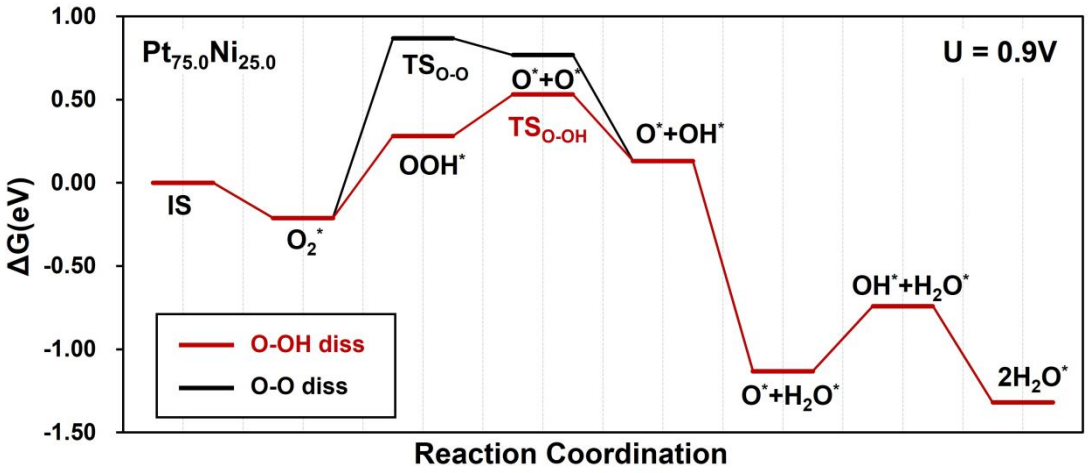

Figure S33. Free energy profile for ORR on the $Pt_{75.0}Ni_{25.0}$(111)-0.16 ML O surface at 0.9V.

5. Dissolution Free Energy of $^{*}MO_4$

As we have shown in the main text, the dissolution free energy ΔG_{diss} is defined as the

$$Pt-Ni-2MO_4+(2x+y)H^+ \rightarrow Pt-Ni-MO_4+H_yMO_{4-x}^{m-}+xH_2O\#(39)$$

$$Pt-Ni-2MO_4+4H^+ \rightarrow Pt-Ni-MO_4+M^{n+}+2H_2O\#(40)$$

In Eq.46-47, the $^{*}MO_4$ group can left from the surface by forms of MO_4^{n-}(VO^{2+}, MnO_4^-, TcO_4^-), H_nMO_4 (H_2MoO_4, $HCrO_4^-$) or M^{n+}(Cr^{3+}, Fe^{3+}, Nb^{3+}, Ta^{3+}, W^{3+}, Ru^{2+}, Os^{2+}, Re^{3+}). If a metal has multiple ionic forms (e.g., Mn^{2+}, Mn^{3+}, $HMnO_4^-$, MnO_4^{2-}). We give detailed examples of each ion forms.

MO_4^{n-}

We take MnO_4^{2-} as the example,

$$PtNi-MnO_4+e^- \rightarrow PtNi+MnO_4^-\#(41)$$

$$\begin{aligned}\Delta G &= G(PtNi)+\mu_{MnO_4^-}-G(PtNi-MnO_4)-\mu_{e^-}\# \\ &= G(PtNi)+\mu^0_{MnO_4^-}+k_BTln(c/c^0)-G(PtNi-MnO_4)-\mu_{e^-}\end{aligned}(42)$$

where the concentration of ions set as c = 10^{-4} mol/L.

According to the definition of electrode potential, the free energy change of Eq. 43 is 0 when at the electrode potential of $E^0_{MnO_4^-/Mn}$. Then, we can get that

$$MnO_4^- + 8H^+ + 7e^- \rightarrow Mn(s)+4H_2O\#(43)$$

$$\Delta G=\mu^0_{Mn}+4\mu_{H_2O}-8\mu_{H^+}-7\mu_{e^-_{MnO_4^-/Mn}}-\mu^0_{MnO_4^-}=0\#(44)$$

where μ^0_{Mn} is the energy of bulk Mn.

$$\begin{aligned}\mu^0_{MnO_4^-} &= \mu^0_{Mn}+4\mu_{H_2O}-8\mu_{H^+}-7\mu_{e^-_{MnO_4^-/Mn}}\# \\ &= \mu^0_{Mn}+4\mu_{H_2O}-8\mu_{H^+}+7\mu^{SHE}_{e^-}-7\mu_{e^-_{MnO_4^-/Mn}}-7\mu^{SHE}_{e^-} \\ &= \mu^0_{Mn}+4\mu_{H_2O}-8\mu_{H^+}+7eE^0_{MnO_4^-/Mn}-7\mu^{SHE}_{e^-}\end{aligned}(45)$$

Substituting Eq. 45 into Eq. 42, we get

$$\begin{aligned}\Delta G &= G(PtNi)+\mu^0_{MnO_4^-}+k_BTln(c/c^0)-G(PtNi-MnO_4)-\mu_{e^-}\# \\ &= G(PtNi)+\mu^0_{Mn}+4\mu_{H_2O}-8\mu_{H^+}+7eE^0_{MnO_4^-/Mn}-7\mu^{SHE}_{e^-} \\ &\quad +k_BTln(c/c^0)-G(PtNi-MnO_4)-\mu_{e^-} \\ &= G(PtNi)-G(PtNi-MnO_4)+\mu^0_{Mn}+4\mu_{H_2O}+7eE^0_{MnO_4^-/Mn}+k_BTln(c/c^0) \\ &\quad -8\mu_{H^+}-7\mu^{SHE}_{e^-}-\mu_{e^-} \\ &= G(PtNi)-G(PtNi-MnO_4)+\mu^0_{Mn}+4\mu_{H_2O}+7eE^0_{MnO_4^-/Mn}+k_BTln(c/c^0) \\ &\quad -8(\mu_{H^+}+\mu_{e^-})+7\mu_{e^-}-7\mu^{SHE}_{e^-} \\ &= G(PtNi)-G(PtNi-MnO_4)+\mu^0_{Mn}+4\mu_{H_2O}+7eE^0_{MnO_4^-/Mn}+k_BTln(c/c^0) \\ &\quad -8\left(\frac{1}{2}\mu_{H_2}-\mu^{SHE}_{e^-}+\mu_{e^-}\right)-7\left(\mu^{SHE}_{e^-}-\mu_{e^-}\right) \\ &= G(PtNi)-G(PtNi-MnO_4)+\mu^0_{Mn}+4\mu_{H_2O}+7eE^0_{MnO_4^-/Mn}+k_BTln(c/c^0) \\ &\quad -4\mu_{H_2}+8eU-7eU \\ &= G(PtNi)-G(PtNi-MnO_4)+\mu^0_{Mn}+4\mu_{H_2O}+7eE^0_{MnO_4^-/Mn}+k_BTln(c/c^0) \\ &\quad -4\mu_{H_2}+eU\end{aligned}(46)$$

And the contribution of c can be further corrected by a term of 0.059lg(c). Thus, the ΔG_{diss} can be summarized as Eq. 47

$$\begin{aligned}\Delta G_{diss} &= G(PtNi)-G(PtNi-MnO_4)+\mu^0_{Mn}+4\mu_{H_2O}+7eE^0_{MnO_4^-/Mn}+0.059\times lg(1\times 10^{-4}) \\ &\quad -4\mu_{H_2}+eU=-0.90\ eV\end{aligned}(47)$$

H_nMO_4

We take H_2MoO_4 as the example,

$$PtNi - MoO_4 + 2H^+ + 2e^- \rightarrow PtNi + H_2MoO_4 \#(48)$$

$$\begin{aligned}\Delta G &= G(PtNi) + \mu_{H_2MoO_4} - G(PtNi - MoO_4) - 2\mu_{H^+} - 2\mu_{e^-} \# \\ &= G(PtNi) + \mu^0_{H_2MoO_4} + k_BTln(c/c^0) - G(PtNi - MoO_4) - 2\mu_{H^+} - 2\mu_{e^-}\end{aligned} \quad (49)$$

where the concentration of ions set as c = 10^{-4} mol/L.

According to the definition of electrode potential, the free energy change of Eq. 50 is 0 when at the electrode potential of $E^0_{H_2MoO_4/Mo}$. Then, we can get that

$$H_2MoO_4(aq) + 6H^+ + 6e^- \rightarrow \mathrm{Mo} + 4H_2O \#(50)$$

$$\Delta G = \mu^0_{Mo} + 4\mu_{H_20} - 6\mu_{H^+} - 6\mu_{e^-_{H_2MoO_4/Mo}} - \mu^0_{H_2MoO_4} = 0 \#(51)$$

where μ^0_{Mo} is the energy of bulk Mo.

$$\begin{aligned}\mu^0_{H_2MoO_4} &= \mu^0_{Mo} + 4\mu_{H_20} - 6\mu_{H^+} - 6\mu_{e^-_{H_2MoO_4/Mo}} \# \\ &= \mu^0_{Mo} + 4\mu_{H_20} - 6\mu_{H^+} + \left(6\mu^{SHE}_{e^-} - 6\mu_{e^-_{H_2MoO_4/Mo}}\right) - 6\mu^{SHE}_{e^-} \\ &= \mu^0_{Mo} + 4\mu_{H_20} - 6\mu_{H^+} + 6eE^0_{H_2MoO_4/Mo} - 6\mu^{SHE}_{e^-}\end{aligned} \quad (52)$$

Substituting Eq. 52 into Eq. 49, we get

$$\begin{aligned}\Delta G &= G(PtNi) + \mu^0_{H_2MoO_4} + k_BTln(c/c^0) - G(PtNi - MoO_4) - 2\mu_{H^+} - 2\mu_{e^-} \# \\ &= G(PtNi) - G(PtNi - MoO_4) \\ &+ \mu^0_{Mo} + 4\mu_{H_20} - 6\mu_{H^+} + 6eE^0_{H_2MoO_4/Mo} - 6\mu^{SHE}_{e^-} + k_BTln(c/c^0) - 2\mu_{H^+} - 2\mu_{e^-} \\ &= G(PtNi) - G(PtNi - MoO_4) + \mu^0_{Mo} + 4\mu_{H_20} + 6eE^0_{H_2MoO_4/Mo} + k_BTln(c/c^0) \\ &\quad -8\mu_{H^+} - 6\mu^{SHE}_{e^-} - 2\mu_{e^-} \\ &= G(PtNi) - G(PtNi - MoO_4) + \mu^0_{Mo} + 4\mu_{H_20} + 6eE^0_{H_2MoO_4/Mo} + k_BTln(c/c^0) \\ &\quad -8(\mu_{H^+} + \mu_{e^-}) - 6\mu^{SHE}_{e^-} + 6\mu_{e^-} \\ &= G(PtNi) - G(PtNi - MoO_4) + \mu^0_{Mo} + 4\mu_{H_20} + 6eE^0_{H_2MoO_4/Mo} + k_BTln(c/c^0) \\ &\quad -8\left(\frac{1}{2}\mu_{H_2} - \mu^{SHE}_{e^-} + \mu_{e^-}\right) - 6\left(\mu^{SHE}_{e^-} - \mu_{e^-}\right) \\ &= G(PtNi) - G(PtNi - MoO_4) + \mu^0_{Mo} + 4\mu_{H_20} + 6eE^0_{H_2MoO_4/Mo} + k_BTln(c/c^0) \\ &\quad -4\mu_{H_2} + 8eU - 6eU \\ &= G(PtNi) - G(PtNi - MoO_4) + \mu^0_{Mo} + 4\mu_{H_20} + 6eE^0_{H_2MoO_4/Mo} + k_BTln(c/c^0) \\ &\quad -4\mu_{H_2} + 2eU\end{aligned} \quad (53)$$

And the contribution of c can be further corrected by a term of 0.059lg(c). Thus, the ΔG_{diss} can be summarized as Eq. 54

$$\begin{aligned}\Delta G_{diss} &= G(PtNi) - G(PtNi - MoO_4) + \mu^0_{Mo} + 4\mu_{H_20} + 6eE^0_{H_2MoO_4/Mo} + 0.059 \times lg(1 \times 10^{-4}) \\ &\quad - 4\mu_{H_2} + 2eU = 0.16\ eV\end{aligned} \quad (54)$$

M^{n+}

We take Cr^{3+} as the example,

$$PtNi - CrO_4 + 8H^+ + 5e^- \rightarrow PtNi + Cr^{3+} + 4H_2O \#(55)$$

$$\begin{aligned}\Delta G &= G(PtNi) + \mu_{Cr^{3+}} + 4\mu_{H_2O} - G(PtNi - CrO_4) - 8\mu_{H^+} - 5\mu_{e^-} \# \\ &= (PtNi) + \mu^0_{Cr^{3+}} + k_BTln(c/c^0) + 4\mu_{H_2O} - G(PtNi - CrO_4) - 8\mu_{H^+} - 5\mu_{e^-}\end{aligned} \quad (56)$$

where the concentration of ions set as c = 10^{-4} mol/L.

To calculate $\mu^0_{Cr^{3+}}$, we use the standard half-electrode potential $E^0_{Cr^{3+}/Cr}$

According to the definition of electrode potential, the free energy change of Eq. 57 is 0 when at the

electrode potential of $E^0_{Cr^{3+}/Cr}$. Then, we can get that

$$Cr^{3+} + 3e^- \rightarrow Cr \# (57)$$

$$\Delta G = \mu^0_{Cr} - \mu^0_{Cr^{3+}} - 3\mu_{e^-_{Cr^{3+}/Cr}} = 0 \# (58)$$

$$\begin{aligned}\mu^0_{Cr^{3+}} = \mu^0_{Cr} - 3\mu_{e^-_{Cr^{3+}/Cr}} = \mu^0_{Cr} - 3\mu_{e^-_{Cr^{3+}/Cr}} = \mu^0_{Cr} + 3\mu_e^{SHE} - 3\mu_{e^-_{Cr^{3+}/Cr}} - 3\mu_e^{SHE} \#\\ = \mu^0_{Cr} + 3eE^0_{Cr^{3+}/Cr} - 3\mu_e^{SHE}\end{aligned} \quad (59)$$

where μ^0_{Cr} is the energy of bulk Cr.

Substituting Eq. 59 into Eq. 56, we get

$$\begin{aligned}\Delta G &= G(PtNi) + \mu^0_{Cr^{3+}} + k_B T ln(c/c^0) + 4\mu_{H_2O} - G(PtNi - CrO_4) - 8\mu_{H^+} - 5\mu_{e^-}\\ &= G(PtNi) + \mu^0_{Cr} + 3eE^0_{Cr^{3+}/Cr} - 3\mu_e^{SHE} + k_B T ln(c/c^0)\\ &\quad + 4\mu_{H_2O} - G(PtNi - CrO_4) - 8\mu_{H^+} - 5\mu_{e^-}\\ &= G(PtNi) - G(PtNi - CrO_4) + 4\mu_{H_2O}\\ &\quad + \mu^0_{Cr} + 3eE^0_{Cr^{3+}/Cr} + k_B T ln(c/c^0) - 3\mu_e^{SHE} - 8(\mu_{H^+} + \mu_{e^-}) + 3\mu_{e^-}\\ &= G(PtNi) - G(PtNi - CrO_4) + 4\mu_{H_2O}\\ &\quad + \mu^0_{Cr} + 3eE^0_{Cr^{3+}/Cr} + k_B T ln(c/c^0) - 8(\mu_{H^+} + \mu_{e^-}) - 3(\mu_e^{SHE} - \mu_{e^-})\\ &= G(PtNi) - G(PtNi - CrO_4) + 4\mu_{H_2O}\\ &\quad + \mu^0_{Cr} + 3eE^0_{Cr^{3+}/Cr} + k_B T ln(c/c^0) - 8\left(\frac{1}{2}\mu_{H_2} - \mu_e^{SHE} + \mu_{e^-}\right) - 3(\mu_e^{SHE} - \mu_{e^-})\\ &= G(PtNi) - G(PtNi - CrO_4) + 4\mu_{H_2O}\\ &\quad + \mu^0_{Cr} + 3eE^0_{Cr^{3+}/Cr} + k_B T ln(c/c^0) - 4\mu_{H_2} + 8(\mu_e^{SHE} - \mu_{e^-}) - 3(\mu_e^{SHE} - \mu_{e^-})\\ &= G(PtNi) - G(PtNi - CrO_4) + 4\mu_{H_2O}\\ &\quad + \mu^0_{Cr} + 3eE^0_{Cr^{3+}/Cr} + k_B T ln(c/c^0) + k_B T ln(c/c^0) - 4\mu_{H_2} + 5(\mu_e^{SHE} - \mu_{e^-})\\ &= G(PtNi) - G(PtNi - CrO_4) + 4\mu_{H_2O}\\ &\quad + \mu^0_{Cr} + 3eE^0_{Cr^{3+}/Cr} + k_B T ln(c/c^0) - 4\mu_{H_2} + 5eU\end{aligned} \quad (60)$$

And the contribution of c can be further corrected by a term of 0.059lg(c). Thus, the ΔG_{diss} can be summarized as Eq. 61

$$\begin{aligned}\Delta G_{diss} &= G(PtNi) - G(PtNi - CrO_4) + 4\mu_{H_2O} + \mu^0_{Cr} + 3eE^0_{Cr^{3+}/Cr} + 0.059 \times lg(1 \times 10^{-4}) - 4\\ &\mu_{H_2} + 5eU = -0.87\ eV\end{aligned} \quad (61)$$

All the results of screened elements are summarized in Table S5-S6. The bold number is the most negative dissolution free energy for each $^*MO_4$ to represent the dissolution free energy of $^*MO_4$.

Table S5. Full list of dissolution free energy of $^*MO_4$

M		ΔG_{diss} (eV)
Mo	$Mo^{3+} + 3e^- \rightarrow Mo(s)\#$ $Pt - Ni - MoO_4 + 8H^+ + 5e^- \rightarrow Pt - Ni + Mo^{3+} + 4H_2O\#$	1.60
	$H_2MoO_4(aq) + 6H^+ + 6e^- \rightarrow Mo(s) + 4H_2O\#$ $Pt - Ni - MoO_4 + 2H^+ + 2e^- \rightarrow Pt - Ni + H_2MoO_4\#$	**0.16**[a]
V	$V^{2+} + 2e^- \rightarrow V(s)\#$ $Pt - Ni - VO_4 + 8H^+ + 6e^- \rightarrow Pt - Ni + V^{2+} + 4H_2O\#$	-0.68
	$VO^{2+} + 2H^+ + 4e^- \rightarrow V(s) + H_2O\#$ $Pt - Ni - VO_4 + 6H^+ + 2e^- \rightarrow Pt - Ni + VO^{2+} + 3H_2O\#$	**-4.51**
Cr	$Cr^{3+} + 3e^- \rightarrow Cr(s)\#$	**-0.87**

	$Pt-Ni-CrO_4+8H^++5e^-\rightarrow Pt-Ni+Cr^{3+}+4H_2O\#$ $HCrO_4^-+7H^++6e^-\rightarrow Cr(s)+4H_2O\#$ $Pt-Ni-CrO_4+H^++2e^-\rightarrow Pt-Ni+HCrO_4^-\#$	2.31
Mn	$Mn^{2+}+2e^-\rightarrow Mn(s)\#$ $Pt-Ni-MnO_4+8H^++6e^-\rightarrow Pt-Ni+Mn^{2+}+4H_2O\#$ $MnO_4^-+8H^++3e^-\rightarrow Mn(s)+4H_2O\#$ $Pt-Ni-MnO_4+e^-\rightarrow Pt-Ni+MnO_4^-\#$	**-1.04** -0.89
Fe	$Fe^{3+}+3e^-\rightarrow Fe(s)\#$ $Pt-Ni-FeO_4+8H^++5e^-\rightarrow Pt-Ni+Fe^{3+}+4H_2O\#$ $FeO_4^{2-}+8H^++6e^-\rightarrow Fe(s)+4H_2O\#$ $Pt-Ni-FeO_4+2e^-\rightarrow Pt-Ni+FeO_4^{2-}\#$	**-1.58** 8.79
Nb	$Nb^{3+}+3e^-\rightarrow Nb(s)\#$ $Pt-Ni-NbO_4+8H^++5e^-\rightarrow Pt-Ni+Nb^{3+}+4H_2O\#$	**-0.48**
Tc	$Tc^{2+}+2e^-\rightarrow Tc(s)\#$ $Pt-Ni-TcO_4+8H^++6e^-\rightarrow Pt-Ni+Tc^{2+}+4H_2O\#$ $TcO_4^-+8H^++7e^-\rightarrow Tc(s)+4H_2O\#$ $Pt-Ni-TcO_4+e^-\rightarrow Pt-Ni+TcO_4^-\#$	2.18 0.19
Ru	$Ru^{2+}+2e^-\rightarrow Ru(s)\#$ $Pt-Ni-RuO_4+8H^++6e^-\rightarrow Pt-Ni+Ru^{2+}+4H_2O\#$	**-0.12**
Os	$Os^{2+}+2e^-\rightarrow Os(s)\#$ $Pt-Ni-OsO_4+8H^++6e^-\rightarrow Pt-Ni+Os^{2+}+4H_2O\#$	**1.42**
Ta	$Ta^{3+}+3e^-\rightarrow Ta(s)\#$ $Pt-Ni-TaO_4+8H^++5e^-\rightarrow Pt-Ni+Ta^{3+}+4H_2O\#$	**1.59**
Re	$Re^{3+}+3e^-\rightarrow Re(s)\#$ $Pt-Ni-ReO_4+8H^++5e^-\rightarrow Pt-Ni+Re^{3+}+4H_2O\#$ $ReO_4^-+8H^++7e^-\rightarrow Re(s)+4H_2O\#$ $Pt-Ni-ReO_4+e^-\rightarrow Pt-Ni+ReO_4^-\#$	**2.45** 3.28
W	$W^{3+}+3e^-\rightarrow W(s)\#$ $Pt-Ni-WO_4+8H^++5e^-\rightarrow Pt-Ni+W^{3+}+4H_2O\#$	**3.23**

[a] The bold number is the most negative dissolution free energy for each $^*MO_4$

Table S6. The most negative dissolution free energy for each $^*MO_4$

$^*MO_4$	ΔG_{diss}(eV)
V	-4.51
Cr	-0.87
Mn	-1.04
Fe	-1.58
Nb	-0.48
Mo	0.16
Tc	0.19
Ru	-0.12
Os	1.42

Ta	1.59
Re	2.45
W	3.23

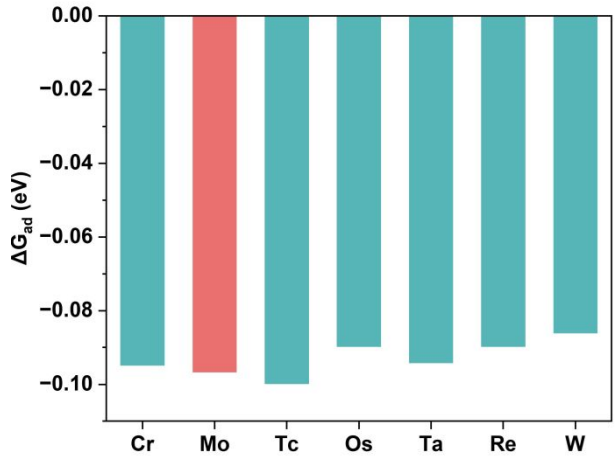

Figure S34. O_2 adsorption energy on the Pt-Ni-$^*MO_4$ surface (M is the screened elements)

6. Dissolution Free Energy of $^{*}MoO_4$

In this section, we elaborate the calculation of dissolution free energy of $^{*}MoO_4$. As the $^{*}MoO_4$ group can left from the surface by forms of H_2MoO_4 and Mo^{3+}, we give detailed calculation of each ion forms of $^{*}MoO_4$.

For the form of H_2MoO_4

$$PtNi - MoO_4 + 2H^+ + 2e^- \rightarrow PtNi + H_2MoO_4 \#(62)$$

$$\begin{aligned}\Delta G &= G(PtNi) + \mu_{H_2MoO_4} - G(PtNi - MoO_4) - 2\mu_{H^+} - 2\mu_{e^-} \# \\ &= G(PtNi) + \mu^0_{H_2MoO_4} + k_BTln(c/c^0) - G(PtNi - MoO_4) - 2\mu_{H^+} - 2\mu_{e^-}\end{aligned} \quad (63)$$

where the concentration of ions set as c = 10^{-4} mol/L. According to the definition of electrode potential, the free energy change of Eq. 62 is 0 when at the electrode potential of $E^0_{H_2MoO_4/Mo}$. Then, we can get that

$$H_2MoO_4(aq) + 6H^+ + 6e^- \rightarrow Mo + 4H_2O \#(64)$$

$$\Delta G = \mu^0_{Mo} + 4\mu_{H_2O} - 6\mu_{H^+} - 6\mu_{e^-_{H_2MoO_4/Mo}} - \mu^0_{H_2MoO_4} = 0 \#(65)$$

where μ^0_{Mo} is the energy of bulk Mo.

$$\begin{aligned}\mu^0_{H_2MoO_4} &= \mu^0_{Mo} + 4\mu_{H_2O} - 6\mu_{H^+} - 6\mu_{e^-_{H_2MoO_4/Mo}} \# \\ &= \mu^0_{Mo} + 4\mu_{H_2O} - 6\mu_{H^+} + \left(6\mu^{SHE}_{e^-} - 6\mu_{e^-_{H_2MoO_4/Mo}}\right) - 6\mu^{SHE}_{e^-} \\ &= \mu^0_{Mo} + 4\mu_{H_2O} - 6\mu_{H^+} + 6eE^0_{H_2MoO_4/Mo} - 6\mu^{SHE}_{e^-}\end{aligned} \quad (66)$$

Substituting Eq. 66 into Eq. 63, we get

$$\begin{aligned}\Delta G &= G(PtNi) + \mu^0_{H_2MoO_4} + k_BTln(c/c^0) - G(PtNi - MoO_4) - 2\mu_{H^+} - 2\mu_{e^-} \# \\ &= G(PtNi) - G(PtNi - MoO_4) \\ &+ \mu^0_{Mo} + 4\mu_{H_2O} - 6\mu_{H^+} + 6eE^0_{H_2MoO_4/Mo} - 6\mu^{SHE}_{e^-} + k_BTln(c/c^0) - 2\mu_{H^+} - 2\mu_{e^-} \\ &= G(PtNi) - G(PtNi - MoO_4) + \mu^0_{Mo} + 4\mu_{H_2O} + 6eE^0_{H_2MoO_4/Mo} + k_BTln(c/c^0) \\ &\quad -8\mu_{H^+} - 6\mu^{SHE}_{e^-} - 2\mu_{e^-} \\ &= G(PtNi) - G(PtNi - MoO_4) + \mu^0_{Mo} + 4\mu_{H_2O} + 6eE^0_{H_2MoO_4/Mo} + k_BTln(c/c^0) \\ &\quad -8(\mu_{H^+} + \mu_{e^-}) - 6\mu^{SHE}_{e^-} + 6\mu_{e^-} \\ &= G(PtNi) - G(PtNi - MoO_4) + \mu^0_{Mo} + 4\mu_{H_2O} + 6eE^0_{H_2MoO_4/Mo} + k_BTln(c/c^0) \\ &\quad -8\left(\frac{1}{2}\mu_{H_2} - \mu^{SHE}_{e^-} + \mu_{e^-}\right) - 6(\mu^{SHE}_{e^-} - \mu_{e^-}) \\ &= G(PtNi) - G(PtNi - MoO_4) + \mu^0_{Mo} + 4\mu_{H_2O} + 6eE^0_{H_2MoO_4/Mo} + k_BTln(c/c^0) \\ &\quad -4\mu_{H_2} + 8eU - 6eU \\ &= G(PtNi) - G(PtNi - MoO_4) + \mu^0_{Mo} + 4\mu_{H_2O} + 6eE^0_{H_2MoO_4/Mo} + k_BTln(c/c^0) \\ &\quad -4\mu_{H_2} + 2eU\end{aligned} \quad (67)$$

Substituting c = 10^{-4} mol/L into Eq. 67, we get

$$\begin{aligned}\Delta G_{diss} &= G(PtNi) - G(PtNi - MoO_4) + \mu^0_{Mo} + 4\mu_{H_2O} + 6eE^0_{H_2MoO_4/Mo} + 0.059 \times lg(1 \times 10^{-4}) \\ &\quad - 4\mu_{H_2} + 2eU = 0.16\ eV\end{aligned} \quad (68)$$

For the form of Mo^{3+},

$$PtNi - 2MoO_4 + 8H^+ + 5e^- \rightarrow PtNi - MoO_4 + Mo^{3+} + 4H_2O \#(69)$$

$$\begin{aligned}\Delta G &= G(PtNi) + \mu_{Mo^{3+}} + 4\mu_{H_2O} - G(PtNi - MoO_4) - 8\mu_{H^+} - 5\mu_{e^-} \# \\ &= (PtNi) + \mu^0_{Mo^{3+}} + k_BTln(c/c^0) + 4\mu_{H_2O} - G(PtNi - MoO_4) - 8\mu_{H^+} - 5\mu_{e^-}\end{aligned} \quad (70)$$

where the concentration of ions set as c = 10^{-4} mol/L.

To calculate $\mu^0_{Mo^{3+}}$, we use the standard half-electrode potential $E^0_{Mo^{3+}/Mo}$

According to the definition of electrode potential, the free energy change of Eq. 71 is 0 when at the electrode potential of $E^0_{Mo^{3+}/Mo}$. Then, we can get that

$$Mo^{3+} + 3e^- \rightarrow Mo \#(71)$$

$$\Delta G = \mu^0_{Mo} - \mu^0_{Mo^{3+}} - 3\mu_{e^-_{Mo^{3+}/Mo}} = 0 \#(72)$$

$$\begin{aligned}\mu^0_{Mo^{3+}} = \mu^0_{Mo} - 3\mu_{e^-_{Mo^{3+}/Mo}} = \mu^0_{Mo} - 3\mu_{e^-_{Mo^{3+}/Mo}} = \mu^0_{Mo} + 3\mu^{SHE}_{e^-} - 3\mu_{e^-_{Mo^{3+}/Mo}} - 3\mu^{SHE}_{e^-} \# \\ = \mu^0_{Mo} + 3eE^0_{Mo^{3+}/Mo} - 3\mu^{SHE}_{e^-}\end{aligned} \quad (73)$$

where μ^0_{Mo} is the energy of bulk Mo.

Substituting Eq. 73 into Eq. 70, we get

$$\begin{aligned}\Delta G &= G(PtNi - MoO_4) + \mu^0_{Mo^{3+}} + k_B T ln(c/c^0) + 4\mu_{H_2O} - G(PtNi - 2MoO_4) - 8\mu_{H^+} - 5\mu_{e^-} \\ &= G(PtNi - MoO_4) + \mu^0_{Mo} + 3eE^0_{Mo^{3+}/Cr} - 3\mu^{SHE}_{e^-} + k_B T ln(c/c^0) \\ &\quad + 4\mu_{H_2O} - G(PtNi - 2MoO_4) - 8\mu_{H^+} - 5\mu_{e^-} \\ &= G(PtNi - MoO_4) - G(PtNi - 2MoO_4) + 4\mu_{H_2O} \\ &\quad + \mu^0_{Mo} + 3eE^0_{Mo^{3+}/Mo} + k_B T ln(c/c^0) - 3\mu^{SHE}_{e^-} - 8(\mu_{H^+} + \mu_{e^-}) + 3\mu_{e^-} \\ &= G(PtNi - MoO_4) - G(PtNi - 2MoO_4) + 4\mu_{H_2O} \\ &\quad + \mu^0_{Mo} + 3eE^0_{Mo^{3+}/Mo} + k_B T ln(c/c^0) - 8(\mu_{H^+} + \mu_{e^-}) - 3(\mu^{SHE}_{e^-} - \mu_{e^-}) \\ &= G(PtNi - MoO_4) - G(PtNi - 2MoO_4) + 4\mu_{H_2O} \\ &\quad + \mu^0_{Mo} + 3eE^0_{Mo^{3+}/Mo} + k_B T ln(c/c^0) - 8\left(\frac{1}{2}\mu_{H_2} - \mu^{SHE}_{e^-} + \mu_{e^-}\right) - 3(\mu^{SHE}_{e^-} - \mu_{e^-}) \\ &= G(PtNi - MoO_4) - G(PtNi - 2MoO_4) + 4\mu_{H_2O} \\ &\quad + \mu^0_{Mo} + 3eE^0_{Mo^{3+}/Mo} + k_B T ln(c/c^0) - 4\mu_{H_2} + 8(\mu^{SHE}_{e^-} - \mu_{e^-}) - 3(\mu^{SHE}_{e^-} - \mu_{e^-}) \\ &= G(PtNi - MoO_4) - G(PtNi - 2MoO_4) + 4\mu_{H_2O} \\ &\quad + \mu^0_{Mo} + 3eE^0_{Mo^{3+}/Mo} + k_B T ln(c/c^0) + k_B T ln(c/c^0) - 4\mu_{H_2} + 5(\mu^{SHE}_{e^-} - \mu_{e^-}) \\ &= G(PtNi - MoO_4) - G(PtNi - 2MoO_4) + 4\mu_{H_2O} \\ &\quad + \mu^0_{Mo} + 3eE^0_{Mo^{3+}/Mo} + k_B T ln(c/c^0) - 4\mu_{H_2} + 5eU\end{aligned} \quad (74)$$

Substituting c = 10^{-4} mol/L into Eq. 74, we get

$$\begin{aligned}\Delta G_{diss} &= G(PtNi - MoO_4) - G(PtNi - 2MoO_4) + 4\mu_{H_2O} + \mu^0_{Mo} + 3e\overline{E^0_{Mo^{3+}}}_{Mo} + 0.059 \times lg \\ &(1 \times 10^{-4}) - 4\mu_{H_2} + 5eU = 1.60\ eV\end{aligned} \quad (75)$$

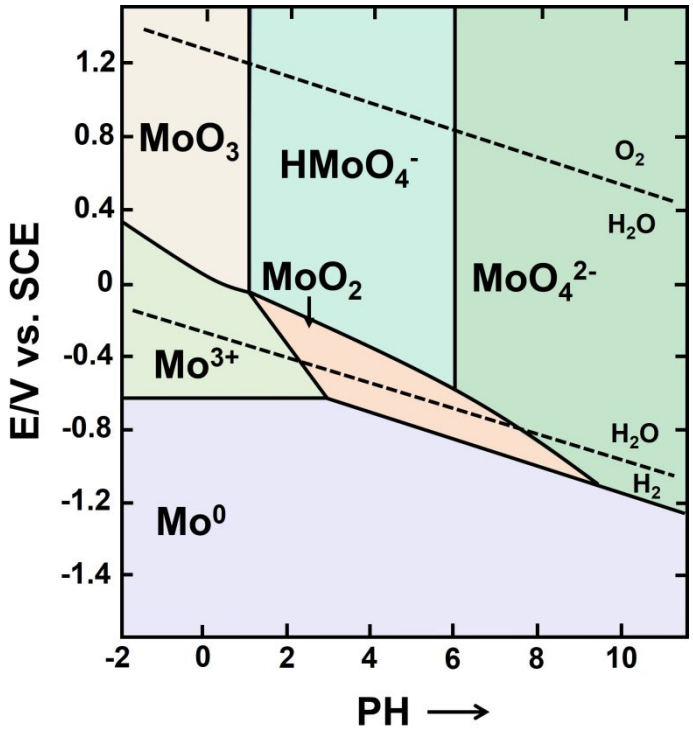

Figure S35. Experimental Pourbaix diagram of the Mo-H_2O system[10]. SCE is the saturated calomel electrode. $\boldsymbol{E_{SHE}}$ is the standard potential of the $\boldsymbol{E_{SCE}}$ at 298.15K (0.2145V).Figure adapted from ref. 10. Copyright 2012 Wiley Publishing Group.

We note that the adsorbed MoO_4 species are water-soluble under alkaline conditions (while it is not under acidic conditions)[6,10-13]. Figure S35 shows the experimental Pourbaix diagram of the Mo-H_2O system. We can see that the standard electrode potential of $E(MoO_4^{2-}/Mo)$ under alkaline conditions (pH > 10) is negative. Accordingly, the Nernst equation [$\Delta G = -nF\ E(MoO_4^{2-}/Mo)$] suggests that the free energy change of $MoO_4^{2-} \rightarrow Mo$ is positive, indicating the adsorbed MoO_4 species are water-soluble under alkaline conditions.

7. The specific activities of ORR catalysts at different CV cycles from experimental literature

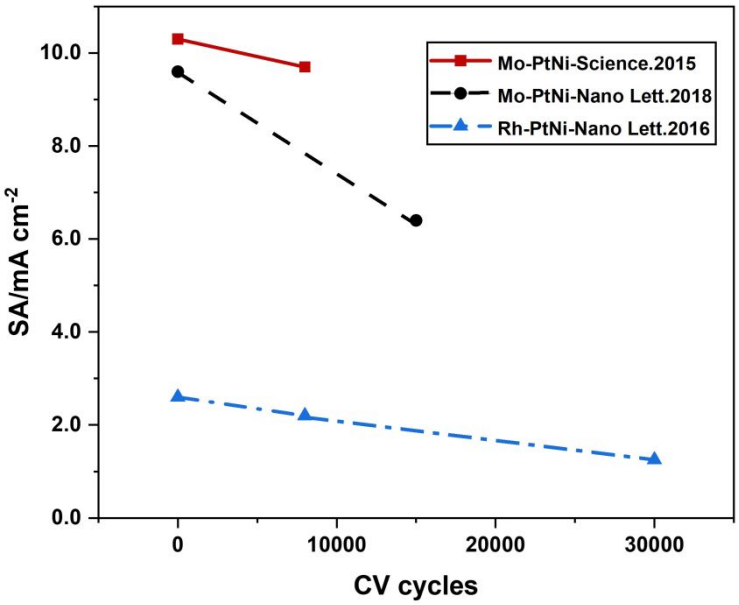

Figure S36. The specific activities (SA) of ORR catalysts at different CV cycles from experimental literature[6, 13-14].

Reference

1. Huang, S.-D.; Shang, C.; Zhang, X.-J.; Liu, Z.-P., Material discovery by combining stochastic surface walking global optimization with a neural network. *Chem. Sci.* **2017,** *8* (9), 6327-6337.

2. Huang, S.-D.; Shang, C.; Kang, P.-L.; Zhang, X.-J.; Liu, Z.-P., LASP: Fast global potential energy surface exploration. *WIRES COMPUT MOL SCI* **2019,** *9* (6).

3. Shang, C.; Liu, Z.-P., Stochastic Surface Walking Method for Structure Prediction and Pathway Searching. *J. Chem. Theory Comput.* **2013,** *9* (3), 1838-1845.

4. Shang, C.; Zhang, X.-J.; Liu, Z.-P., Stochastic surface walking method for crystal structure and phase transition pathway prediction. *Phys. Chem. Chem. Phys.* **2014,** *16* (33), 17845-17856.

5. Zhang, X.-J.; Shang, C.; Liu, Z.-P., Stochastic surface walking reaction sampling for resolving heterogeneous catalytic reaction network: A revisit to the mechanism of water-gas shift reaction on Cu. *J. Chem. Phys.* **2017,** *147* (15), 152706.

6. Huang, X.; Zhao, Z.; Cao, L.; Chen, Y.; Zhu, E.; Lin, Z.; Li, M.; Yan, A.; Zettl, A.; Wang, Y. M.; Duan, X.; Mueller, T.; Huang, Y., High-performance transition metal-doped Pt3Ni octahedra for oxygen reduction reaction. *Science* **2015,** *348* (6240), 1230-1234.

7. Li, Y.-F.; Liu, Z.-P., Particle Size, Shape and Activity for Photocatalysis on Titania Anatase Nanoparticles in Aqueous Surroundings. *J. Am. Chem. Soc.* **2011,** *133* (39), 15743-15752.

8. Bard Allen, J.; Faulkner Larry, R., Electrochemical methods: fundamentals and applications. Wiley New York: 2001.

9. Bosch, R.-W.; Féron, D.; Celis, J.-P., *Electrochemistry in light water reactors: reference electrodes, measurement, corrosion and tribocorrosion issues*. Elsevier: 2007.

10. Saji, V. S.; Lee, C.-W., Molybdenum, Molybdenum Oxides, and their Electrochemistry. *ChemSusChem* **2012,** *5* (7), 1146-1161.

11. Jiang, K.; Zhao, D.; Guo, S.; Zhang, X.; Zhu, X.; Guo, J.; Lu, G.; Huang, X., Efficient oxygen reduction catalysis by subnanometer Pt alloy nanowires. *Sci. Adv. 3* (2), e1601705.

12. Li, M.; Zhao, Z.; Cheng, T.; Fortunelli, A.; Chen, C.-Y.; Yu, R.; Zhang, Q.; Gu, L.; Merinov, B. V.; Lin, Z.; Zhu, E.; Yu, T.; Jia, Q.; Guo, J.; Zhang, L.; Goddard, W. A.; Huang, Y.; Duan, X., Ultrafine jagged platinum nanowires enable ultrahigh mass activity for the oxygen reduction reaction. *Science* **2016,** *354* (6318), 1414-1419.

13. Jia, Q.; Zhao, Z.; Cao, L.; Li, J.; Ghoshal, S.; Davies, V.; Stavitski, E.; Attenkofer, K.; Liu, Z.; Li, M.; Duan, X.; Mukerjee, S.; Mueller, T.; Huang, Y., Roles of Mo Surface Dopants in Enhancing the ORR Performance of Octahedral PtNi Nanoparticles. *Nano Lett.* **2018,** *18* (2), 798-804.

14. Beermann, V.; Gocyla, M.; Willinger, E.; Rudi, S.; Heggen, M.; Dunin-Borkowski, R. E.; Willinger, M.-G.; Strasser, P., Rh-Doped Pt–Ni Octahedral Nanoparticles: Understanding the Correlation between Elemental Distribution, Oxygen Reduction Reaction, and Shape Stability. *Nano Lett.* **2016,** *16* (3), 1719-1725.